Master's thesis

NTNU
Norwegian University of Science and Technology
Faculty of Information Technology and Electrical Engineering
Department of Engineering Cybernetics

Sindre Persaud Møller

Dynamic Optimization of a District Heating System using Model Predictive Control

Master's thesis in Industrial Cybernetics
Supervisor: Lars Imsland
June 2019

NTNU
Norwegian University of
Science and Technology

Sindre Persaud Møller

Dynamic Optimization of a District Heating System using Model Predictive Control

Master's thesis in Industrial Cybernetics
Supervisor: Lars Imsland
June 2019

Norwegian University of Science and Technology
Faculty of Information Technology and Electrical Engineering
Department of Engineering Cybernetics

Abstract

To operate a District Heating System (DHS) can be a complex task. The suppliers must continuously manage a varying demand of energy in a large and complex network, where heat losses can be significant. In order to produce optimally subject to delays, losses and last but not least energy demand, a predictive controller can be a important tool to utilize.

In this thesis a complete process model of the DHS at Stjørdal has been developed and further optimized, by using Nonlinear Model Predictive Control (NMPC). The regulatory and economic objectives has been merged together into a single level optimization problem, often called Dynamic Real-Time Optimization (DRTO), in order to improve both flexibility and accuracy. The goal has been to provide the requested power consumption by the aggregated consumers in the network, while minimizing the supply pressure and temperature at the plant as much as possible.

The process model has been developed based on preliminary work performed by Møller (2018). A finite volume approximation has been used to describe the heat propagation in the network, while the pressure was modeled as a lumped system. A linear correlation between the measured power consumption and mass flow, together with the energy balance, was used to model the mass flow and return temperature at the consumer. Furthermore was the DRTO designed by using both unreachable setpoints and infeasible soft constraints to express the economic objectives. Two cases was experimented with in order to test the effect of having the power consumption in the prediction.

Apart from minor deviations during peak consumption, the model matched the measurements relatively well during validation. There were close to no deviation in the modeled mass flow and return temperature at the majority of the consumers. However the return temperature at consumers with large consumption, were observed to have low sensitivity compared to the measurements. This was because the model relied heavily on the linear correlation, which did not catch the characteristics of the heat exchanger at the large consumers accurately enough. As a consequence the controller became relatively restrained from adjusting the temperature during optimization, since one of the large consumers had a low return temperature through the majority of the simulation. The effect of the low sensitivity, became particularly evident when the controller was tested in the second case. Without any information about the power consumption in the prediction horizon, the break in the regulative constraints only increased slightly.

Moreover were the controller able to reduce the supply temperature on average between 8 and 13 °C, with one occasion were a regulative constraint were broken. Additionally were oscillations observed in the temperature during low flow rates. These challenges were a result of using a fixed amount of evaluation points on the return temperature. This is because the delay in the heat propagation changed according to the mass flow of each consumer. By using a fixed amount of evaluation points it ultimately became a trade-off between breaking the regulatory constraint, or having oscillations in the supply temperature. Furthermore were the pressure not comparable with the measurements due to the modelling approach of the mass flow. However the results showed that the pressure was kept at adequate levels in order to provide the consumer with the requested flow.

Sammendrag

Å styre et fjernvarmenettverk kan være en utfordrende oppgave. Leverandøren må kontinuerlig håndtere varierende forbruk i et stort og komplekst nettverk, hvor varmetapet kan være betydelig. For å kunne produsere optimalt, med hensyn til forsinkelser, tap og ikke minst forbruksmønster, kan modellbasert prediktiv regulering være et viktig verktøy.

I denne oppgaven er en prosessmodell av fjernvarmenettverket ved Stjørdal blitt utviklet og videre optimalisert, ved bruk av modellbasert prediktiv regulering (NMPC). De regulative og økonomiske målene har blitt slått sammen til ett optimaliseringsproblem, som ofte blir kalt Dynamic Real-Time Optimization (DRTO), for å oppnå større fleksibilitet og nøyaktighet. Det overordnede målet har vært å forsyne kundene med den forespurte energien, og samtidig redusere forsyningstemperatur og trykk så mye som mulig.

Prosessmodellen har vært utviklet basert på et tidligere arbeid utført av (Møller 2018). Varmeforplantningen har blitt approksimert ved bruk av kontrollvolummetoden, mens trykket ble uttrykt i hvert rørstrekk. En lineær korrelasjon mellom målt energiforbruk og massestrøm, sammen med energibalansen, ble brukt til å modellere massestrøm og returtemperatur hos hver kunde. Videre ble optimaliseringsproblemet utviklet vha metodene ”unreachable setpoint” og ”infeasible soft constraint” for å inkludere de økonomiske målene i regulatoren. To problemstillinger ble så testet for å undersøke effekten av å ha informasjon om energiforbruket tilgjengelig i prediksjonshorisonten.

Sett bort ifra mindre avvik ved stort energiforbruk, stemte modellen svært godt med målingene. Det var nærmest ingen avvik i den modellerte massestrømmen og retur temperaturen hos majoriteten av kundene. Likevel ble det oppdaget svært lav sensitivitet i den modellerte returtemperaturen hos kunder med stort forbruk, sammenligner med måledata. Dette var fordi modellen var avhengig av den lineære korrelasjonen, som videre ikke klarte å beskrive karakteristikken til varmeveksleren hos de større kundene nøyaktig nok. Konsekvensen ble at kontrolleren ble holdt tilbake fra å endre mye på tilførselstemperaturen, siden en av de større kundene hadde en lav returtemperatur gjennom store deler av simuleringen. Effekten av den lave sensitiviteten ble enda tydeligere når kontrolleren ikke hadde informasjon om energiforbruket på forhånd. Resultatet ble at de regulative beskrankningene kun ble brutt i litt større grad, sammenlignet med når kontrolleren hadde full informasjon om energiforbruket.

Videre var kontrolleren i stand til å redusere tilførselstemperaturen i snitt med 8 til 13 °C, samtidig med kun ett tilfelle hvor de regulative beskrankningene ble brutt. I tillegg ble det observert oscillasjoner i temperaturen ved lav strømningshastighet. Disse utfordringene var et resultat av at det ble brukt en konstant mengde evalueringspunkt på returtemperaturen hos kundene. Dette var fordi temperaturforsinkelsen kontinuerlig ble endret etter den angitte massestrømmen hos hver kunde. Ved å bruke en konstant mengde punkt, måtte det gjøres en avveining mellom brudd på beskrankninger eller ha oscilleringer i tilførselstemperaturen. Avslutningsvis ble trykket ikke sammenlignet med måledata, på grunn av måten massestrømmen ble modellert. Resultatet viste likevel at trykket ble justert etter den ønskede massestrømmen hos hver kunde.

Preface

This Master's thesis is part of the compulsory 30 credits subject TTK4900 at the Norwegian University of Science and Technology. The thesis has been written in collaboration with Cybernetica AS, who initially defined the research problem.

Cybernetica has provided the necessary software tools to develop, simulate and control the process model. More specifically has the applications used in this thesis been the in-house software packages Modelfit, CENIT and RealSim. Additionally has Matlab been utilized. The thesis has been developed based on some of the previous work performed by the author, in a specialization project during autumn 2018.

I would like to express my gratitude and thank all the employees at Cybernetica for their support and tools to perform this project. Especially I would like to thank my Co-supervisors; Svein Olav Hauger and Peter Singstad for their support and assistance with a challenging research problem. I would also like to thank my supervisor Lars Imsland at NTNU for his support and advices during guidance sessions.

Finally I would like to thank Edgar Markhus, Åmund Utne and Toril Hovde at Statkraft AS, for providing technical information and insight about the district heating system at Stjørdal.

Table of Contents

List of Tables

List of Figures

Nomenclature

Abbreviations

AMTD:	Arithmetic Mean Temperature Difference
DRTO:	Dynamic Real-Time Optimization
NMPC:	Nonlinear Model Predictive Control
DV:	Disturbance Variable
MV:	Manipulated Variable
CV:	Controlled Variable
SQP:	Sequential Quadratic Programming
MHE:	Moving Horizon Estimator
EKF:	Extended kalman Filter

Symbols

$\dot{m}$	=	Mass flow$[kg/s]$
q	=	Volumetric flow $[m^3/s]$
c_p	=	Specific heat capacity of water $[J/(kg°C)]$
A	=	Cross sectional area of the pipe $[m2]$
k'	=	Thermal loss coefficient between pipe and ground $\frac{J}{m^2 s°C}$
T_{gnd}	=	Temperature of the surrounding ground $[°C]$
T	=	temperature of the water $[°C]$
v	=	Fluid velocity $[m3/h]$
c_p	=	Specific heat capacity of water $[J/(kg°C)]$
A	=	Surface area of the pipe $[m2]$
Q	=	Heat transfer $[W]$
P	=	Pressure $[MPa]$
$D1$	=	Inner inner diameter $[mm]$
D2	=	Outer pipe diameter[mm]
D3	=	Diameter of pipe including insulation [mm]
λ_p	=	Conductivity in the steelpipe $[W/(mK)]$
λ_i	=	Conductivity in the insulation $[W/(mK)]$
m	=	Mass [kg]
r	=	Radius [mm]
Δx	=	Distance [m]
h_l	=	Head loss [m]
V	=	Volume $[m^3]$
ρ	=	Density $[kg/m^3]$
z	=	Height [m]
g	=	gravitaional constant $[m/s^2]$
K_v	=	Valve constant
J	=	Jacobian matrix
n	=	number of control volumes

u	=	input
x	=	State variable
y	=	Measured variable
z	=	Derived variable
N	=	Horizon length
L	=	Length of pipe at consumer [m]

Chapter 1

Introduction

1.1 Motivation

According to Centre for Sustainable Energy Studies, a high activity scenario of energy demand in Norway, could result in a increased total energy consumption by 43 TWh from 2010 to 2050 (CENSES 2015). The Norwegian Water Resources and Energy Directorate predicts that the total electricity consumption in Norway will increase from 133 TWh in 2016 to 157 TWh in 2035 (NVE 2018). The main reason for this estimated increase, comes from electrification of oilplatforms, new data centers, a more power demanding industry, and last but not least electrification of the transport industry. Fossil cars, trucks and ferries are either being fully electrified or will be using a hybrid version which will drastically increase the need of electricity in the future.

In 2015, Norway was among the 196 countries that established The Paris Agreement, which legally bound the countries into a climate deal. The goal was to keep the global temperature increase below $2°C$ compared to pre-industrial levels, and also to limit the consequences that global warming could bring. In order to meet this goal, all the countries are looking for solutions to decrease CO2 emissions, like for instance increasing the prices of fossil power production.

The increased energy demand in Norway will to some extent be supplied from Europe, since Norway is connected to the European power supply market. This solution serves as a good contribution, especially during droughts (like summer 2018), to keep the prices from skyrocketing. However the European price market are higher than the average Norwegian, which could drive the prices up (E24 2019). Together with the Paris agreement that requires a reduction in energy consumption from fossil fuels, this could result in a high electricity price in Norway. Seen in context with the predicted increase in energy demand in Norway the next decades, this should encourage more effective use of energy where ever possible.

District heating systems (DHS will be used as an abbreviation from now on) has been an important heat source in several European cities of varying sizes. The recovery of energy from waste, represents a large and seldom used energy source in Norway, and could provide a cheap option for residential heating compared to conventional electric source. By for instance incinerating trash or waste-chips from timber, and transport the heat by water, a whole city could benefit from a more energy-effective supply. As a result could the load on the electric grid be significantly reduced. This technology enables efficient and economical utilization of energy sources that earlier have been wasted (Kauko et al. 2018). If the world are to become fossile-free in the future, systems that utilizes waste heat could play an important role.

To operate a large DHS is a rather complex task. The suppliers in the DHS must continuously manage a varying demand in large and complex networks, which will be further described in chapter 2.3 (Kauko et al. 2018). A high level of process control which can predict peaks before they occur, and at the same time keep the delivered flow and temperature at a minimum, could be an important tool in order to operate the plant efficiently.

The heat propagation in the network can further be in the range of several hours with both heat and pressure losses to be accounted for. Without any accurate information about the network due to the complexity, the DHS-supplier have to compensate with a high distribution temperature and pressure. This further leads to higher energy losses, and low efficiency in the heat exchangers. In order to produce optimally subject to delays, losses and last but not least the demand, a good model of the consumer and the heat propagation throughout the network is essential, according to Åmund Utne, Senior Advisor at Statkraft (Meeting at Statkraft 30.01.19).

1.2 District Heating Systems

This chapter describes the qualitative theory regarding district heating systems with relevance to the Stjørdal network. It provides an overview of the most vital components of the network, their purpose, and some of the most important aspects of them regarding modelling and control.

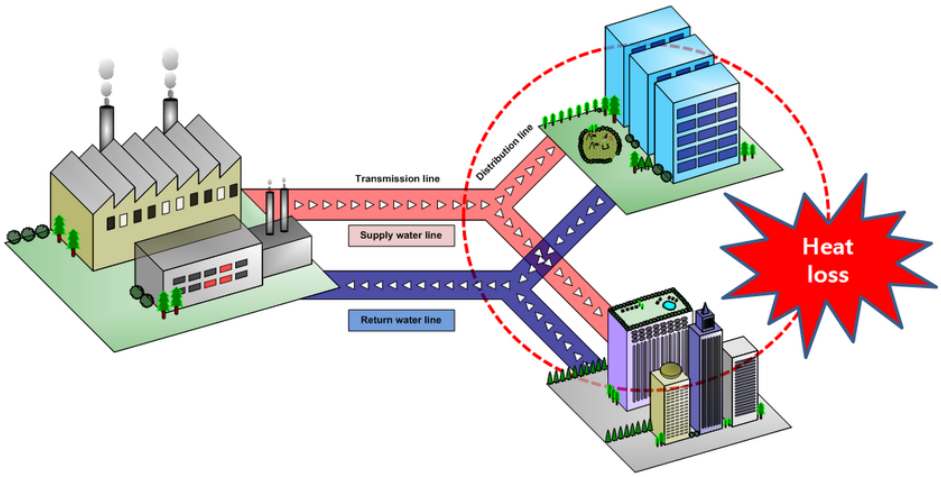

Figure 1.1: District Heating System (Byun et al. 2019)

1.2.1 District Heating

A DHS uses hot water or steam that circulates between a heat central and consumers via a distribution network. The consumers then use the water for heating either as floor heating or with radiators, and for heating tap water. As displayed in figure 1.1, are the main components in such a system production plant, transmission line and consumer substations of varying sizes. There are various types of consumers in a DHS. A data center or retail store could be both consumer and supplier through the year. For instance a store could have surplus heat during the summer that could be fed into the grid system, but during the winter months it would require heat from the grid (Kauko et al. 2018). There could also be consumers that uses the heat in order to cool down equipment (Statkraft 2019a). However in the Stjørdal network there are only regular consumers that uses the supplied heat for heating (Utne 2018). This thesis will therefore not go into more detail on this topic.

1.2.2 Production Plant

There are various energy sources that can be used for heat production e.g. bio-fuels, electricity, waste incineration, oil or natural gas (SNL 2019). The production plant at Stjørdal primarily burns woodchips in order to keep the water heated. In addition are there two large electric boilers available if needed. It is common to have several types of energy sources available in larger networks due to the following reasons (Statkraft 2019b) :

- Being able to switch between different energy sources based on what is the cheapest at a given time.
- It is necessary to have at least one backup source for redundancy if the primary one fails.
- During the peak hours or peak season of consumption, there might be need of several energy sources at the same time in order to handle the demand.

Naturally one would want to use as much of the environmentally friendly energy sources as possible. In order to separate between the preferred and the non-preferred sources, the first one is called base load and the latter is called peak load. The peak load then corresponds to less favourable energy sources, e.g., oil or gas (Statkraft 2019b). If the consumption increases above the available base load of the plant, the remaining therefore has to be supplemented by the peak load.

The required temperature in the network is dependant on several factors, such as layout, laws and regulations, power consumption, and last but not least the varying ambient temperature. The supply temperature at Stjørdal usually varies between 110 and 90 °Celsius, and the return temperature varies between 50 and 60 °C (Utne 2018). A typical delta temperature is therefore about 50 °C, which means a large amount of the supplied energy is not being utilized. Although a lower supply temperature is desirable, are laws and regulations preventing it from being lower than 70 °C at the inlet of each consumer. This is due to the risk of Legionella bacteria (Statkraft 2019c).

The plant at Stjørdal is currently operated by three large water pumps set up in parallel, were one pump can produce a maximum pressure of 16 bar and mass flow of 361 m^3/h (Grundfos 2019). Together they produce the necessary pressure in order to transport the water out to the work. A production plant can also have accumulated hot water stored in large tanks at the production site or close to large consumers, in order to quickly compensate for large increases in consumption. Statkraft is however not using water storage at Stjørdal, so it will not be included in this thesis.

1.2.3 Distribution Network

The district heating system can be split into a primary and secondary side, where the primary side consist of the distribution network, and the secondary side consist of the consumer substation as shown in figure 1.2. A distribution network usually consist of several loops and branches stretching out in all directions. The network could span tens of kilometers, causing large delays in the heat transportation, since the production plants are often located in the outskirts of the city. In order to retain as much of the heat as possible, the pipes at Stjørdal are insulated with polyurethane-foam which is a type of polymer.

The network usually increases over time with new consumers being added gradually. These new additions could be installed with new technology or standards, or even from different suppliers. The result could be a large web of heat exchangers, pipes and manholes with different quality and designs, according to Åmund Utne, Senior Advisor at Statkraft (Meeting at Statkraft 30.01.19). Without proper documentation, it could be a

difficult task to model such system if for instance several heat exchangers acts differently than presumed.

1.2.4 Consumer Substations

The secondary side of the DHS, i.e., the consumer substation, consists of a smaller network within the consumer building. A consumer can be defined as a building with heat demands in terms of hot water and/or space heating, such as residential buildings, offices, public buildings or industrial areas. A heat exchanger hydraulically separates the heat central and consumer from the distribution network (no fluid is transferred), which can be observed in figure 1.2. The figure illustrates how the heat central supplies heat into the distribution network by using two large heat exchangers, and then ultimately the network is able to deliver the heat through a smaller exchanger placed at the consumer.

From a modeling point of view the substation only contains a heat exchanger, PID controller and a valve. In reality there are several meters of pipe around the house which separates into two heat exchangers, one for heated water and one for the space heating. In addition there are circulation pumps, expansion tanks and radiators, but these are usually not included in a model. The system is developed such that the consumer can set a desired temperature on the controller, which further changes the valve position accordingly. In the simplified schematic shown in figure 1.2, the valve is located right after the heat exchanger on the right side of the figure. If the valve opening is increased, the pressure difference between the supply (red) and return line (blue) is reduced. The pump at the production plant then has to increase the supply pressure in order to keep the difference at the plant constant. If the pump can not deliver more water (or further increasing the mass flow does not result in more heat transfer), then the supply temperature has to be increased.

The supplied heat to the heat exchanger during a given amount of time, can be expressed as an energy consumption at the consumer. The term peak will also be used about the consumer referring to times with large consumption (peak consumption), whereas base consumption will only be referred to as consumption.

In the network at Stjørdal, the consumer has the responsibility of acquiring and maintaining the heat exchanger (since it is usually inside the building). As a result, Statkraft has no possibility of measuring mass flow or temperature on the secondary side. This also includes the valve position on the primary side. Additionally are the characteristics of the heat exchanger at each consumer unknown, since Statkraft has no database of what type of exchanger has been installed. The consequence is limited information about the consumers in the network.

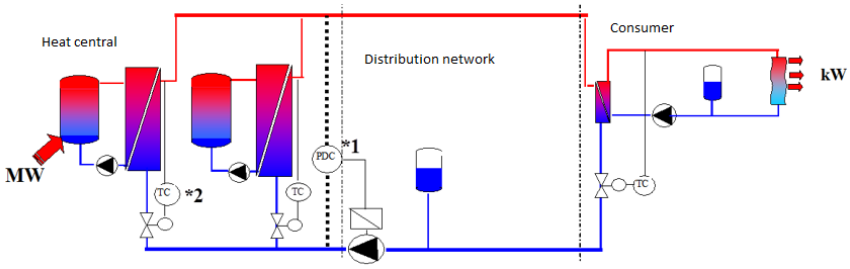

Figure 1.2: Simplified district heating system (Utne 2018).

1.3 Previous Work

Substantial work has been conducted in the field of district heating. The main focus when describing the studies below, has been the modeling approach of the distribution network and consumer together with the setup of the MPC. In addition were some studies not relevant to the DHS directly, but the general topic of optimization were studied in order to find inspiration of how to develop the controller.

There are several possibilities when modelling the heat and pressure propagation through a distribution network. A common method is to use Modelica when implementing a physical approach. Giraud et al. (2015) presented a Modelica library containing two different pipe models to describe the heat propagation in a DHS. Both models were based on the first law of thermodynamics, expressed as a partial derivative equation, but with different approaches to obtain an ODE. The first method spatially discretized the model by using a finite volume method. By implementing a collection of axially distributed control volumes, the PDE was transformed into a ODE. A node method, including the method of characteristics, were also tested were the PDE was integrated along a fluid's particle path line. Along these path lines, namely a characteristic curve, the PDE became an ODE. As a result could the exact solution of the temperature dynamics in the distribution system be described. After comparison of computational cost, the node method had a reduction in complexity by a factor of 40.

The pressure was modeled with one balance equation per pipe section. Several pre-made pipe-libraries were utilized in order to model the mass flow directly. The consumer substation was developed by using a Logarithmic Mean Temperature Difference method, while a pre-made valve component described the pressure loss. The validation were performed on a 470m pre-insulated pipe with relatively good results. The model showed only small errors compared to the measurements, but did however struggle to reach the peak temperature when a input step was performed.

(Hermansson and Kos 2017) used Matlab and Open Modelica to develop a pipe and consumer model of a DHS. Similarly to (Giraud et al. 2015), were a finite volume method utilized to transform the PDE to an ODE in order to express the heat propagation. The heat loss throughout the network was modeled by using a heat transfer coefficient in each control volume, that were calculated by Prandtl's and Nusselt's number. The pressure loss

through the network was modeled by using Churchill's equation. With this method both turbulent as well as laminar flow could be handled. The consumer substation were modeled with a heat exchanger from the library. When validated, the distribution and consumer model produced relatively good results, even when tested on larger parts of a network.

Several other examples of studies that utilized the method of characteristics were observed, e.g, (Hamre 2017), (Hägg 2016) and (ZHOU et al. 2014). (Hamre 2017) introduced a few empirical approaches in order to describe the complete distribution system at Stjørdal. The pressure loss through the network were modeled with a physical approach of using the Colebrook-White equation. By additionally using Wood - Charles linearization, the flow-pressure equations were transformed into a linear system of equations. The node method was utilized, in addition to the method of characteristics, in order to model both the heat propagation through the network and the return temperature at each consumer. The mass flow at each consumer were modeled as a weighted average based on the measured power consumption, together with estimated time delays to each consumer. The developed models were validated with a sampling time of one hour, and showed promising results.

The use of Model Predictive Control (MPC) can be a effective tool when handling multiple-input multiple-output systems, including constraints and regulatory objectives (Foss and Heirung 2016). Due to the system complexity in a DHS, the utilization of MPC can be a useful tool to determine optimal temperature and pressure levels (Giraud et al. 2017). The possibility of handling nonlinear constraints, makes the MPC a powerful tool to deal with nonlinear systems such as a DHS.

There are typically several objectives when implementing a MPC algorithm. A common method, used in both Hamre (2017) and Svenheim Rene (2016), were to divide the objectives into two layers of cost functions. The first layer included the cost function in the MPC, which handled the regulatory objectives. The second function (named slow model) handled the economic objectives, but less frequently and it was simulated to steady state before setpoints were fed to the MPC layer. Hamre (2017) implemented the controller by using SQP and fmincon function in Matlab. The economic layer provided the ideal constant supply temperature and flow to be delivered to each consumer, based on load predictions. In addition were regulatory objectives implemented in the form of constraints on return temperature. The result showed that the supply temperature were reduced, while the mass flow was increased. However the modeled return temperature at the plant was significantly higher than the historical measurements throughout the simulation, and Hamre suggested several possible reasons for this.

Svenheim Rene (2016) also implemented a MPC algorithm to optimize his model. The control hierarchy were similarly to (Hamre 2017) separated at the top with a slow model. Only the power demand was used as feedback in the control loop however, and the goal became to achieve an overall zero energy difference between the input from the consumers and the output of the plant. The algorithm were able to reduce the average supply temperature by approximately 18 °C through a 24 hour simulation.

A few studies has tested the possibility of merging the economic and regulatory objectives into one layer. (Giraud et al. 2017) utilized MPC based on a previously built nonlinear model in Modelica. In this study both the regulatory and economic criteria were imple-

mented in the same objective function. By using this method, the setpoints for an optimal combination of the supply temperature and mass flow were updated more frequently. This enabled more dynamic optimization, by including the economic objectives in the MPC cost function. The study was performed on a high temperature mesh-free network, including heat storage capacity, with a mixed integer linear program and a time step of 15 minutes. By taking into consideration the fuel and electricity consumption, together with several regulatory constraints, the algorithm were able to reduce production cost by 8 % compared to the more simple controller tested in (Giraud et al. 2015). The algorithm were programmed with an in-house optimal control software called PEGASE, while the optimization problem were programmed by using C++.

(Willersrud et al. 2013) also tested the possibility of merging the two objectives into one layer. The controller was implemented to optimize the production at an oil rig, by utilizing two methods to handle the economic objectives. The first one utilized unreachable setpoints and the second used infeasible soft constraints. Both methods were able to find the optimum, while the second method resulted in a more aggressive controller. This approach of optimization is often referred to as Dynamic Real-Time Optimization (DRTO) or Economic MPC. In this thesis DRTO will be used as an abbreviation.

To sum up the most common approaches of modelling a DHS, has Modelica or Matlab been the most common software to utilize, and especially when a physical approach were preferred. This could be because of its favourable properties regarding handling for instance spatial discretization. However by using either characteristic path lines or finite control volumes has the heat propagation through the network been described. The pressure has in most cases been modeled as a lumped system with general flow-pressure equations. The consumer has in general been modeled as a valve, heat exchanger and controller, although various methods has been used to actually describe the mass flow and return temperature at the consumer. The MPC controller has in several cases been developed as a two layer problem, however a trend towards integrating the economic and regulative objectives has been observed.

1.3.1 Previous relevant work performed by the author

As mentioned in the preface has there been performed previous work by the author on the DHS at Stjørdal, through a specialization project during autumn 2018. In this project were a physical model developed to describe the heat propagation and pressure development of certain parts of the Stjørdal network. The pipe model was discretized by using a finite differencing scheme, together with control volumes. The pressure was further modelled as a lumped system, with the pressure loss described by Haaland's equation. Møller (2018) developed additionally two different consumer models. The first model was based on the valve position at the consumer, which further affected the pressure difference. By using Newton's method, with the flow-pressure equations describing the network, the mass flow distribution in each pipe segment and consumer was found. However there were no measurements of the valve position to be used. In order to have a consumer input, a linear correlation between the valve position and the power consumption was used. The second modelling approach was based on the energy balance together with an arithmetic mean temperature difference (AMTD) in the heat exchanger.

The validation of the two models was performed on two smaller parts of the Stjørdal network. The first part was a single branch with two consumers, and the second was a loop with four consumers. By comparing with historical data, the valve model was observed more accurate than the AMTD method. Especially during hours of low power consumption and during a transient period when a consumer drastically increased or decreased its consumption. However when implementing the valve model in the loop network, the newton iterations did not converge to adequate values, and validation was not possible. The AMTD method showed a similar pattern as with the single branch, experiencing deviations during low power consumption.

1.4 Assumptions

In the process of developing a process model from scratch, several overall assumptions about the network was required. There are about 70 consumers in the Stjørdal network, and all of them had to be included in the model in order to make it as realistic as possible. This involved modelling the pipe-layout stretching out to each consumer, which could be very time-consuming to develop and make the runtime of the simulation inadequate. However by aggregating some of the consumers together, the model is kept on a small enough level for the simulation time to be sufficient, and without losing to much accuracy in the model. Based on the geographical layout of the consumers it was therefore assumed that the DHS contained 15 aggregated consumers.

In addition it has been assumed that there already exists a optimal plant model that describes the heat production at the plant. Incineration of woodchips, heating up water in the heat exchanger, and adjusting pump pressure has therefore been assumed sufficiently fast. This also accompanying the assumption that the low level controllers adjusting pump speed, incineration and valve positions, behaves flawlessly and with adequate transients at all times to produce the required values set by the MPC. This also includes the low level controller at each consumer that are adjusting the valve position, in order to describe the power consumption. Moreover has it been assumed that the local optimum found by the optimization algorithm also is a global optimum. Furthermore has the measurements, provided by Statkraft AS, been assumed accurate enough to be used for verification of the model.

1.5 Objective

The goal of this thesis is to develop a process model that describes the temperature, mass flow and pressure throughout the DHS at Stjørdal. Additionally is a consumer substation, explicitly describing the mass flow and return temperature, to be implemented at each aggregated consumer. The model is further to be validated against historical data to observe the accuracy. DRTO should further be utilized with the goal of reducing the supply temperature compared to the historical data, but at the same time deliver the requested power to each consumer. The algorithm is to be constructed as a single level Nonlinear Model Predictive Controller, by using soft constraints and setpoints.

1.6 Outline of Thesis

This master thesis is structured such that the reader is firstly introduced to the importance of this research in chapter 1. The goal is to give the reader a bigger perspective of the benefit of utilizing DHS in large networks, together with the importance of optimizing these processes in order to minimize waste. In addition is a brief introduction to the most important components in a DHS provided, together with a literature review, assumptions and finally the objective of this thesis.

In chapter 2 will the reader be given an introduction to the underlying model theory, which will be necessary to understand the modelling approach of the network. In chapter 2.2 are the theory used to describe the return temperature and mass flow at the consumer substations provided, together with the approach of aggregating the consumers.

In order to understand the implementation of the controller, the reader is firstly introduced to the general control theory in chapter 3. This includes the development of the cost function based on different objectives, and understanding the closed control loop. Since Cybernetica has developed their own software tools for simulating and performing process optimization, the reader is also introduced to each of these tools in chapter 4. In chapter 5 the theory from chapter 3 is applied, in order to develop the process model of the Stjørdal network. Additionally the model is validated against historical data and presented graphically, following discussion and conclusions. In the process of developing a physical model there will often be deviations from the measurements, and the sources of these errors can be comprehensive. However the most important sources of errors are described in chapter 5.3.

The process of implementing both economical and regulatory objectives, as well as tuning the controller is described in chapter 6. Two cases has been tested, and the results, following discussion and conclusions, are presented. An overall conclusion based on the findings from both the modelling and control, are further presented in chapter 7. A final chapter describing the possibility of future work on this topic is presented in chapter 8.

Chapter 2

Process Model Theory

As described in chapter 1.3 there are several possible approaches to model a DHS. In this chapter the theory behind the chosen modelling approach of the DHS is presented. Furthermore are the theory describing the modelling approach of the consumer substation presented. A large part of the underlying theory describing the heat and pressure loss is based from Møller (2018), but more aspects has been taken into consideration and inadequate descriptions has been further detailed.

In order to calculate the heat- and pressure loss, the following assumptions have been made:

- The system is modeled quasi-dynamic, which means that temperature is modelled dynamic and pressure is modelled static. This is because the fast pressure dynamics will not affect the more slow heat propagation in any noteworthy way. As a consequence is the water assumed incompressible as well.
- The heat does not accumulate in either the wall or insulation of the pipe.
- Specific heat, density and viscosity is kept constant.
- The flow is assumed turbulent throughout the network.
- Minor pressure losses, e.g, losses from bends, fittings and entrances in the pipes are neglected. Additionally is the heat loss to the surroundings in the heat exchanger neglected.

2.1 Pipe Model

In Møller (2018) the pipe system was spatially approximated with a finite amount of control volumes. A control volume describing a small pipe length, Δx , of the system was described as shown in figure 2.1. $T_{x+\Delta x}$ expresses the temperature inside the control volume, where the water is assumed ideally mixed. T_x represents the temperature one control volume upstream (in front), with the difference between them being the heat loss. This way a series of control volumes can be put in a consecutive order creating a network of pipes, while the following continuity principle regarding the mass flow has to hold:

$$\dot{m}_{out} = \dot{m}_{in}$$

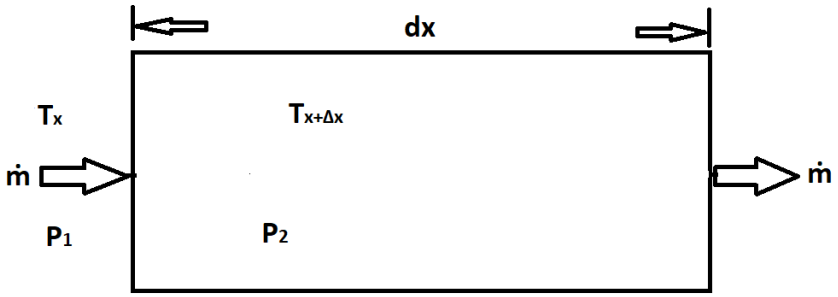

Figure 2.1: Control volume with length dx Møller (2018)

2.1.1 Heat model

Møller (2018) used the partial differential equation in 2.1 to express the energy balance, in terms of heat, of the pipe system. In this equation ρ is the density of the water, c_p is the specific heat coefficient, A is the area, T is temperature, v is the velocity and Q_{loss} is the heat loss. However before the equation can be used to express the heat propagation in a pipe network, it has to be transformed into an ODE by handling the spatial derivative, $\frac{\delta T}{\delta x}$.

$$\rho c_p A \left(\frac{\delta T}{\delta t} + v \frac{\delta T}{\delta x} \right) + Q_{loss} = 0 \tag{2.1}$$

As pointed out in chapter 1.3 there are different ways to obtain the outlet temperature of a pipe. The node method used in both Hamre (2017) and Giraud et al. (2015) integrates equation 2.1 along a fluid's path line following the method of characteristics. However Møller (2018) suggests that using method of characteristics could cause discontinuity and stiffness issues when implemented with a MPC. Instead a finite difference approximation is used to spatially discretized the equation. The spatial derivative is then approximated as

shown in equation 2.2 into a small part of the pipe network, Δx, which makes it possible to produce a collection of axially distributed control volumes as shown in figure 2.1. Equation 2.1 is then transformed into an ordinary differential equation, which can be solved with an integration scheme in order to describe the temperature in each control volume. (Thomas 1999)

$$\frac{\delta T}{\delta x} \approx \frac{T_{x+\Delta x} - T_x}{\Delta x} \tag{2.2}$$

The heat loss, Q_{loss} in equation 2.1, can be determined by using Fourier's law of thermal conduction as shown below (Cengel and A.Boles 2011):

$$Q_{loss} = -Ak'(T - T_{gnd})$$

The k' represents the thermal transmittance through the pipe, and T_{gnd} is the ground temperature. The transmittance can be calculated by using the thermal conductivity, λ, together with the thickness of the pipe and insulation (Thermopedia 2019). The thickness in a insulated pipe, can further be divided into three significant diameters as shown in figure 2.2. D1 represents the diameter of the inner pipe where the water flows. D2 represents the inner pipe including the wall thickness. D3 displays the outer diameter of the pipe which includes the insulation. By using these diameters and the thermal conductivity, the thermal transmittance can be calculated as shown in equation 2.3. By using this method a separate thermal transmittance has to be calculated for each combination of pipe diameter and insulation thickness that exists in the network. (Thermopedia 2019)

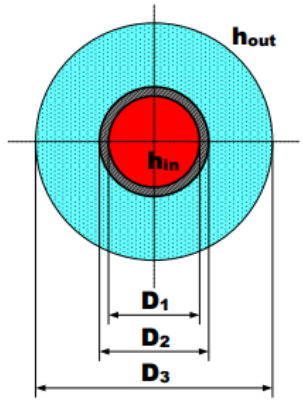

Figure 2.2: Diameters of an insulated pipe. Morvay and D. (2008)

The thermal conductivity of polyurethane and steel, λ_i and λ_p , is temperature dependent and is therefore likely to change through the network. In order to reduce the number of variables in the model, has the conductivity initially been averaged and then adjusted by

parameter estimation. The temperature in the distribution network is given to be between $110°C$ and $50°C$. However one of the goals of this thesis is to reduce the supply and return temperature and therefore has an average of 70 °C been used, which equals about 0.027 $\frac{W}{mK}$ (EngineeringToolbox 2019b). The conductivity of the steel pipe can further be averaged to 17 $\frac{W}{mK}$ (EngineeringToolbox 2019a).

$$k' = \frac{1}{\frac{D_3 \log(\frac{D_2}{D_1})}{2\lambda_p} + \frac{D_3 \log \frac{D_3}{D_2}}{2\lambda_i}} \tag{2.3}$$

The heat propagation in the DHS can finally now be modeled by using equation 2.4, where m is the mass of the control volume. The equation is essentially the same as equation 2.1, but with the spatial approximation, rewriting of Q_{loss} and constants, and some rearranging. The outlet temperature of a control volume with length Δx can now be calculated by using an integration scheme, e.g., Explicit Euler.

$$\frac{\delta T_{x+\Delta x}}{\delta t} = \frac{\dot{m}}{m}(T_x - T_{x+\Delta x}) - \frac{k' 2\pi r \Delta x (T - T_{gnd})}{c_p m} \tag{2.4}$$

2.1.2 Pressure model

In order to determine the mass flow going through the network, the pressure loss has to be accounted for. The pressure transient is not included in the model as stated in the assumptions, so the pipe pressure can be expressed as a lumped system. By modelling the pressure as static, we can utilize the conservation of energy law per unit mass as shown in equation 2.5. In this equation P_1 and P_2 respectively denotes the pressure at the start and at the end of a pipe segment (Fox et al. 2016). The term gh_l represents the pressure loss measured in meters (head loss).

$$\left(\frac{P_1}{\rho} + \frac{{v_1}^2}{2} + gz_1\right) - \left(\frac{P_2}{\rho} + \frac{{v_2}^2}{2} + gz_2\right) = gh_l \tag{2.5}$$

The conservation of mass principle can be applied to the pipe section in terms of mass flux. For a steady and incompressible flow where the cross section does not change, the following holds:

$$v_1 = v_2$$

The network at Stjørdal is blessed with very small elevation differences, and therefore can the terms z_1 and z_2 be removed. With the continuity principle and some rearranging, equation 2.5 can be simplified to the following equation:

$$P_1 - P_2 = \Delta P_{loss} \tag{2.6}$$

ΔP_{loss} can be derived from the Darcy-Weisbach equation shown in equation 2.7. In this equation f is the friction coefficient, Δx is the pipe length (not necessarily the same length as the control volume defined in last chapter), D is the diameter, g is the acceleration of gravity, and $\bar{v}$ is the average fluid velocity. (Wikipedia 2019)

$$\Delta P_{loss} = f\frac{\Delta x \bar{v}^2}{2Dg} \tag{2.7}$$

The equation can further be rewritten to express the pressure loss in terms of volumetric flow, w, which then becomes as follows:

$$\Delta P_{loss} = f\frac{8\Delta x \rho w^2}{\pi^2 g D^5} \tag{2.8}$$

The friction factor, f, for turbulent flow can be determined by the Colebrook-White equation shown in equation 2.9. The equations uses the Reynoldsnumber Re, pipe diameter D, and roughness ϵ to determine the friction factor.

$$\frac{1}{\sqrt{f}} = -2\log\left(\frac{\epsilon}{3.7D} - \frac{2.51}{Re\sqrt{f}}\right) \tag{2.9}$$

This equation is implicit and therefore requires an iterative scheme to be solved. Instead of iterating for a solution, Haaland's approximation has been used and is shown in equation 2.10. The approximation claims to be within $\pm$ 2% error if the Reynoldsnumber is greater than 3000 (Kiijärvi 2019).

$$\frac{1}{\sqrt{f}} = -1.8\log\left(\frac{\epsilon}{3.7D}^{1.11} + \frac{6.9}{Re}\right) \tag{2.10}$$

The Reynoldsnumber predicts fluid patterns based on turbulent or laminar flow situations, and is further decribed below:

$$Re = \frac{vD}{\nu}$$

The kinematic viscosity, ν, describes how resistive the fluid is to shear stress, and is often called thickness. This is an important property in order to calculate a good estimate of the pipe friction. The kinematic viscosity of water depends on the temperature. As mentioned in chapter 2.2 are the temperature in the distribution system ranging between 50-110 $^\circ C$. An average viscosity of $0.4116 * 10^{-6}\frac{m^2}{s}$ has therefore been used initially, which corresponds to 70 $^\circ C$ (ToolBox 2019) .

The relative roughness is usually difficult to determine with high precision in a DHS. The large amount of pipes undergoes varying loads regarding pressure, temperatures and flow

velocities. In order to estimate the roughness, several factors has to be considered. For instance how the welding was done when installed, pipe age, pH value of fluid, average flow amount, and pipe-material. Naturally it is not possible to account for all these factors, and therefore has averaged values from Statkraft been used.

In order to have a more convenient expression when developing a large distribution model, equation 2.8 has been rewritten to a more simplified expression, i.e, the constants has been merged together into a friction constant K_{pipe}.

$$\Delta P_{loss} = K_{pipe} w^2$$

We can then replace the head loss term in equation 2.6 to the following expression:

$$P_2 = P_1 - K_{pipe} w^2 \tag{2.11}$$

Finally equation 2.11 expresses the complete pressure loss in a pipe section. In such a section there could be several control volumes, where the heat propagation can be expressed by utilizing equation 2.4 in each volume.

2.2 Consumer substation

In order to model a complete DHS, the return temperature and mass flow at each consumer must be calculated. As stated in chapter 2.4, can a consumer be simplified to a valve, controller and a heat exchanger. The PID controller adjusts a valve opening, by varying the stem position, which further controls how much water flows through the heat exchanger. This ultimately controls the amount of heat transfer the consumer receives.

2.2.1 Heat exchanger model

Since the stem position is the decisive factor of the amount of heat transfer to the consumer, this would preferably be the input from the consumer. Unfortunately it is not possible to measure this position, but only the heat transfer rate between the primary and secondary side. By assuming that the controller changed the stem position instantly, Møller (2018) assumed in his explicit consumer model that the heat transfer changed instantly when the setpoint or ambient temperature changed. However since there were no information regarding the flow or temperature on the secondary side of the heat exchanger, their respective values were set to a constant. This resulted in deviations in both mass flow and return temperature, with for instance return temperatures decreasing when historical data indicated there should have been an increase. A different approach could be conducted by using the conservation of energy as shown in the equation below Cengel and A.Boles 2011:

$$Q = c_p q (T_{supply} - T_{return}) \tag{2.12}$$

In this equation the supply temperature, T_{supply}, at the consumer is given by the heat propagation in the system. The mass flow, q, and return temperature, T_{return}, are unknowns, and requires a second equation in order to be determined. By analyzing the power consumption and mass flow from historical data, a linear correlation was discovered. This correlation could be varying depending on the setup of the heat exchanger and pump on the secondary side, and therefore had to be performed on each consumer. The two required equations to calculate the return temperature and mass flow at each consumers is shown in equation 2.13 and 2.14, where a linear correlation between power consumption and mass flow is assumed. Depending on the measurements from the consumer, a linear correlation between the power consumption and return temperature could also be more suitable.

$$q_i = \frac{dq_i}{dQ_i} Q_i + b \quad i = 1, 2, 3...M(consumers) \tag{2.13}$$

$$T_{return_i} = T_{inn_i} - \frac{Q_i}{c_p q_i} \tag{2.14}$$

A DHS consists typically of several loops and branches, where the mass flow in each pipe segment has to be determined. In each of these loops there will be an equilibrium pressure point either at a consumer that receives water from two pipe segments at once, or there are no movement in the water at one pipe segment. This equilibrium point could move along the loop depending on the change in power consumption, and therefore must several possible points be accounted for. By using the pressure loss expressed in equation 2.1.2, the equilibrium can be found by moving along the pipe from each side, and gradually adding the losses in each pipe segment. At some point the pressure has to be equal, which produces N equilibrium equations depending on how many loops there are in the network. If the loops are connected, the equilibrium equations has to be solved simultaneously in order to maintain the mass continuity principle. By first determining the mass flow in each consumer with equation 2.13, the flow in each pipe segment can then be found by using the pressure equilibrium equations.

In order to solve the equilibrium equations simultaneously, an iterative scheme has to be utilized. The Newton algorithm can be used as a efficient tool to calculate the root of a system of nonlinear equations, by utilizing the first derivative (Nocedal and Wright 2006). Suppose that there are N equilibrium equations (with N variables) that is set equal to zero, and put into a vector $F(x)$. The partial derivatives of these equations can then be expressed as the Jacobian matrix J. In order to start the iteration an initial guess of each variable has to be made, which should not be too far away from the solution. To obtain a sufficient solution that fulfills the equations equalling zero, an iteration is performed k+1 steps where the updated values x_{k+1_N} of each variable is calculated as displayed below (Nocedal and Wright 2006):

$$x_{k+1} = x_k - J^{-1} F(x) \tag{2.15}$$

An advantage of the Newton algorithm is that it converges within relatively few iterations. This is desirable when the runtime of each sample in the simulation has a maximum limit depending on the sampling frequency.

2.2.2 Aggregation of consumers

A DHS is in general a large network consisting of many consumers and pipe sections. In order to make the model more suitable for simulation purposes, aggregation of consumers are necessary. A basic principle of aggregation can be shown in figure 2.3 where two branches shown on the left side, is aggregated into a single serial line on the right.

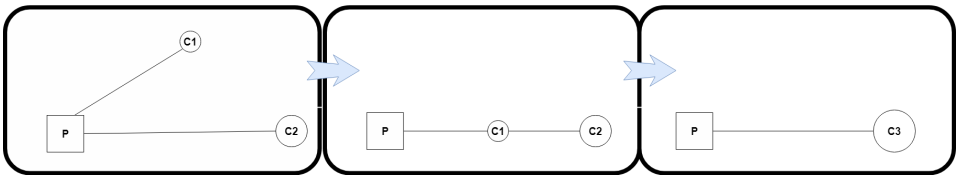

Figure 2.3: Principle of aggregating two branches into a serial line. Developed by using online tool at www.draw.io

In (Larsen, Bøhm, and Wigbels 2004) and (Hägg 2016) two methods for network aggregation in a DHS was presented, the German and the Danish method. The Danish method does not consider the pressure drop when the consumers are aggregated, but does however consider heat loss in the pipes. By using the German method the heat loss is not considered, since it is assumed that the return temperature of each consumer is the same (Larsen, Bøhm, and Wigbels 2004). The German method can handle loops but they have to be transformed into a serial line, while the danish method does not support loops. Straightforwardly these methods are meant to reduce the number of consumers into a straight line, and aggregate consumers that possibly has large distances between them. This is a very effective tool in terms of aggregation, but at the cost of not knowing the geographical area of the aggregated consumer and possibly expressing the consumers inaccurately.

Since the pipe system at Stjørdal contains several loops and relatively precise information about the consumer substation were desirable, a slightly different method have been used. The aggregation was instead performed on consumers in geographically close areas. This means that only consumers that received water from the same ”main” pipeline was aggregated together. In figure 2.3 two consumers, C1 and C2, are receiving water from the same pipe section, P. Assumed that C2 is larger than C1, then C1 can be aggregated onto C2 as displayed. Depending on the size difference between these consumers, C3 will be moved towards the original placement of C2. Ultimately this will result in increased complexity and time spent creating these consumers, but the reward will be accuracy and more possibilities in the network layout.

Chapter 3

Control Theory

In this chapter the general optimization problem will be described, including relevant features and examples for the DHS. In the final subsections the underlying control and NMPC theory is presented.

3.1 Dynamic Optimization

According to (Foss and Heirung 2016), an optimization problem consists of an objective function, e.g. $f(z)$, which is further maximized or minimized with respect to certain decision variables and constraints. The constraints could either be equality, $i \in \mathcal{E}$, or inequality constraints $i \in I$ as shown in the following equation:

$$\begin{aligned} &\underset{z\in\mathbb{R}^n}{\text{minimize}} \quad f(z) \\ &\text{subject to} \quad c_i(z) \geq 0,\ i \in I \quad and \quad c_i(z) = 0,\ i \in \mathcal{E} \end{aligned} \tag{3.1}$$

Equality constraints in the DHS could typically be the nonlinear differential equations, describing the heat propagation through the network. Other equality constraints could also be the maximum amount of mass flow that the pump physically can produce. In industrial processes a typical inequality constraint is used to prevent the optimization-algorithm to move into negative values, for instance a negative mass flow through the pump.

The differential equations of the system, expressed in discrete time, are dependent on the previous state x_k, and the input u_k, as shown in equation 3.2. The initial point is represented as x_o. The system is then solved N discrete time samples into the future, which is called the prediction horizon. According to Svein Olav Hauger, Senior Specialist at Cybernetica, the horizon should be set with sufficiently length, so that the last input has taken completely effect.

$$x_{k+1} = g(x_k, u_k), \quad x(0) = x_o \quad k =, ..., N-1 \tag{3.2}$$

The objective function in equation 3.1 can now be rewritten to include the relevant equality and inequality constraints as shown in equation 3.3 (Foss and Heirung 2016). A constraint is also included on the rate of change of the inputs, by Δu_k. At sample k, the algorithm will use the given inputs to minimize $f(z)$ over the given prediction horizon, while staying within the specified constraints.

$$\underset{z\in\mathbb{R}^n}{\text{minimize}} \quad f(z) = \sum_{k=0}^{N-1} f_k(x_{k+1}, u_k)$$

subject to

$$\begin{aligned} x_{t+k} &= g(x_k, u_k) && k = 0, ..., N-1 \\ x_o, u_1 &= given \\ x^{low} &\leq x_k \leq x^{high} && k = 1, ..., N \\ u^{low} &\leq u_k \leq u^{high} && k = 0, ..., N-1 \\ \Delta u^{low} &\leq \Delta u_k \leq \Delta u^{high} && k = 0, ..., N-1 \end{aligned}$$

$where$

$$\begin{aligned} x &\in \mathbb{R} \\ u &\in \mathbb{R} \\ \Delta u_k &= u_k - u_{k-1} \\ z^T &= (x_1^T, ...x_N^T, u_0^T, ..., u_{N-1}^T) \end{aligned} \tag{3.3}$$

Since one of the equality constraints consists of nonlinear equations, the optimization problem becomes non-convex which could result in several local optimums. The algorithm could then be trapped in such a point, and unable to find the global solution (Foss and Heirung 2016). The design of the objective function is therefore important in order to increase the possibility of finding the global solution. The most common way of representing the objective function of a quadratic programming problem is shown in equation 3.4 (Foss and Heirung 2016).

$$f(z) = \sum_{t=0}^{N-1} \frac{1}{2} x_{k+1}^T Q_{k+1} x_{k+1} + d_{x,k+1} x_{k+1} + \frac{1}{2} u_k^T R_k u_k + d_{u,k} u_k$$

$where$

$$\begin{aligned} Q_k &\geq 0 \\ R_k &\geq 0 \end{aligned} \tag{3.4}$$

The first term in the equation, $\frac{1}{2} x_{k+1}^T Q_{k+1} x_{k+1}$, represents the states and the weighting on each of them. If any of the sates becomes large, the algorithm will focus on decreasing them sufficiently. The matrix Q has diagonal elements, which makes it possible to penalize

each state relative to other states, by increasing or decreasing their respective value. For instance if a large value is put on the first element, the algorithm will focus more on minimizing the first state relative to the others. The same possibilities can be done on the inputs with the term $\frac{1}{2}u_k^T R_k u_k$, where R_k only has elements on the diagonal. Several modifications can be performed on the objective function depending on the optimization problem. In context with a nonlinear system, several modifications have been utilized (Foss and Heirung 2016):

- A state reference trajectory could be suitable if the state are to follow a desired reference, i.e., $x_k \rightarrow (x_k - x_k^{ref})$. Then the algorithm should then try to make the current state equal to the reference, in order to minimize the objective function.
- Instead of using the state directly, a derived variable could be used. This could be the case if a measurement from the system were to be used, and not the state itself. The transform from state feedback to output feedback can then be described as x_k $\rightarrow$z$_k$ = h(x_k). In a DHS this output could be for instance return temperature or mass flow, and will be further described later.
- The input to the system can not be changed infinitely fast since the pump and the burning of woodchips has a delay. Additionally could very fast changes potentially cause wear and tear on the equipment. Therefore are the following term $\frac{1}{2}\Delta u_t^T R_{\Delta t} \Delta u_t$ added in order to penalize such behavior. Δu_t represents the difference between current input and the next, and $R_{\Delta t}$ is the weight matrix.
- A challenge that could arise in nonlinear systems are infeasible solutions, i.e., solutions outside the bounds given by the constraints. A common solution is implementation of slack variables, ϵ_k. This transforms the original constraint to allow some deviation. The modification of the constraint can be expressed as shown in equation 3.5, where the output z has been used. The principle is also displayed in figure 3.1, where the output Z has constraint at Z_{max}. This way the objective function can perform the optimization, and additionally ensure feasibility.

$$\begin{aligned} z^{min} \leq & z_k \leq z^{max} \rightarrow z^{min} - \epsilon_k \leq z_k \leq z^{max} + \epsilon_k \\ 0 \leq & \epsilon_k \leq \epsilon_{k,max} \end{aligned} \tag{3.5}$$

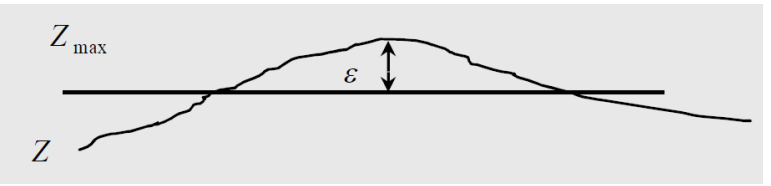

Figure 3.1: Utilization of slack variable in constraints (Dyrset et al. 2017)

The objective function can then finally be assembled by including the described modifications, as displayed in equation 3.6. The soft constraint is implemented in the objective

function as a linear term, $\rho_{k+1}^T \epsilon_{k+1}$, including a significantly smaller weighted quadratic term, $\frac{1}{2}\epsilon_{k+1}^T S_{k+1}\epsilon_{k+1}$, with the diagonal weight matrix S. Usually are either the linear or quadratic terms utilized. The quadratic term is used if several variables are breaking their respective constraint simultaneously, and a trade-off has to be made between how large their slack variable should be. In contrast is the linear term used if an exact penalty is desirable, where the variable with largest weight should be the only deciding slack variable. The latter is the most typical one to use. Moreover are the number of decision variables, n, determined by the number of states, n_x, and number of inputs, n_u.

$$\begin{aligned}\underset{z\in\mathbb{R}^n}{\text{minimize}} \quad f(z) = \sum_{k=0}^{N-1} (&\frac{1}{2}(z_{k+1} - z_{k+1}^{ref})^T Q_{k+1}(z_{k+1} - z_{k+1}^{ref}) \\ &+ d_{z,k+1}^T (z_{k+1} - z_{k+1}^{ref}) + \frac{1}{2} u_k^T R_k u_k + d_{u,k+1}^T u_k \\ &+ \frac{1}{2}\Delta u_k^T R_{\Delta k} \Delta u_k + \rho_{k+1}^T \epsilon_{k+1} + \frac{1}{2}\epsilon_{k+1}^T S_{k+1}\epsilon_{k+1}\end{aligned}$$

$where$

$$\begin{aligned} Q_k &\geq 0 && k = 1, ..., N \\ R_k &\geq 0 && k = 0, ..., N-1 \\ \epsilon_k \in \mathbb{R}^{n_z} &\geq 0 && k = 1, ..., N \\ \rho_k \in \mathbb{R}^{n_z} &\geq 0 && k = 1, ..., N \\ u &\in \mathbb{R}^{n_u} \\ z &\in \mathbb{R}^{n_z} \\ n &= N(n_x + n_u) \end{aligned} \tag{3.6}$$

As a final remark, can the objective function be displayed in a simpler fashion for easier display later in the thesis. The simpler version is described with a matrix formulation, which as shown in equation 3.7.

$$\begin{aligned}\text{Minimize} \quad J = &\frac{1}{2}(Z - Z^{ref})^T Q (Z - Z^{ref}) + \frac{1}{2} U^T R_1 U + \frac{1}{2}\Delta U^T R_2 \Delta U \\ &+ \rho^T \epsilon + \frac{1}{2}\epsilon^T S \epsilon\end{aligned} \tag{3.7}$$

3.2 Nonlinear Model Predictive Control

As mentioned in section 2.2, are PID-controllers implemented at each consumer in order to control the mass flow. In a large DHS there are many such classical controllers at both consumers and at the production plant, in order to ensure correct mass flow or temperature. These controllers are part of the lower level in the control hierarchy shown in figure 3.2. In the hierarchy the two lowest levels consist of measurement equipment and the process itself, which provides realtime data to the control system. Above are the PID-controllers which aims to make the flow or temperature reach a given setpoint. At this level the sampling frequencies are high, with new inputs frequently being given to the specific equipment, e.g., a pump.

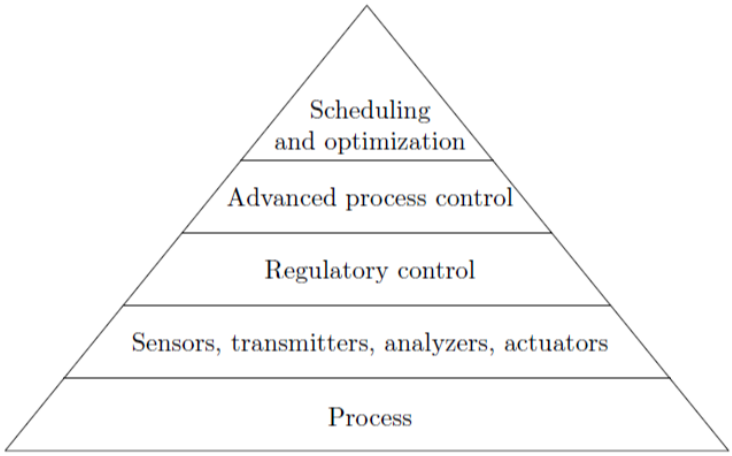

Figure 3.2: Illustration of the control hierarchy, where the two top layers are proposed merged together. (Foss and Heirung 2016)

At the Advanced process control level, the overall controller for the whole process lies. The Model Predictive controller (MPC) is a common tool to calculate the optimal setpoints of all the lower-level controllers simultaneously, in order to optimize the complete process. By developing a plant replacement model, the model can be simulated a number of time steps into the future and predict how the process will behave. Combined with frequent measurement updates from the process, an estimator can be utilized in order to find a optimal input sequence at each time step.

The highest level in the control hierarchy includes the optimization and scheduling application. At this level the desired production plans could be implemented, which are usually based on optimizing the process in terms of revenue, waste, robustness or customer satisfaction. These criteria are often referred to as economic objectives. The economic objectives would traditionally be developed based on manual analysis of the process, or as an output from a separate economic optimization application. The application would be run

less frequently, and to steady state, as performed in (Svenheim Rene 2016) and (Hamre 2017). The output are then implemented as setpoints to the MPC. However in order to reach the desired economic objectives Willersrud et al. (2013) suggests merging the two top layers into one, described as Dynamic Real-Time Optimization (DRTO). It is further suggested to divide the controlled variables, z, into two categories:

- Variables that should track a reference and/or stay within bounds, denoted z_{track}.
- Variables to be optimized, denoted z_{opt}. This would be for instance cost, revenue, etc.

This way the process control and economic process optimization are more integrated. The single layer control hierarchy will also be able to react better to disturbances. Additionally can weighting of the economic objectives be performed in reference to the regulatory ones.

The optimization problem described in equation 3.3 is according to Foss and Heirung (2016) an open loop optimization problem. This means that it is only calculating the optimal solution once, and the solution is used throughout the prediction horizon. This would possibly be sufficient if the process model had no modelling errors, and there were no unforeseen disturbances occurring in the process. However when developing a process model with a physical approach, there will always be errors and disturbances. A better solution would therefore be to use measurements from the system, and regularly calculate new sets of inputs. This method is called closed loop optimization and is one of the core aspects of the MPC. In this thesis the system to be optimized is nonlinear, and therefore are the algorithm referred to as Nonlinear MPC (NMPC).

There are usually two types of feedback that can be implemented with a NMPC. With state feedback the states are measurable from the process, and can be used directly. However this is seldom a possibility in a real plant, and is neither the case in the DHS at Stjørdal. Instead are there usually some measurable outputs from the process, e.g., the returning temperature at the plant, which can be used. This is called output feedback, where the output is used to estimate the states by using an estimator. The measurements are often affected by noise which has to be taken into consideration as well. To overcome the challenges of noise, disturbances and modelling errors, the output from the process is compared with the output from the plant replacement model. The result is then fed into the estimator, which ultimately produces an accurate estimate of the states and parameters from the process.

The two most common estimators used in nonlinear systems are Extended Kalman filter (EKF), and Moving horizon estimators (MHE). The EKF can handle nonlinear systems quite efficiently, and at relatively low computational cost. By using measurements observed over time, and statistical analysis, gain factors can be multiplied to the estimated states in order to drive them to its true value. The MHE estimates the states by solving an optimization problem with a moving, fixed-size window of measurements. The problem is formulated as a quadratic programming problem with a time interval $k \in [0, N]$ where N is the horizon length.

In figure 3.3, courtesy of Cybernetica AS, the setup of a MPC with output feedback is demonstrated with the real process connected. However in this thesis the model will instead be used together with historical inputs that has been applied to the plant, and then the historical outputs will be compared with the output of the model. The figure is therefore meant to illustrate how the process model can be combined with an estimator and controller. It shows the controller and how it applies the manipulated variables (MV), u, to both the real plant and the model. Additionally are the disturbance variables (DV), v, shown as an measurable input to both the process and the model. Measurements are then taken from the process, y, and the model, $\bar{y}$. The deviation between them are further fed into the estimator in order estimate the states and parameters. The estimator then feeds these values back into the model. The controlled variables (CV), often expressed as z or x, can then be derived from these updated states. The CV can then be used by the controller to produce a new set of inputs, which ultimately creates a closed control loop.

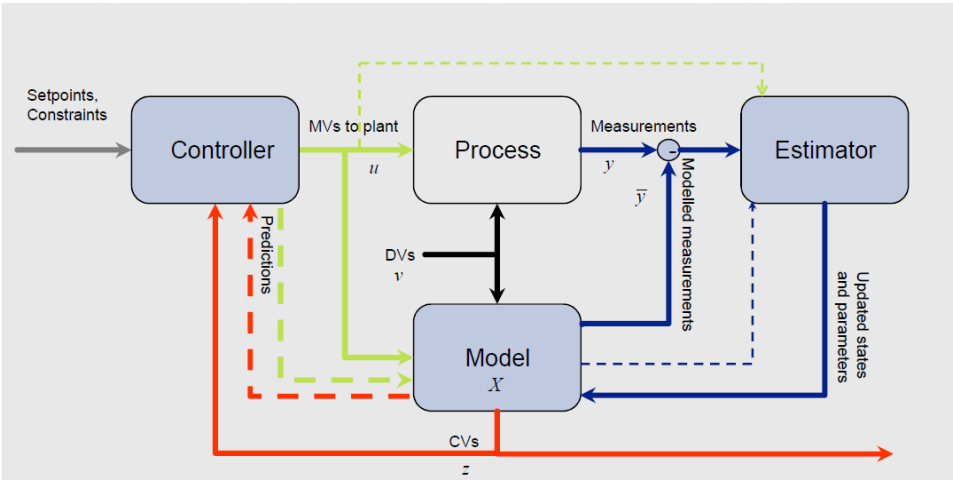

Figure 3.3: NMPC with output feedback (Dyrset et al. 2017)

The loop shown in figure 3.3 can be further described at current time sample t', as displayed in figure 3.4. The figure shows how the plant can be controlled by using the CV and MV respectively, x_k and u_k, and how they vary in time. At the bottom graph the past MVs that has been applied, and the CVs that has been measured from the plant is shown. At current time, t', the controller performs the MPC procedure which can be observed in the upper graph. The solution to the open loop optimization problem at $t = t'$ produces the following set of MVs, presented as the red line in the graph, $t' + N - 1$ time samples ahead. A predicted trajectory of the CV is then calculated, and can be seen as the blue dots in the graph, which is simulated $t' + N$ steps ahead. However, only the first control move is fed into the controller and a new solution is calculated at the next time step. The MV and CV will therefore possibly change at each time step so that the plant always has an updated trajectory. The length of the predicted horizon is usually a constant N, and is called a receding horizon.

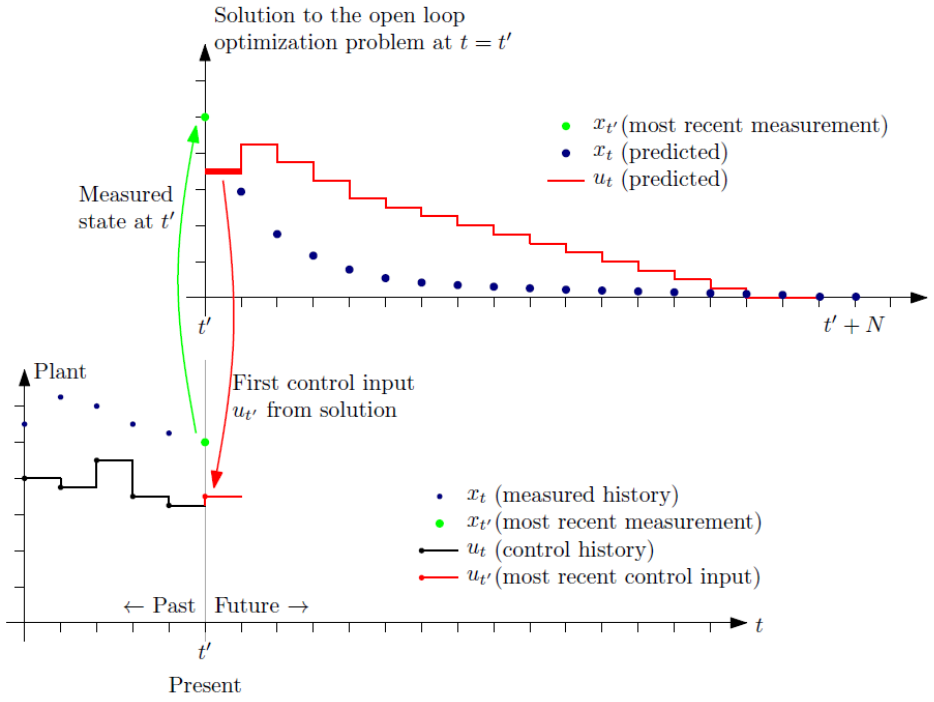

0

Figure 3.4: Illustration of the NMPC procedure including predictions and historical values (Foss and Heirung 2016)

As seen in figure 3.4 the NMPC solves the optimization problem using the current state as initial state $x_o = x_{t'}$, which further gives an optimal input $u_{t'}$ at each time step. From Foss and Heirung (2016) the pseudo algorithm for the state feedback MPC procedure is stated below:

for k = 0, 1, 2... do
Compute an estimate of the current state $x_{t'}$ based on the measured data up until time t'.
Solve a dynamic optimization problem on the prediction horizon from t' to $t' + N$ with $x_{t'}$ as the initial condition.
Apply the first control move $u_{t'}$ from the solution above.
end for

When calculating the trajectory, the input vector will have the size of $N * n_u$, i.e., one variable for each time sample for each MV. It is however desirable to reduce the number of decision variables if possible, since the optimization problem can easily become very

computational demanding to solve. By setting the input constant for a certain number of samples into the horizon, the runtime can be significantly reduced and could therefore be an important contribution to secure a robust NMPC application. This method is called input blocking, where the horizon consists of several ”blocks” of constant inputs (Foss and Heirung 2016). The method can be illustrated in figure 3.5, which is a similar graph to the one presented in figure 3.4. It shows an example of predicted and historical MVs and CVs. Looking at the MV history to the left, the time between each change of the input can be observed (changed every time step). However in the MV prediction, the input is observed to be constant in each block.

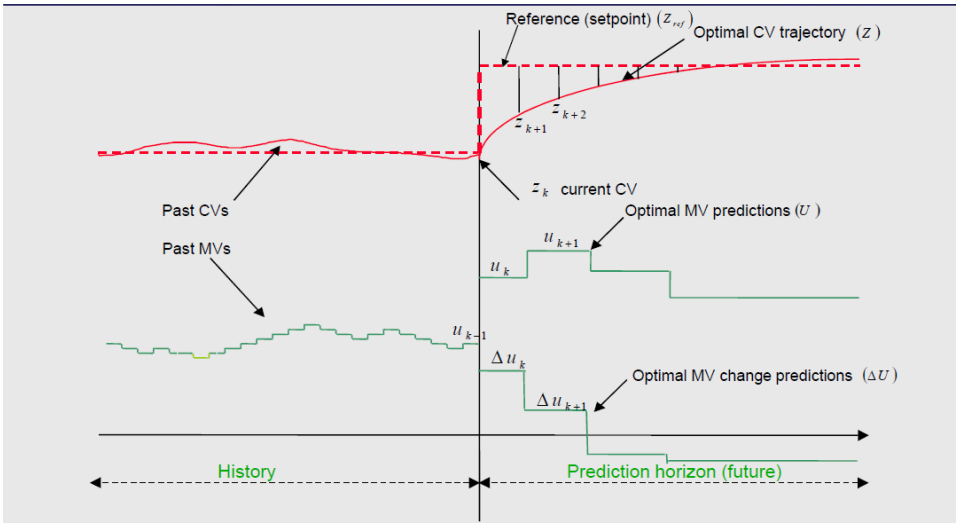

Figure 3.5: Illustration of the NMPC procedure with input blocking, delta input blocking and evaluation points (Dyrset et al. 2017)

The number of required blocks are dependent of how quickly the input has to change, and has to be tuned according to the dynamics in the system and desired behavior of the controller. In addition can the number of input blocks be specified independently for each MV if necessary, and may even vary in time. This could be useful if for instance the characteristics of the system changes during the simulation. Additionally can the optimal change on the input, Δu_k, be predicted, and put into blocks as shown in figure 3.5.

Similarly as input blocking reduces the number of decision variables in the input, a reduction of evaluation points of the CV can have the same effect. The evaluation points represents the specific future time sample where the MPC is evaluating the optimization criterion (Dyrset et al. 2017). These points are initially evaluated at each sample in the horizon. However depending on what is being measured, the number of points can be reduced to for instance every other point in the horizon. The reduction of evaluated points between the current time sample and the end of the predicted horizon, is illustrated in figure 3.5. It can be observed that the CV, Z_k, is only evaluated at Z_{k+1}, Z_{k+2} etc, which less frequent than the sampling time. How many points needed is dependent on the sys-

tem and the desired behavior of the controller. The amount of variables can also be set independently to each other, and varying with time if needed. This could be an important feature if there are variables in the system that does not require evaluation at each sample.

In a large nonlinear system, such as a DHS, both input blocking and specified CV evaluation points could be important tools in order to keep the solving time per sample sufficient. It is important to emphasize that the solving time per sample has to be less than the time between each sample, or else the controller will not be able to simulate the predictions fast enough to be used in an online application. Therefore are the tuning process of these tools important in order to have a effective, but at the same time robust controller.

In this thesis, the regulatory and economic objectives are to be implemented into the common objective function described in equation 3.7. Since the economic objective is typically to minimize a variable as much as possible but not necessarily knowing how much, a reference value can be hard to define. Willersrud et al. (2013) suggested two methods in order to achieve economic optimum. The first one sets an unrealistic high or low setpoint on the optimized controlled variable. In addition are the regulatory objectives that are implemented with setpoints to track, included as z_{trac}. These two objectives are then included in the objective function as shown in equation 3.8. For clarification are the elements in the weight matrices Q_{track} and Q_{opt}, on diagonal form and assumed constant in time. It is however worth noting that this method, according to Willersrud et al. (2013), could affect the solution because the term is included in the gradient of the objective function. This could further cause difficulties when tuning and unexpected behavior, if not taken into consideration. The method is illustrated in figure 3.6 were the output, Z, is to be minimized. By implementing a unreachable lower setpoint, Z_{ref}, the output is minimized as much as possible.

$$\begin{aligned} \underset{z\in\mathbb{R}^n}{\text{minimize}} \quad f(z) = \sum_{i=1}^{N} &((z_{track,k+i} - z_{trac}^{ref})^T Q_{trac}(z_{track,k+i} - z_{trac}^{ref}) \\ &+((z_{opt,k+i} - z_{opt}^{ref})^T Q_{opt}(z_{opt,k+i} - z_{opt}^{ref}) \end{aligned} \tag{3.8}$$

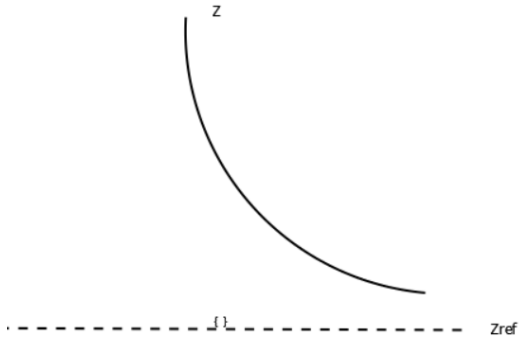

Figure 3.6: Illustration of the unreachable setpoint. Created with the software Dia

The second approach uses infeasible soft-constraints and exact penalty function for production optimization. By selecting a lower constraint, $z_{opt,min}$, and a upper constraint, $z_{opt,max}$, in a desired direction and to a value that can not occur, the variable z_{opt} will be optimized. In other words will z_{opt} always be infeasible with respect to this constraint, but with the inclusion of slack variables in the objective function a feasible solution can be found. In a minimization problem these constraints and slack variable will have the following form:

$$
\begin{aligned}
&z_{opt,min} \leq z_{opt,max} \leq z_{opt,k+i} \\
&r_{opt}^{T} \epsilon_{opt,k+i} = r_{opt}^{T}(z_{opt,k+i} - z_{opt,max}) \\
&\epsilon_{opt,k+i} = z_{opt,k+i} - z_{opt,max} \geq 0
\end{aligned}
$$

By using this method the breaking of constraint, in contrast to the first method with deviation from setpoint, is penalized. The result is a linear cost term, opposed to the quadratic cost in the first method. The cost terms can then be developed as shown in equation 3.9. The method is further illustrated in figure 3.7 with the output , Z, an upper and lower constraint, Z_{max} and Z_{min}, and the slack variable. In this situation the output is minimized towards the unreachable Z_{max}, while the slack variable represents the deviation from the constraint.

$$
\underset{z \in \mathbb{R}^n}{\text{minimize}} f(z) = \sum_{i=1}^{N} \quad (r_{trac}^{T} \epsilon_{trac,k+i} + r_{opt}^{T} \epsilon_{opt,k+i}) \tag{3.9}
$$

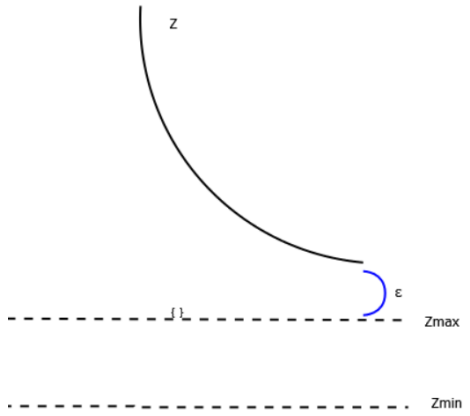

Figure 3.7: Illustration of the infeasible soft constraint. Created with the software Dia.

3.2.1 Solving Nonlinear Optimization Problems

In order to solve the optimization problem, a relatively complex solver is required due to the nonlinear constraints making it non-convex. The Sequential Quadratic Programming (SQP) shows good strength when solving these types of optimization problems. In SQP the problem is reformulated as a sequence of smaller quadratic problems, which ultimately are approximations to the nonlinear objective function. The problem will then be solved iteratively with the number of steps equal number of subproblems to be solved. (Nocedal and Wright 2006)

The principle can be illustrated in figure 3.8. To the left a nonlinear function to be minimized is shown. The algorithm will first do a quadratic approximation of the function around the current point, and then find the minimum of this smaller quadratic problem. It then finds the function value closest to this minimum, accompanied by a line search, and use it as the new current point for the next subproblem. To the right the effect of using several quadratic problems are illustrated. The quadratic sub program can be shown in equation 3.10, where f(x) is an approximation of the highly nonlinear objective function at iterate x_k. $\mathscr{L}$ is the Lagrangian function, and p is the step direction of the next iterate found by an iterative scheme, e.g., Newtons method described in chapter 2.2.

$$f(x) \approx f(x_k) + \nabla f(x_k)^T p + \frac{1}{2} p^T \nabla^2_{xx} \mathscr{L}(x_k, \lambda_k) p \tag{3.10}$$

As shown in figure 3.10, there could be a local minimum that are closest to the current point, and the SQP could therefore get stuck. Even though the global minimum could be found depending on the starting point, the method is usually extended in order to ensure that the optimum is global. However such methods will not be explained in any detail in this thesis.

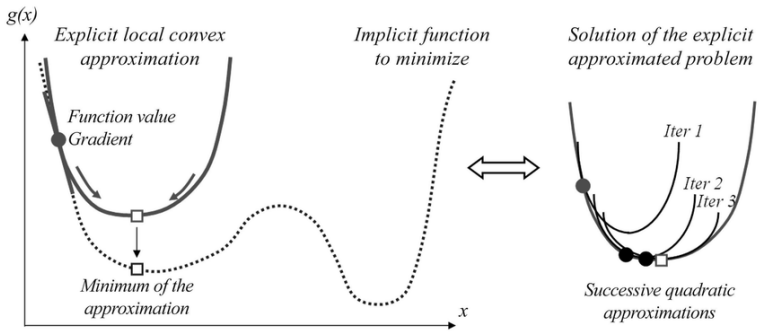

Figure 3.8: Illustration of the SQP algorithm (Bruyneel 2019)

Chapter 4

Software Tools

In several of the previous works described in chapter 1.3, a Modelica-based programming language was utilized to model the pipe system. Compared to other languages Modelica has certain advantages when it comes to creating process models. For instance are the equations not treated as assignments but as expressions, and there are several built in operators that easily can be used. (Hägg 2016) used in his thesis a built in operator in order to keep track of the spatial distribution of heat. Depending on the type of model being developed, Modelica could therefore be a very efficient tool to use.

In Cybernetica the standard programming language is C, which also has been used in this thesis. It requires a more manual setup by the user, but the reward is a more flexible software where everything is built from scratch. Cybernetica has also developed their own general template that all models can be created in. This template acts as a framework that the user can utilize to develop their own model, including several mathematical libraries. Additionally there are several integration schemes that can be used, however the standard Explicit Euler has been chosen in this thesis. In addition has Cybernetica developed their own software to simulate the model, estimate parameters and initial conditions, and last but not least develop and tune the NMPC. These software packages has been utilized to develop the process model of the DHS at Stjørdal, and tune the controller.

In order to use the model as a plant replacement for optimization and control, it is essential to simulate and validate the quality of it. More specifically are the modelling errors, disturbances and possibly left out information, observed by comparing the model with historical measurements. Modelfit has been developed by Cybernetica AS to perform these types of simulations and to do parameter estimation (Dyrset et al. 2017). Although no controllers or online estimation is included in Modelfit, offline parameter and initial state estimation is possible. By including large datasets with input for each time sample of the simulation horizon, the model can be simulated by using a built-in estimator. In addition can measurements from the process be added and compared with the output of the model. By using the SQP algorithm explained in chapter 3.2.1, the deviation between model and historical measurements can be minimized. Modelfit finds the optimal parameters and initial states

that minimizes this deviation. The objective function value is then plotted at each step of the algorithm, to show how the parameter adjustments are reducing the deviations between the model and measurements. This way the model can easily be validated, and tuned to better fit the real process.

When the model has been validated and the optimized parameters has been found, the controller can be implemented and tested. The two software packages Cenit (version 6.9) and RealSim provides these possibilities. Cenit is a powerful software suite for nonlinear model predictive control, and is divided into a user interface (MMI) and the kernel (Dyrset et al. 2017). The interface displays the MVs, CVs and estimates, with both historical and prediction values. In addition can the user implement desired regulatory and economic objectives of the optimization algorithm, in the form of setpoints or soft constraints. The kernel handles the NMPC and estimator (Extended Kalman Filter or Moving horizon). The third software in this package is RealSim. It functions as a simulation tool and test-bench for the NMPC application. By communication through an OPC server, the process and Cenit can send updated MVs and CVs between them, as required in the control loop displayed in figure 3.3. It is important to mention that the simulator may use a different model than the model implemented in the controller, but in this thesis they will be the same.

Moreover has Matlab been utilized separately if the previously mentioned software were not sufficient. Matlab encompasses a large numerical computing environment, and has been used to perform numerical and symbolic calculations that further was implemented into the model. This complete package of software can be linked together as shown in figure 4.1. It displays an overview of Cybernetica's products (and Matlab), and what purpose they have when developing a process model.

A final software that has been used for database purposes was MYSQL. Cenit has been developed to easily communicate with an external database as for instance MYSQL. After implementing the database, Cenit was able to send MVs, CVs and other variables of interest at each time sample directly to it. By using external scripts the data was then outputted from the database, that could be used for plotting in Matlab.

In figure 4.2 the workflow of developing a process model and a optimization application is shown. From the start the process knowledge is used to developed a model in a preferred programming language. By utilizing the described tools that Cybernetica has developed, the process model can be simulated and compared with logged measurements and further refined by parameter estimation. By using Cenit and Realsim, a NMPC application can then be implemented and tuned in order to reach an regulatory and/or economic objective.

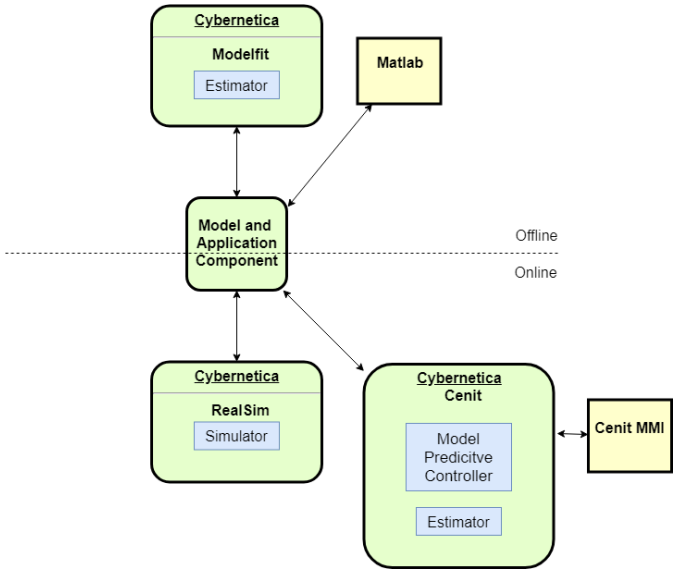

Figure 4.1: Overview of the software packages used in this thesis. (Dyrset et al. 2017)

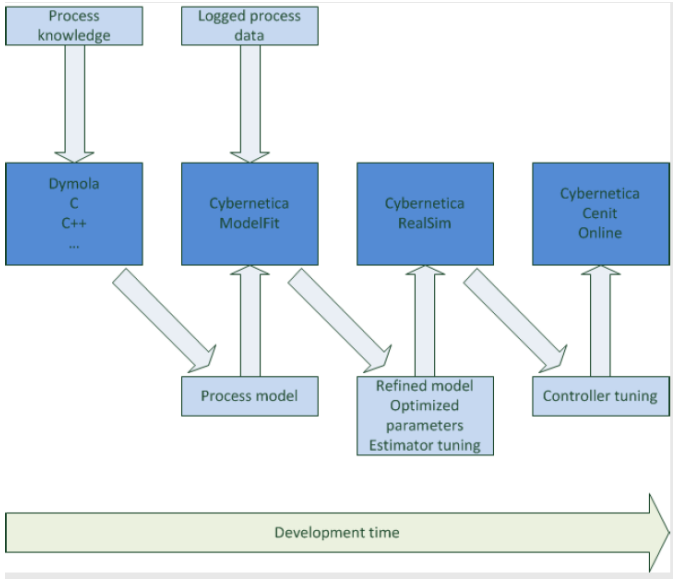

Figure 4.2: Workflow of the different software packages when developing a process model and controller. (Dyrset et al. 2017)

Chapter 5

Modelling and Validation

The modelling of the process was performed by using the software tools and template described in chapter 4. Due to the complexity of the Stjørdal network it was necessary to validate the model to ensure correct responses. The model was therefore simulated in Modelfit with a sampling time of 10 minutes, by using historical data from the first week of February 2019. The power consumption for each consumer can be found in appendix B.4 - B.9. Certain assumptions regarding the model have also been made:

- The absolute roughness in the pipes was set to 0.05mm as advised from Åmund Utne, Senior Advisor at Statkraft.
- The length of the pipes on the primary side of the consumer substation, has been assumed to be 50 meters.
- The inlet temperature in the secondary side of the consumer heat exchanger, is assumed to be at least 295 K.
- Historical data of the power consumption and mass flow, has been used to calculate mass flow through each consumer. Since the provided measurements from Statkraft only shows the actual delivered power, it is possible that the consumer in reality requested more power. During modelling and validation it has however been assumed that the measured power consumption of a consumer was also equal the requested power consumption at all times.

5.1 Modelling the Stjørdal network

The Stjørdal network is a complex network including two nested loops and several branches as shown in figure 5.1. The blue lines indicates the main supply lines in the network, the red dots being junctions, and the green large dot is the production plant. The network consist in total about 70 consumer substations varying from small apartment blocks to large schools or industrial buildings. In order to keep the consumption of single consumers anonymous and since not all consumers needed aggregation, each consumer is not shown geographically on the map. Instead are three consumers shown in figure 5.2 as an example of how the aggregation was performed. The shown distances does not reflect the exact distances in the network, but are meant to illustrate a method. The real distances were acquired from a map-database provided by Statkraft, that displayed the geographical placement of each consumer, including all pipe sections with the corresponding diameters. The consumers were aggregated together by using the geographical distance between them and their respective power consumption. For illustration purposes one could assume the following power consumption shown in table 5.1.

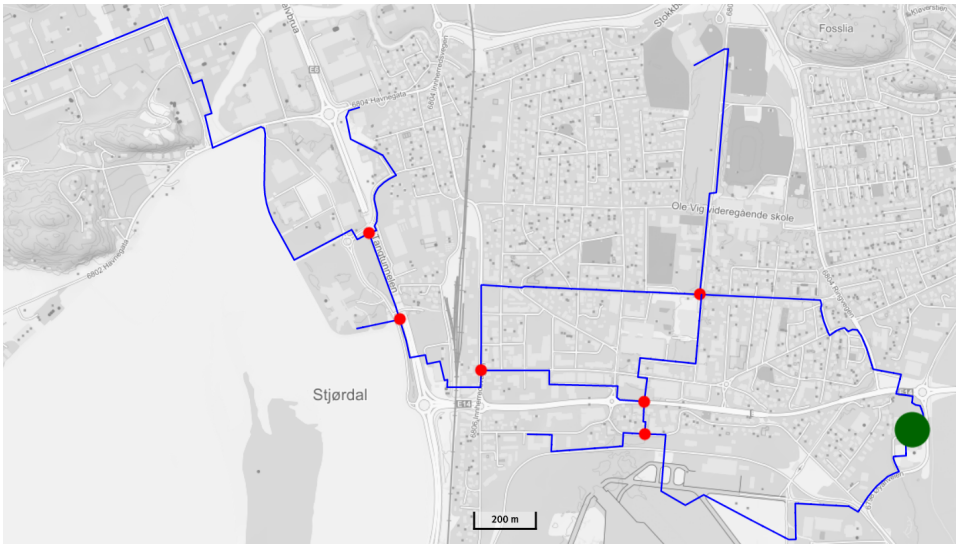

Figure 5.1: Map of Stjordal network where the green dot is the production plant and the red dots are junctions. The map was developed by using norgeskart.no

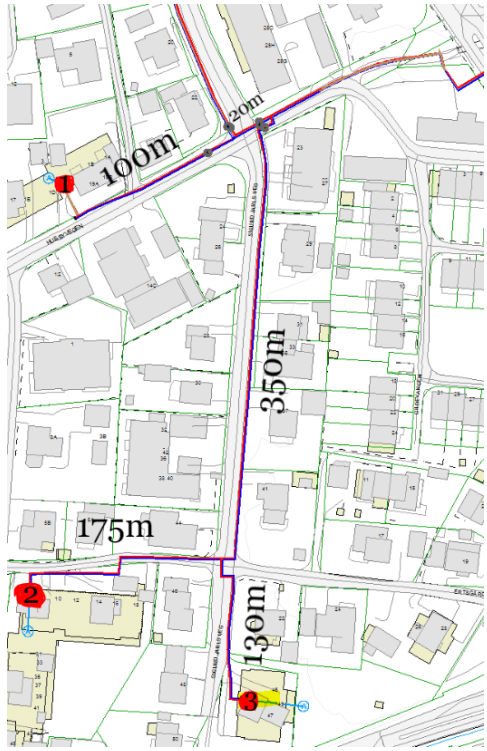

Figure 5.2: Cutout from a map-database provided by Statkraft, showing three single consumers that are being aggregated into one.

Consumer	Size
1	5kW
2	10kW
3	5kW

Table 5.1: Fictitious power consumption of three consumers shown in figure 5.2.

Since the second consumer is twice the size of the first and third, it is weighted twice as much when placing of the aggregated consumer is performed. In this example the first consumer is 120m from the junction, the second is 525m away and the third is 480m from the junction. The placement of the new aggregated consumer then becomes $120m * \frac{1}{4} + 480m * \frac{1}{4} + 525m * \frac{1}{2} = 412.5m$. The result is therefore a new consumer that is 412.5m from the junction, and has the power consumption of all three consumers combined. The same approach was utilized in the whole network, where the average power consumption at each consumer was used. However certain exceptions had to be made:

- Only consumers receiving water from the same ”main” pipeline were aggregated together.

- If the distance between any of the consumers became too large, they were split into two consumers. However a few exceptions were made; In figure 5.1 there is a large pipe branch to the left in the picture. All the consumers along this branch receives water from the same ”main” pipeline, but some had relatively large distances between them. In order to keep the number of consumers within manageable amounts, several of them were aggregated together. In order to define the consumer that were furthest away from the plant, two consumers furthest out to the upper left in the map were separated out.

In figure 5.3 the block diagram of the aggregated consumers are shown, where the same two nested loops can be observed. The supply line is displayed as red, and the return line as blue. Although not displayed in the figure, is it assumed that the return line has the same layout as the supply line. Moreover is information given in each pipe section. The first part indicates mass flow number, qi, $i = 1, ...19$, and mass flow to each consumer, qj $j = a, ...p$. The second number shows the code of the diameter of the pipe, which has to be seen in context with the table in appendix A.1. The third and final number indicates the length of the pipe section, expressed in meters. The power consumption of each consumer is displayed as Q_i, $i = a, ...p$. Three pressure points are also displayed in the network, more specifically P4, P7 and P14. These will be used later in this thesis.

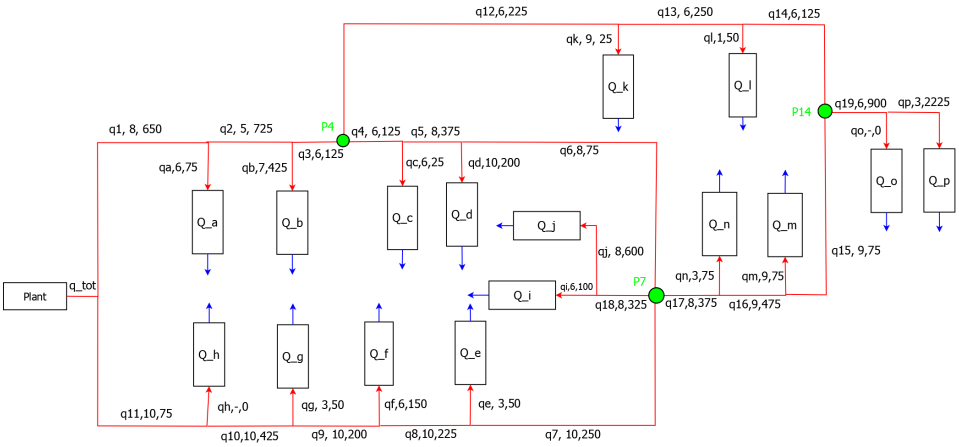

Figure 5.3: Blockdiagram of the consumers in the Stjørdal network.

5.1.1 Heat propagation in the distribution network

The heat propagation through the DHS at Stjørdal was modelled based on the relevant theory in chapter 3. By using a series of control volumes added one after another, the whole network shown in figure 5.3 were developed. It is however not easy to know how large the control volume should be, since it is highly dependent on the system. Not much time was spent researching on this, but ultimately it will be a trade-off between accuracy and computational speed. A total length of 25 meters was used based on Cybernetica’s experience from other industries with large pipe systems. By utilizing the Euler integration

scheme on equation 2.4, the temperature at each time step and in each control volume could be calculated. The thermal transmittance was further calculated in each combination of pipe diameter and insulation thickness. Finally by including the return temperature from each consumer, the same amount of control volumes were used to describe the return lines back to the plant.

5.1.2 Temperature and mass flow in consumer substation

In order to determine the mass flow and return temperature at each consumer, both equations in 2.13 and 2.14 are utilized. They require historical data that correlates the power consumption, with either the mass flow or temperature difference at the heat exchanger. The power consumption will typically vary through the day, depending on what type of consumer it is (e.g., residential or office building). A long enough time span of measurements is therefore important in order to have a function that could handle both low and high load requests from the consumer. The historical data from the first week of February 2019 has been used in this thesis. This week was chosen due to large variations in the ambient air temperature. The temperature was measured to vary between -18.5 and 4.8°C during this time period (Yr.no 2019), and the temperature each day can be closer inspected in appendix A.2. The chosen time span is therefore well suited in order to include the consumption during varying temperatures.

Instead of including the graphs of the correlation between the power consumption, mass flow and return temperature of each consumer, have a few distinct ones been included instead. On an overall basis, the correlation between the power consumption and mass flow of each consumer was found to have a relatively good fit during this period. In appendix C.1 the resulting linear equations describing the mass flow at each consumer, is displayed. In table 5.2 the coefficient of determination, R^2, is shown for each consumer. The coefficient describes how well the two variables fits a linear relationship, where 1 indicates a perfect fit while 0 indicates no correlation. The lowest correlation was found at consumer A with a coefficient of 0.798, and the best was found at consumer L with a coefficient of 0.977. A second order and logarithmic correlation was also tested on some of the consumers with lower coefficients, but it did not increase in any significant way and therefore was the linear relation kept. The return temperature was observed not to correlate particularly well with the consumption, due to a distinct larger spread on the datapoints. Especially consumer A, D, F, I and K, appeard to have close to no correlation, and consumer B, G, H, J and L had, if not linear, some correlation. Additionally was a distinct offset on the mass flow observed at consumer E at the end of the measurements, which can be shown in appendix B.2. This could be due to changes performed on the heat exchanger, more exchangers were included, or simply a change in settings at the secondary side.

Consumer	Coefficient of Determination
A	0.798
B	0.973
C	0.965
D	0.878
E	0.963
F	0.857
G	0.827
H	0.954
I	0.974
J	0.974
K	0.908
L	0.977
M	0.904
N	0.935
O	0.972
P	0.907

Table 5.2: The coefficients of determination found when plotting the mass flow against the power consumption of all consumers

Consumer A and B have been observed in more detail, since they are able to display the disparities in the consumers. In table 5.2 they represent a consumer with good correlation, and one with a not so good correlation. This way both ends of the coefficient scale is presented. In figure 5.4 the mass flow is plotted against the power consumption of consumer A . In the graph it can be observed a spread of the datapoints, causing a significant variation of mass flow to produce the same amount power. It can also be observed a minimum mass flow limit at 4 kg/s. In this area the power consumption still changes, although the flow is kept constant. The correlation between the delta temperature and power consumption of consumer A is shown in figure 5.5. It can be observed an even larger spread on the datapoints, and the coefficient from the regression analysis is to low to be used.

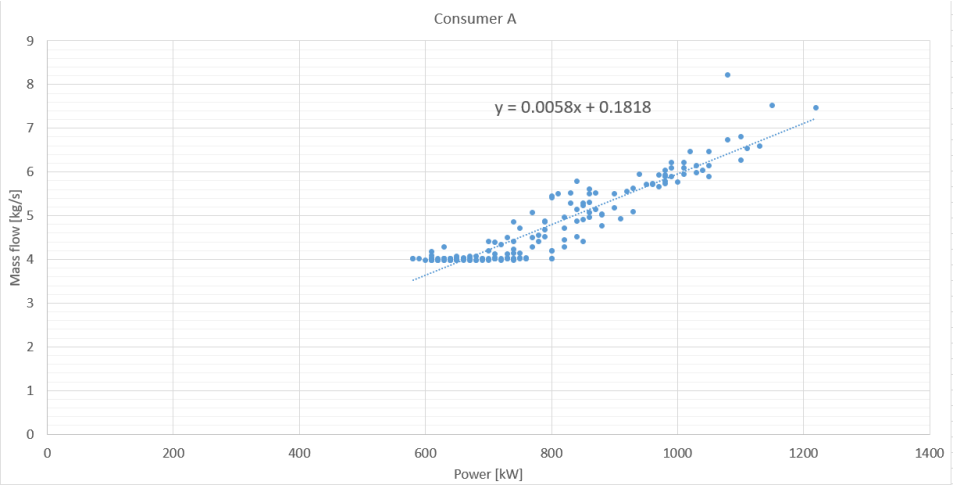

Figure 5.4: Power vs Mass flow of consumer A.

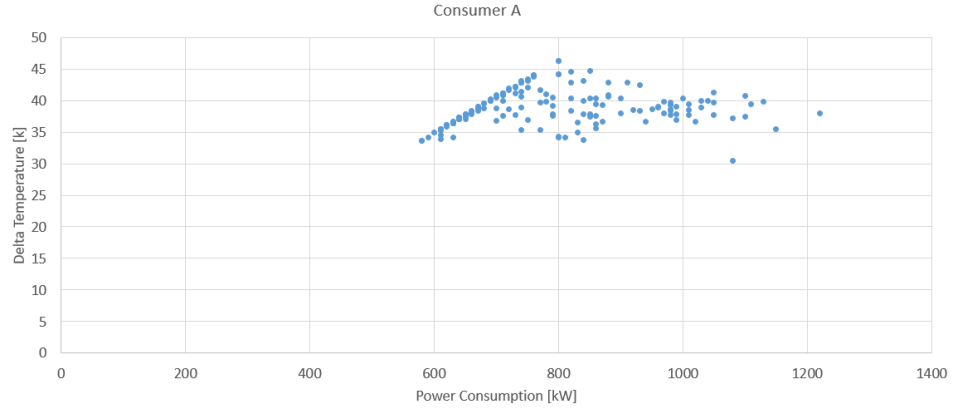

Figure 5.5: Power vs return temperature of consumer A.

In figure 5.6 the measured power consumption is plotted against the mass flow of consumer B. A linear correlation is observed to fit very well. In contrast to consumer A the mass flow is able to approach zero, which indicates there are no minimum limit at this consumer. In figure 5.7 the delta temperature is plotted against the power consumption of consumer B. In contrast to consumer A, there are less spread on the datapoints and perhaps a logarithmic function would fit sufficiently.

Based on the observations, there is reason to believe that the consumers could have personal setups in their substation regarding both components and control. According Åmund Utne, Senior Advisor at Statkraft (Meeting at Statkraft 30.01.19), the pump on the secondary side has different modes (e.g., constant flow, delta pressure driven flow, outlet temperature driven flow). This indicates that the flow and inlet temperature on the secondary side can not be set to constant values as done in Møller (2018).

By using this approach of calculating the mass flow, it can potentially become an infinite large or small positive number based on the input power consumption. In order to restrain the calculated mass flow, a upper and lower constraint in the model has been implemented.

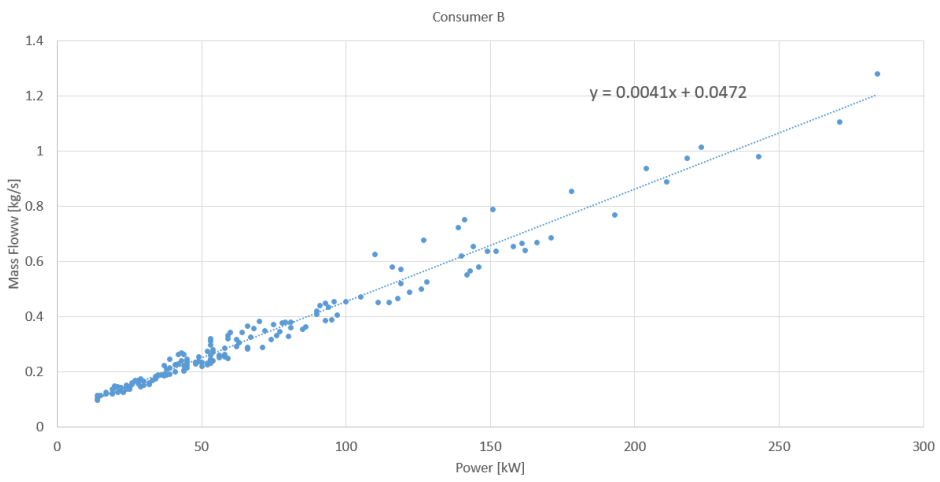

Figure 5.6: Mass flow vs power consumption consumer B

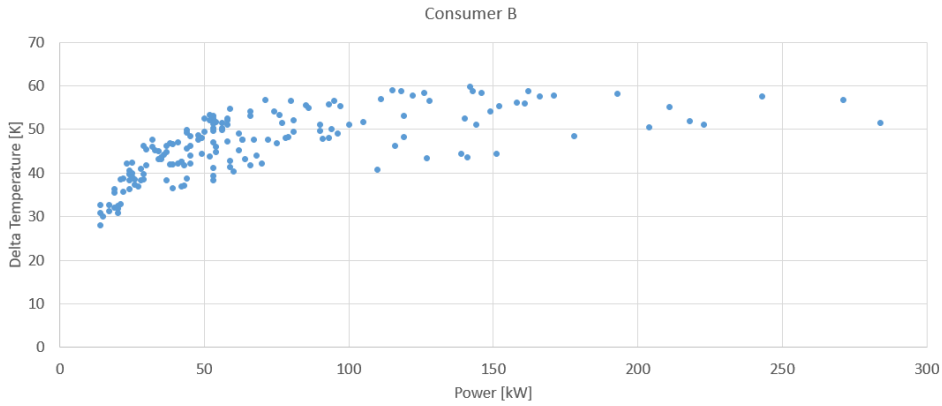

Figure 5.7: Return temperature vs power consumer B

Moreover can the return temperature be calculated as shown in equation 2.14, by using the energy balance. Based on the equation, can the temperature potentially become unphysical if the mass flow becomes too large. Although a constraint has been implemented on the mass flow, it could have a higher upper bound than the minimum possible return temperature. It was assumed a minimum inlet temperature on the secondary side of the heat exchanger of 295 K. This assumption was implemented as the lower bound of the outlet temperature on the primary side, since the outlet temperature on the warm side of a heat exchanger can not be lower than the inlet temperature on the cold side. The return temperature will then be restrained from going below 22 °C. In addition was a softmax function implemented on the return temperature. Simply speaking is the algorithm in a MPC calculating a prediction horizon by testing the sensitivity in the model. If the variable experiences a ”kink” at any point, for instance with a hard ”IF” statement at the minimum return temperature, the MPC could struggle to perform predictions. The softmax function simply takes two values, one higher than the other, and together with a scale it removes the kink by smoothing it. The function is displayed in equation 5.1, where T_r is the smoothed return temperature, s is the scale, T is the original return temperature, and T_{min} is the lower bound set at 295 K. An illustration of the softmax is shown in figure 5.8, where the blue line is the original function, and the green is after the softmax function is used.

$$T_r = s(T + log(1.0 + e^{(T_{min} - T)})) \tag{5.1}$$

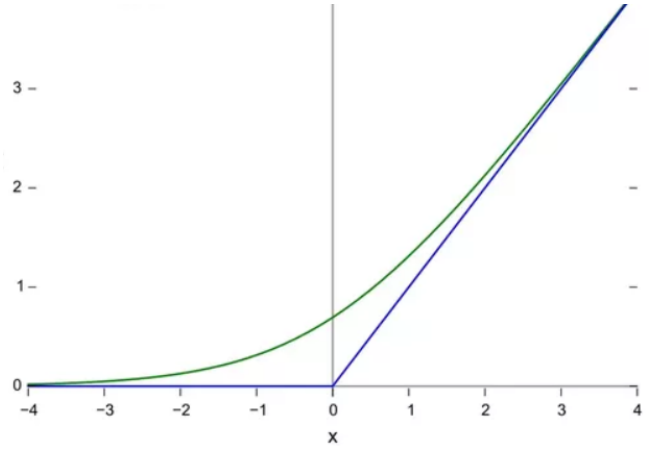

Figure 5.8: Illustration of the softmax function (Patnia 2018)

5.1.3 Pressure propagation and mass flow in the distribution network

The Stjørdal network consists of two loops and three larger branches as shown in figure 5.1. In order to calculate how much water flows in each pipe section of the DHS, the equilibrium point in each loop has to be determined by using the flow-pressure equation as described in chapter 3.2.1. As an example one could assume that P4 and P14 in figure 5.3 is an equilibrium point. In the first loop the pressure moving along the line from each side has to be equal at P4, which ultimately produces equation 5.2 with mass flow q_i, supply pressure P_S and loss constant K_i where $i = 1, 2, 3...11$. The mass flow in each pipe section are unknown, and has to be expressed by the consumer mass flows found by the linear correlation with the power consumption. Since the system contains two loops, there will be two equilibrium equations and two unknown mass flows that has to be iterated on. The resulting equations can be shown in 5.3 and 5.4.

$$\begin{aligned} P_s - K_1 q_1^2 - K_2 q_2^2 - K_3 q_3^2 = P_s - K_{11} q_{11}^2 - K_{10} q_{10}^2 - K_9 q_9^2 - \\ K_8 q_8^2 - K_7 q_7^2 - K_6 q_6^2 - K_5 q_5^2 - K_4 q_4^2 \end{aligned} \tag{5.2}$$

$$\begin{aligned} q_{tot} &= q_a + q_b + q_c + ...q_p \\ q_1 &= unknown \\ q_2 &= (q_1 - q_a) \\ q_3 &= (q_1 - q_a - q_b) \\ q_{11} &= (q_{tot} - q_1) \\ q_{10} &= (q_{tot} - q_1 - q_h) \\ q_9 &= (q_{tot} - q_1 - q_h - q_g) \\ q_8 &= (q_{tot} - q_1 - q_h - q_g - q_f) \\ q_7 &= (q_{tot} - q_1 - q_h - q_g - q_f - q_e) \end{aligned} \tag{5.3}$$

$$
\begin{aligned}
q_{12} &= unknown \\
q6 &= (tot - q1 - q_h - q_g - q_f - q_e - q_j - q_i - (q_o + q_p + q_m + q_n + q_k + q_l - q_{12})) \\
q5 &= (tot - q1 - q_h - q_g - q_f - q_e - q_j - q_i - (q_o + q_p + q_m + q_n + q_k + q_l - q_{12}) - q_d) \\
q4 &= (tot - q1 - q_h - q_g - q_f - q_e - q_j - q_i - (q_p + q_o + q_m + q_n + q_k + q_l - q_{12}) - q_d - q_c)
\end{aligned} \tag{5.4}
$$

By inserting equation 5.4 and 5.3 into equation 5.2 and doing some rearranging, the final equation describes the pressure equilibrium at P4 as shown in equation 5.5. The two unknown mass flows, q_1 and q_{12}, are further to be calculated by including a second equation from the second loop.

$$
\begin{aligned}
f_1 = {} & K_1 q_1^2 + K_2(q_1 - q_a)^2 + K_3(q_1 - q_a - q_b)^2 - K_{11}(q_{tot} - q_1)^2 - \\
& K_{10}(q_{tot} - q_1 - q_h)^2 - K_9(q_{tot} - q_1 - q_h - q_g)^2 - K_8(q_{tot} - \\
& q_1 - q_h - q_g - q_f)^2 - K_7(q_{tot} - q_1 - q_h - q_g - q_f - q_e)^2 - K_6(tot - \\
& q1 - q_h - q_g - q_f - q_e - q_j - q_i - (q_o + q_p + q_m + q_n + q_k + q_l - q_{12}))^2 - \\
& K_5(tot - q1 - q_h - q_g - q_f - q_e - q_j - q_i - (q_o + q_p + q_m + q_n + q_k + q_l - \\
& q_{12}) - q_d)^2 - K_4(tot - q1 - q_h - q_g - q_f - q_e - q_j - q_i - \\
& (q_p + q_o + q_m + q_n + q_k + q_l - q_{12}) - q_d - q_c)^2 = 0
\end{aligned} \tag{5.5}
$$

Furthermore can the second equation similarly be produced by assuming a pressure equilibrium at P14. In equation 5.6 the pressure equilibrium at P14 is described as the pressure loss from each side of the outer loop , which starts at P4 and P7, and presumably then meets at P14. By doing the same rearranging and substitution, the resulting equation is shown in equation 5.8.

$$
\begin{aligned}
P_s - K_1 q_1^2 - K_2 q_2^2 - K_3 q_3^2 - K_{12} q_{12}^2 - K_{13} q_{13}^2 - K_{14} q_{14}^2 = {} & P_s - K_{11} q_{11}^2 - K_{10} q_{10}^2 - \\
& K_9 q_9^2 - K_8 q_8^2 - K_{17} q_{17}^2 - K_{16} q_{16}^2 - K_{15} q_{15}^2
\end{aligned} \tag{5.6}
$$

$$
\begin{aligned}
q_{13} &= (q_{12} - q_k) \\
q_{14} &= (q_{12} - q_k - q_l) \\
q15 &= (q_k + q_l + q_o + q_p - q_{12}) \\
q16 &= (q_k + q_l + q_o + q_m + q_p - q_{12}) \\
q17 &= (q_k + q_l + q_o + q_m + q_n + q_p - q_{12})
\end{aligned} \tag{5.7}
$$

$$
\begin{aligned}
f_2 = {} & K_1 q_1^2 + K_2(q_1 - q_a)^2 + K_3(q_1 - q_a - q_b)^2 + K_{12} q_{12}^2 + K_{13}(q_{12} - \\
& q_k)^2 + K_{14}(q_{12} - q_k - q_l)^2 - K_{11}(q_{tot} - q_1)^2 - K_{10}(q_{tot} - q_1 - q_h)^2 - \\
& K_9(q_{tot} - q_1 - q_h - q_g)^2 - K_8(q_{tot} - q_1 - q_h - q_g - q_f)^2 - K_{17}(q_k + q_l + \\
& q_o + q_m + q_n + q_p - q_{12})^2 - K_{16}(q_k + q_l + q_o + q_m + q_p - q_{12})^2 - \\
& K_{15}(q_k + q_l + q_o + q_p - q_{12})^2
\end{aligned} \tag{5.8}
$$

The two equations in 5.5 and 5.8 can now be solved with respect to the unknown mass flows q_1 and q_{12}. Additionally can equation 5.3, 5.4 and 5.7 be used to determine the mass flow in each pipe segment. In order to find the correct distribution of mass flow, an iterative scheme has to be utilized. By using Newton's method as shown in equation 2.15, the mass flow q_1 and q_{12} can be determined with high accuracy. Since the system consist of two equilibrium equations, the Jacobi becomes a 2 x 2 matrix with the following elements:

$$J = \begin{bmatrix} \frac{\partial f_1}{\partial q_1} & \frac{\partial f_1}{\partial q_{12}} \\ \frac{\partial f_2}{\partial q_1} & \frac{\partial f_2}{\partial q_{12}} \end{bmatrix} \tag{5.9}$$

Due to the low dimension of the Jacobi, the inverse of the matrix can be calculated symbolically by Matlab, and then implemented directly into the model. Equation 5.5 and 5.8 is included in the 2 x 1 vector $F(q1, q12)$ in equation 5.10. The resulting values of q_1 and q_{12} are then presented after k iterations in the 2 x 1 vector q_{k+1}. The starting point will depend on the initial input and disturbances to the system, and therefore were several points tested in a "trial and error" method during the simulations.

$$q_{k+1} = q_k - J^{-1}F(q_1, q_{12}) \tag{5.10}$$

Furthermore if one pipe section shows a negative value, this indicates that the mass flow is travelling the opposite direction. Then equation 5.2 and 5.6 has to be rearranged according to the new equilibrium point, and the distribution of the mass flow has to be recalculated. Eventually will all the pipe sections have a positive mass flow, which indicates a correct equilibrium point. This iterative method has to be utilized if any of the boundary conditions changes, since this could potentially change how the mass flow is distributed in the system.

By utilizing this method, the mass flow in each consumer substation becomes completely disconnected from the supply pressure and temperature since it is only dependent on the power consumption. A challenge that Møller (2018) experienced when using the pressure to determine the mass flow distribution, was the lack of information about the valve position at the consumer. Therefore was a correlation between the valve position and power consumption was utilized. However a different approach could be used in order to create the connection between the pressure and mass flow. By assuming a known constant return pressure at the plant, the pressure at each side (supply and return) of the consumer can be calculated by using equation 2.11. The delta pressure across the consumer can then be used to calculate the pressure loss in the valve, heat exchanger and pipes, as shown in equation 5.11.

$$\Delta P_c = \Delta P_{valve} + \Delta P_{pipe} + \Delta P_{HE} \tag{5.11}$$

The delta pressure in the valve can be described as shown in equation 5.12. The mass flow, q_{max}, is not the requested mass flow that is being acquired by the linear correlation in figure 5.6, but a maximum deliverable mass flow based on the valve being fully opened. By using this assumption, the valve position, s, can be set to a constant value of one. The valve constant, K_v, has further been determined from the datasheet of the most common

valve that has been used at Stjørdal, and is shown in appendix B.31. The loss in the pipe can be calculated by using equation 2.1.2, but with the maximum deliverable flow as shown in equation 5.13. The pressure loss from the heat exchanger was calculated by using a pressure loss tool developed by the supplier SWEP, which has supplied several of the heat exchangers to the network at Stjørdal. As shown in Appendix B.30, can the pressure loss be approximated, based on the datapoints, to follow a second order function. A complete expression with q_{max} as the only unknown is further shown in equation 5.14.

$$\Delta P_{valve} = \left(\frac{q_{max}}{sK_v}\right)^2 \tag{5.12}$$

$$\Delta P_{pipe} = K_{pipe} q_{max}^2 \tag{5.13}$$

$$\Delta P_c = \left(\frac{q_{max}}{K_v}\right)^2 + K_{pipe} q_{max}^2 + 0.0889 q_{max}^2 + 0.0771 q_{max} - 0.0492 \tag{5.14}$$

Furthermore by rearranging equation 5.14 with respect to q_{max}, the final equation can be expressed as shown in 5.15. The constants, C and ρ, represents a required conversion from respectively m^3/h to kg/s, and m^3/s to kg/s so that each term has the same units. The constant L, represents the length of the pipe on the primary side of the consumer substation. When the supply pressure changes, then the maximum mass flow has to be recalculated since this will affect the pressure loss across each of the consumers in the network. Furthermore by calculating the difference between the requested mass flow and the deliverable maximum mass flow, a controller can use this information to either increase or decrease the supply pressure in order supply the network correctly. This ultimately creates the connection between the mass flow and network pressure that were required. As a final note, has the expression inside the square root a possibility of becoming negative if the delta pressure becomes too low. Therefore has precautions been taken, by restraining the expression from becoming less than zero.

$$q_{max} = \frac{\sqrt{-0.0608 - s(\frac{C}{K_v})^2 - \frac{K_{pipe}L}{\rho^2} + \Delta P_c}}{s(\frac{C}{K_v})^2 + \frac{K_{pipe}L}{\rho^2} + 0.09} \tag{5.15}$$

5.2 Validation

Due to the complex network at Stjørdal, it was important to validate the model in order to ensure correct responses compared to the historical data. It was however not possible to validate the pressure in the network, due to the modelling approach. In this thesis the mass flow is calculated directly from the power consumption, and not by the supply pressure. As described in chapter 4 where the return pressure at the plant set to a constant, and then the supply pressure was adjusted so that the maximum deliverable flow equaled the requested flow. This approach is different from how the plant is currently operated, where a constant pressure difference between the supply and return line at the plant is used. A constant pressure difference would however not be feasible, since the approach depends on a significant change at the consumer when the supply pressure changes. The chosen model and regulative setup, has therefore been proposed as an alternative in order to overcome the missing information in the consumer substation and the complexity that (Møller 2018) faced. During validation, the temperature becomes disconnected from the pressure by only using the correlation to the power consumption to determine the mass flow at each consumer. The following variables were validated with historical data:

- Temperature difference (difference between inlet and outlet on the primary side) at each consumer.
- Return temperature at the production plant.
- Mass flow at each consumer.
- Total mass flow at the plant.

5.2.1 Offline parameter estimation

In figure 5.9 the return temperature at the plant before the parameter estimation is shown. The red line indicates the model and the blue line shows the historical data. It can be observed a significant deviation between the model and the measurements the first hours of the simulation. The deviation can be explained from the initial states and power consumption from the consumers. The measured return temperature in the beginning of the simulation, will be a result of the supply temperature, heat propagation and power consumption in the network several hours before the first sample. Therefore would such a simulation be required in order to achieve correct values in all states at the start. The effect of these deviations will however decrease as the simulation progresses and eventually disappear completely. As a solution when doing the offline parameter estimation, the estimation was not performed in the first 130 samples. An alternative solution would be to simulate the system long enough to reach the states with the longest time constant, and use these states as initial values in the simulation performed in this thesis. This method basically just increases the total simulation, since the effect of the error will disappear regardless.

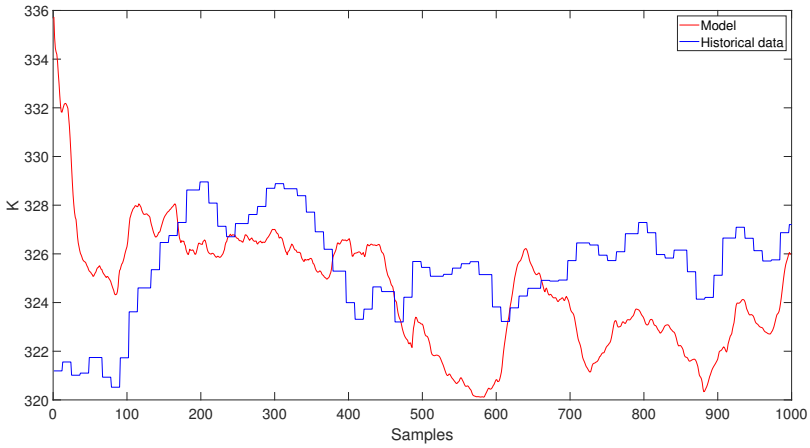

Figure 5.9: Return temperature at plant.

The parameter estimation was performed in two steps. First the specific heat coefficient for each consumer was estimated by using the delta temperature as output. The temperature drop through a heat exchanger can be significant and depends on the type of heat exchanger and consumption. It is however not known what type of heat exchanger each consumer is using at Stjørdal, since each of the consumers buys and maintains their own equipment. This way Statkraft has no record of what equipment each consumer is using. In equation 2.14, c_p, is the only parameter used to describe the return temperature from the consumer, and therefore the only value the estimator could influence. This is because the inlet temperature does not affect the temperature difference at the consumer, since it would affect the outlet temperature just as much. The mass flow is calculated di-

rectly by the power consumption, and is therefore not affected by any of the parameters during validation. In table 5.3 the specific heat at each consumer is shown after a parameter estimation is performed. The SQP algorithm was given an initial value of 4200 $J/(kgK)$, with a possible range between 4180 and 4260 $J/(kgK)$. As shown in the figure, were several values estimated to the maximum value of 4260 by the algorithm. In figure 5.10 the reduction of the objective function value during the estimation is shown. After one iteration the SQP is able to reduce the function value from about 179000 to 170842, which indicates a better fit to the measurements.

Specific heat constant of each consumer	Value after estimation
cp,a	4260
cp,b	4256
cp,c	4196
cp,d	4260
cp,e	4260
cp,f	4260
cp,g	4260
cp,h	4260
cp,i	4180
cp,j	4260
cp,k	4260
cp,l	4260
cp,m	4260
cp,n	4260
cp,o	4260
cp,p	4260

Table 5.3: Estimation of specific heat parameter at each consumer

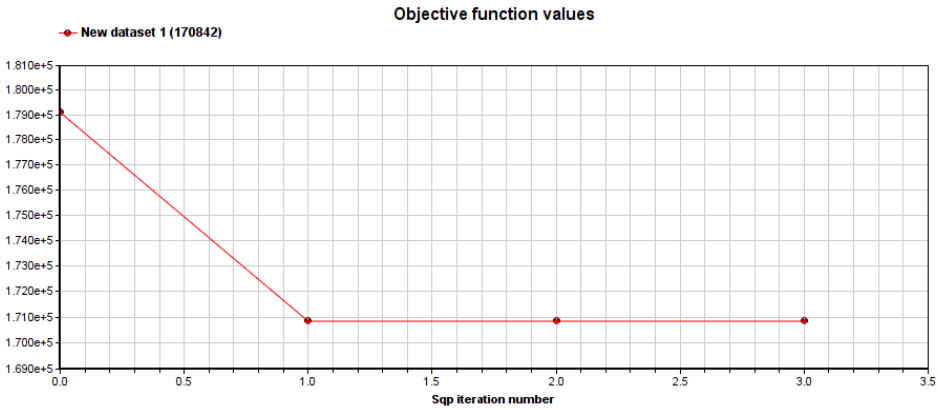

Figure 5.10: Illustration of the reduction in objective function value after parameter estimation of the specific heat at each consumer

The second parameter estimation was performed on the rest of the parameters that could influence the return temperature at the plant. All of the parameters shown in table 5.4 are used several places in the model to calculate the temperature, and therefore had to be estimated simultaneously. The table displays the updated values of each parameter after performing the offline estimation in Modelfit. The first parameter, T_{gnd}, represents the temperature surrounding the pipe. By using the database from the Norwegian Meteorological Institute, it was possible to use measurements taken 0.5m into the ground at Stjørdal (MET 2019). During the first week of February 2019 the temperature indicated about 274.15 K. The parameter was therefore set to the given value, with a range from 272 to 276 K. The second parameter, k , has been implemented as a factor multiplied with the thermal transmittance, k', described in chapter 2.1. The factor has been multiplied with each of the calculated thermal transmittance, which has been used in all the combinations of pipe diameter and insulation thickness found in Appendix A.1. The range of the factor was set between 0.1 and 5, and initial value set to 1. The third parameter, c_p, was initially set to 4200 $J/(kgK)$, with a range between 4180 and 4260 $J/(kgK)$ corresponding to a water temperature between 20-130 °C. The fourth and last parameter, ρ, was initially set to 970 kg/m^3, with a range between 935 to 1000 corresponding to a water temperature between 20-130 °C.

Variable	Value after estimation
Surrounding temperature, T_{gnd} [K]	276
Thermal transmittance factor, k	0.3413
Specific heat water, cp [J/(kg*K)]	4180
Density water, ρ [kg/mˆ3]	935

Table 5.4: Result after parameter estimation number two

In figure 5.11 the objective function value of the estimation of the four remaining parameters are shown. The return temperature at the plant was used as output for comparison with the historical data. After one iteration of the SQP algorithm, the objective function value decreased from about 3500 to 1600. This shows that the algorithm was able to better fit the output of the model to the historical data. It should be noted that the values from the first parameter estimation were used when performing the second.

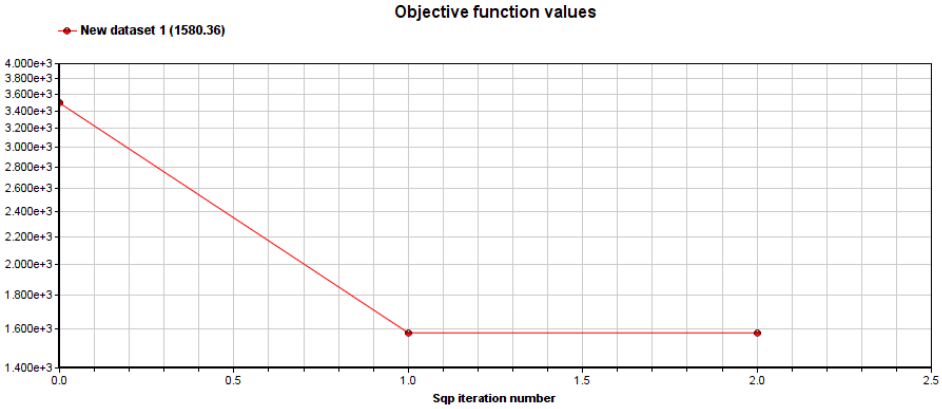

Figure 5.11: Illustration of the reduction in objective function value after estimation of the four remaining parameters

5.2.2 Validating temperature and mass flow

In order to keep the number of graphs within manageable amounts, are the mass flow of the majority of consumers are shown in appendix B.10 - B.13, while a few distinct consumers have been displayed in more detail. However as an overall comment, the model showed a relatively good fit compared to the measurement at the majority of the consumers. Deviations were observed during large peaks of consumption, where the model slightly underestimated the value in some cases. Similarly to the mass flow of each consumer, has the delta temperature of the majority of consumers been moved to Appendix B.14 - B.17 in order to keep the number of graphs within manageable amounts. A larger overall deviation, compared to the mass flow, was observed at all consumers. Consumer B, G, J, L, M, N, P shows relatively good fit compared to the historical data, while consumer A, C, D, E, I, K and O does not follow the historical data very well. The model appears to lack sensitivity when calculating the temperature difference at these consumers, and are close to being constant. The measurements are to a greater extent fluctuating through the simulation. It appears however that the average value of the model is close to the average measurement value.

Moreover has consumer A, B, and E been observed in more detail, in order to further analyze the most distinct results. In figure 5.12 and 5.13 are the mass flow at consumer A and B displayed, with results from both the model and historical data. They are used as an example of one ”good matched” and one ”bad matched” consumer, where consumer A experiences one of the largest deviations and consumer B has one of the lowest. The red line indicates the model, and the blue line shows the historical data. The flow at consumer A has a relatively good match at the first part of the simulation, but at the end of the week the historical data indicates a stable mass flow at about 4 kg/s, while the model fluctuates between 3.5 and 4.5 kg/s. The large deviation at the second part of the week could be explained from figure 5.4 where consumer A clearly has a lower limit on the mass flow, while the model uses a linear correlation which can reach zero. The mass flow at consumer

B has in contrast to A a much better fit when compared to the measurements. Apart from not entirely reaching some of the peaks, the model is close to a perfect fit. The good match can also be explained from the high value in the coefficient of determination at consumer B.

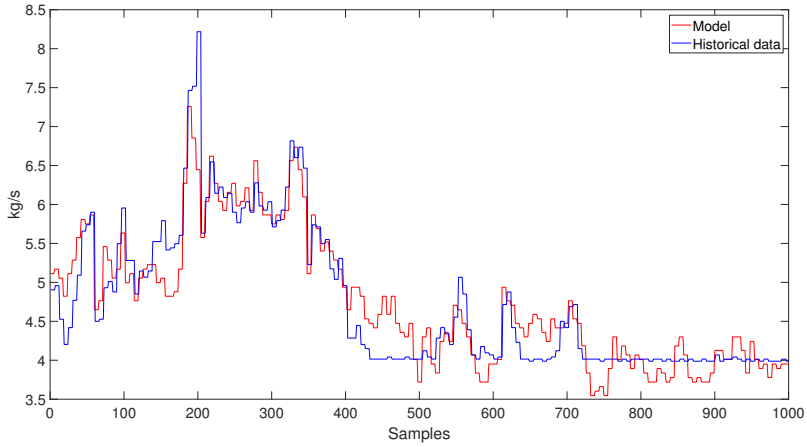

Figure 5.12: Mass flow consumer A.

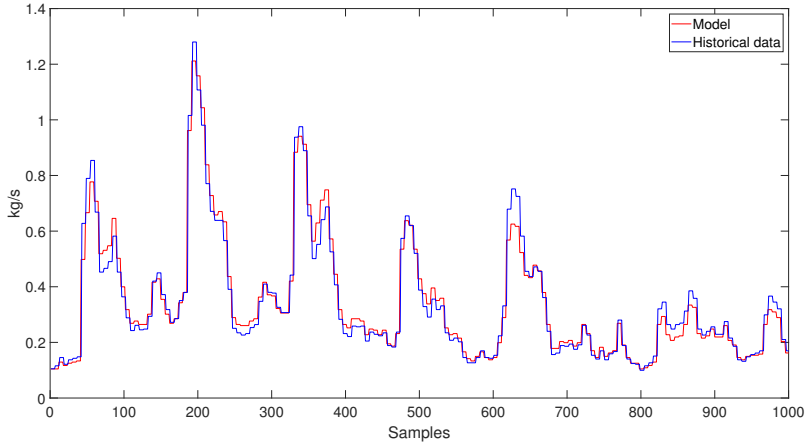

Figure 5.13: Mass flow consumer B.

In figure 5.14 the temperature difference (difference between inlet and outlet on the primary side) of consumer A are shown. At consumer A the measurements ranges between 30 and 46 °C, while the model is close to being constant at about 39 °C. However if the average value of the measurements is compared to the average model values, the deviation is only 0.09 °C. In figure 5.15 the delta temperature of consumer B is shown. The model follows the historical measurements far better than A. In the first part of the week the model experiences some deviation during the peaks, with deviations between 3- 5 °C. In the second part of the week the model has an average lower deviation, but in the opposite direction. It shows a higher delta temperature than the measurements, with maximum deviation about 5 °C at the peaks.

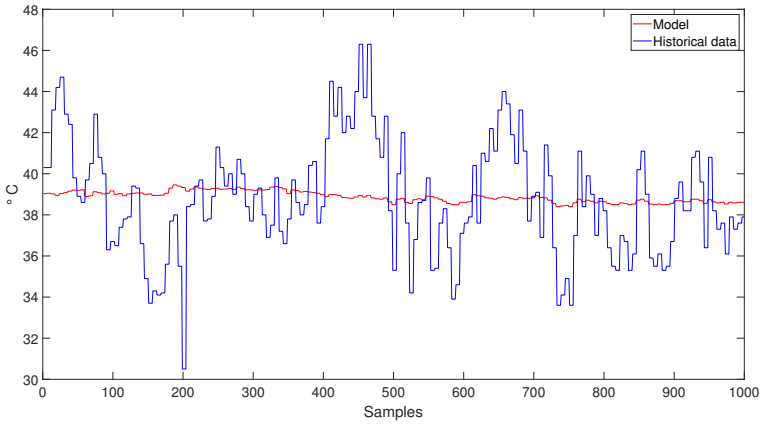

Figure 5.14: Delta temperature consumer A.

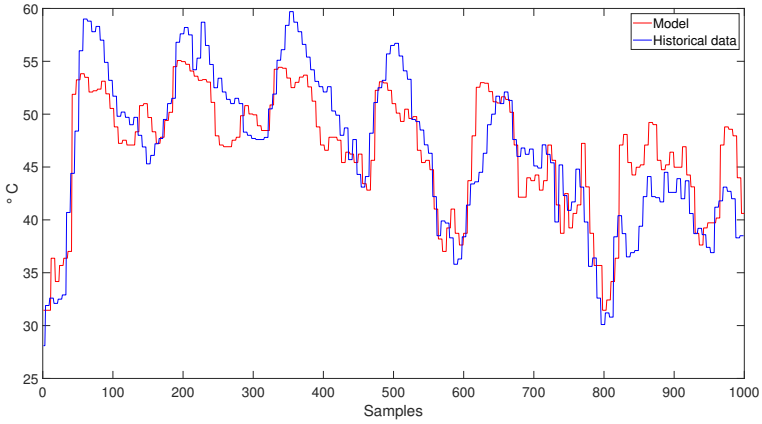

Figure 5.15: Delta temperature consumer B.

In figure 5.16 the mass flow of consumer E is shown. The model matches the measurements relatively well, but experiences a distinct deviation after 800 samples where the measured mass flow is increased about 0.5 kg/s throughout the rest of the simulation. This shift can not be observed in the modeled mass flow. The same pattern can be observed in the delta temperature of the consumer. In figure 5.17 the model experiences some deviations through the simulation, with the measurements fluctuating more than the model. After 800 samples the delta temperature drops to about 25 °C until the end of the simulation.

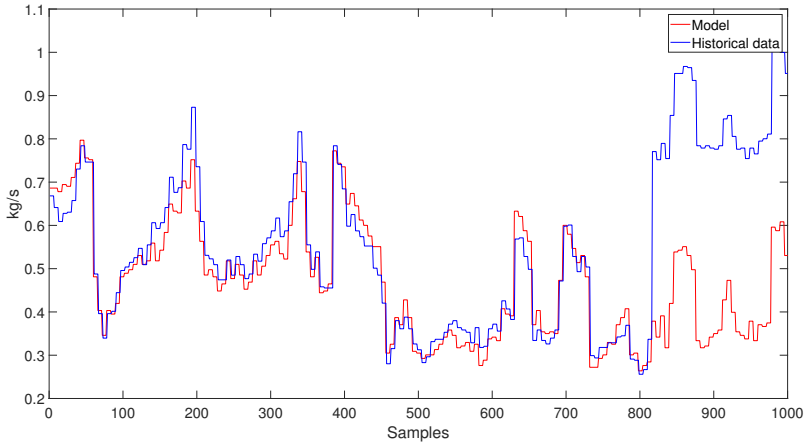

Figure 5.16: Mass flow consumer E.

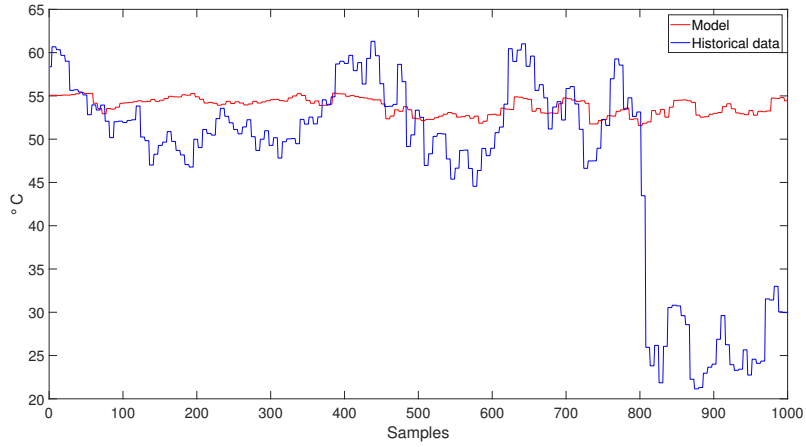

Figure 5.17: Delta temperature consumer E.

Furthermore in figure 5.18 are the return temperature at consumer B, J and L displayed. They represent some of the smaller consumers in the network, and therefore has a different characteristic in their respective heat exchanger compared to the large consumers. A step in the power consumption, from the largest possible value to the lowest, was performed at each respective consumer, while the supply temperature was kept constant. The purpose of this graph is therefore to display the effect of only changing the power consumption. It can be observed a relative large step at the return temperature at each consumer, ranging between 13 - 24 °C. It can also be observed that consumer B and J increases their temperature, while the return temperature at consumer L is reduced.

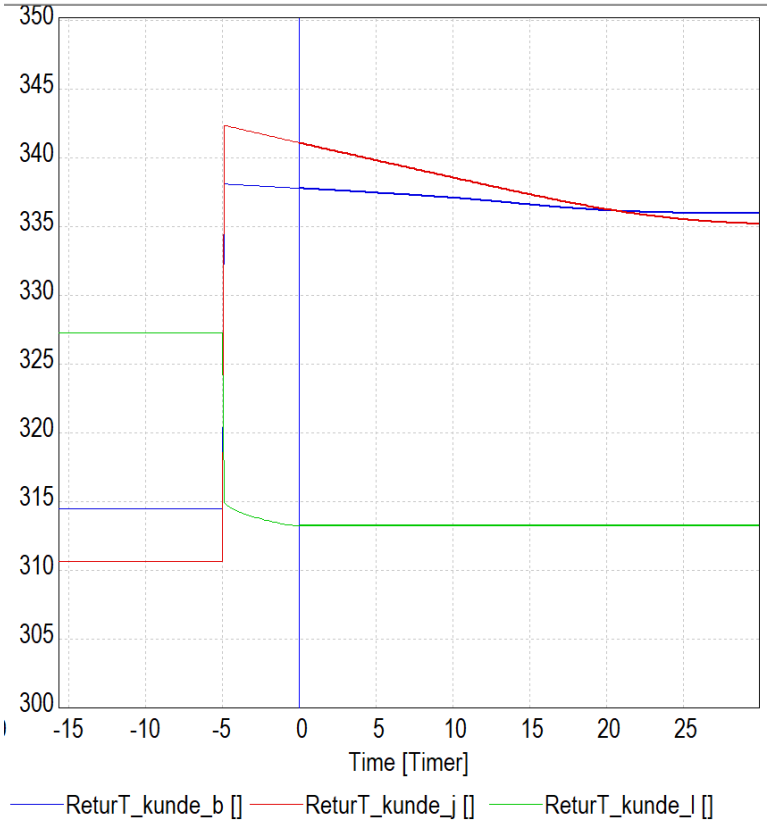

Figure 5.18: Step in consumption from max to min at consumer B, J and L

In figure 5.19 a step from the largest possible power consumption to the lowest, was performed on the large consumers in the network. It can be observed a relatively small effect on the return temperature, ranging between 1.5 - 4 °C. It therefore appears that the large consumers have low sensitivity in their return temperature. Apart from consumer C and K are all consumers increasing their return temperature due to this step.

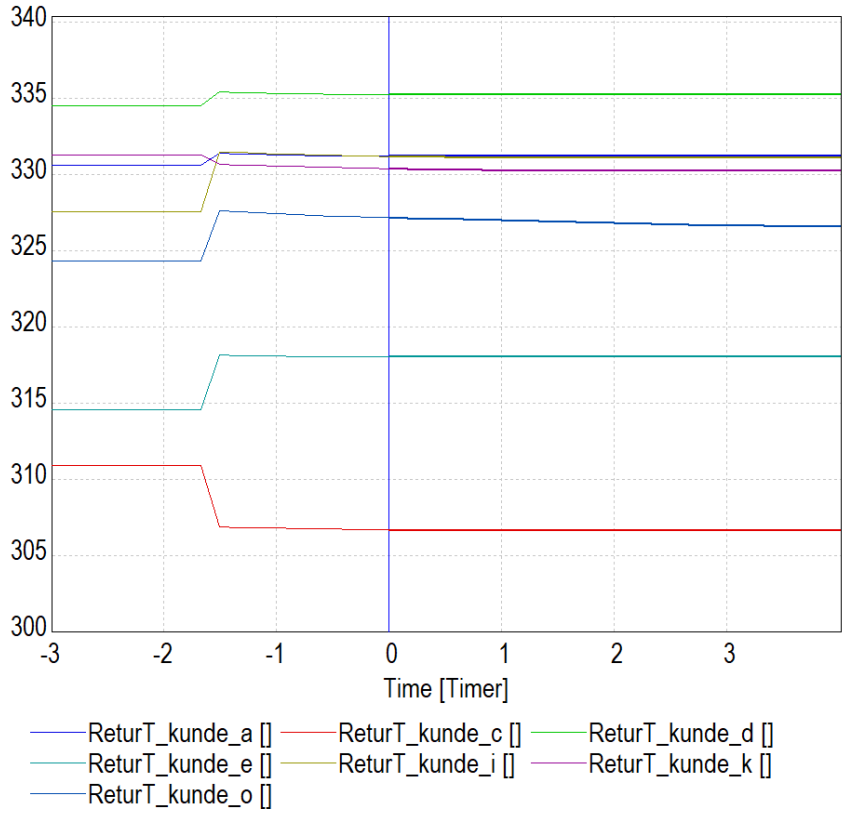

Figure 5.19: Step in consumption from max to min at consumer A, C, D, E, I, K and O

In figure 5.20 the total mass flow from the plant is plotted. The red line indicates the model, and the blue line shows the historical data. The model shows relatively small deviations compared to the historical measurements during the first part of the simulation. However during hours of peak or low consumption, the model starts to deviate. It can be observed deviations about 6 kg/s too short at sample 200 and 330. During the second part of the week the average mass flow is reduced, and therefore there are no large peaks. The average deviation is however observed to increase, where the model regularly underestimates the mass flow by around 4-5 kg/s. The deviation can be further explained in figure 5.21, where the total mass flow measured at the plant has been compared with the measured mass flow at each consumer that has further been summed up. The measurements from each consumer were collected from Statkraft's database, Energiguiden. The total

mass flow were measured at the plant, and collected from manual extraction by the plant operators. It can be observed a distinct deviation between these two measurements. On average is the measurement at the plant 3.48 kg/s larger than the summed up mass flows. In this graph the x-axis displays the number of hours into the week.

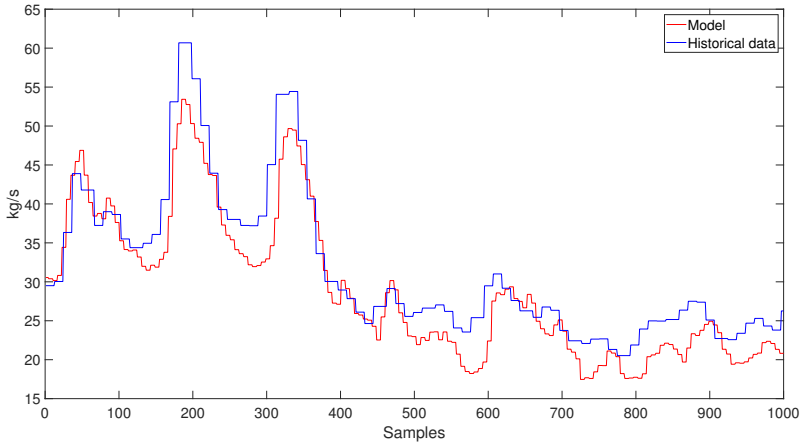

Figure 5.20: Mass flow at the plant.

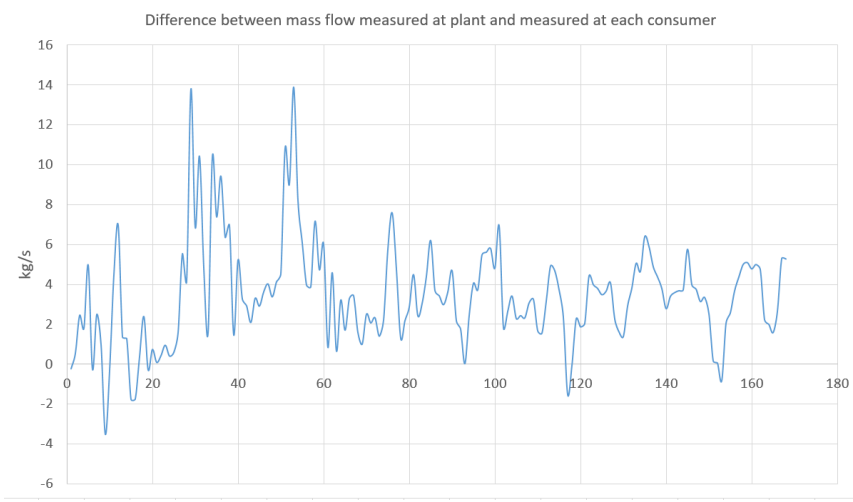

Figure 5.21: Difference between total mass flow measured at plant and measured at each consumer

After the offline parameter estimation was performed, the updated return temperature can be shown in figure 5.22.The parameter estimation can be observed to have shifted the function upwards, ultimately decreased the deviations compared to the historical data. The first 130 samples were not included when performing the parameter estimation, and are therefore not taken into consideration. Apart from two peaks at sample 420 and 650, the model follows the measurements relatively good. The largest deviation happens at sample 420 with a deviation of 5.5 Kelvin, where the model has increased the temperature while the measurement shows a further decrease. During the second part of the week the model follows the measurement increasingly, where the last 300 samples indicates close to a perfect fit. The return temperature does however still deviate more from the measurements than the mass flow. This is expected since the return temperature is based on temperature states, the heat propagation throughout the network, and heat extraction at each consumer. In contrast is the mass flow only depending on the linear correlation with the power consumption, and are therefore less prone to deviations.

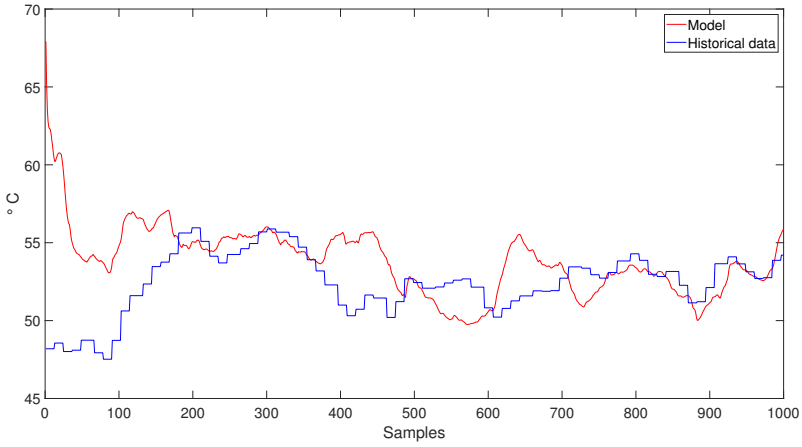

Figure 5.22: Return temperature at plant.

5.3 Sources of error in model and validation

When creating a process model there will naturally be several sources of error. These errors are in most cases due to lack of information, or necessary simplifications in order to create the model. As a consequence the model might deviate compared to the historical data, and this must be considered when further implementing a controller and estimator. The most significant sources can be further described below:

- When modelling the heat propagation of the DHS, a finite volume method was utilized. This is an approximation compared to using the exact solution.
- The heat was assumed not to accumulate in the pipe wall or insulation, which would be the case in reality.
- Haaland's approximation of the implicit Colebrook-White equation has been used in order to describe the pressure loss in the DHS. This method could cause errors, especially in the case of low Reynolds number.
- The flow is assumed turbulent throughout the network. This is not necessarily the case throughout the network, and especially in the heat exchanger at smaller consumers the flow could tend to move slow enough to become laminar. As seen in the Appendix B.29, the Reynolds number in one of the heat exchangers used at Stjørdal indicates a laminar flow.
- In order to include all the consumers in the network, an aggregation method was necessary. When aggregating several consumer into one larger one, there will be deviations compared to modelling all separately. in table 5.1 the weight between each of the consumers is assumed constant. In reality these would change through the simulation, and require the aggregated consumer to be moved slightly.
- As observed could the historical data be affected by sources of error. Based on two separate measurements, there could be different sources causing the uncertainty and hard to pinpoint which one is correct. In addition when the data is being collected and stored in large databases, data truncation could occur and cause errors as well.

5.4 Discussion

By observing the measured power consumption, mass flow and return temperature of the consumers, a relatively large spread in size and behavior can be seen. In context with the geographical spread between the consumers, the Stjørdal network can be a complex network to model. Some discrepancies were therefore unavoidable when developing the process model, and they have to be taken into consideration during validation and further when developing a corresponding controller. In that context was the offline parameter estimation in Modelfit, a useful tool to compensate for some of these discrepancies. In the estimation of four different parameters, it was observed a significant decrease in the objective function value, where the value represented the deviation between the model and measurements. It was therefore evident that the SQP algorithm were able to fit the model

with the measurements in a better way by adjusting the parameters. When graphically comparing the return temperature at the plant, before and after the estimation, a significant improvement in the fit was observed, noting that the first 130 samples were not taken into consideration.

The coefficient of determination indicated a good linear correlation between the measured power consumption and mass flow at the majority of the consumers. Due to this high correlation, the modeled mass flow was able to match the measurements relatively good. However some consumers did experience minor deviations. These were typically observed during large peaks in flow consumption. This indicates that the correlation between power consumption and mass flow could be less linear during these hours, and different types of correlation depending on the magnitude of the consumption should be tested. The reason for the large peaks of power consumption in the first part of the week compared to the second, could be explained by the outside temperature. From Appendix A.2 the outside temperature is at the lowest on the second day with -18.5 °C. The temperature then increases to 4.8 °C on the sixth day. This large increase in temperature will cause the average power consumption (together with the mass flow) to drastically drop during the week. Overall this causes a larger spread in datapoints of both the model and measurement.

Moreover had consumer A a lower lower limit on the mass flow in the measurements, causing larger deviations during hours of low consumption. This indicated that instead of changing the mass flow any further, the temperature difference was adjusted so that the resulting power changed. Consumer E experienced large sudden deviations in the mass flow and delta temperature, which were clearly connected. This deviation has to be seen in context with appendix B.32 displaying the measured power consumption and mass flow of consumer E. It can be observed a clear offset in some of the datapoints, going upwards, compared to the rest. These datapoints indicates that there has been a change in the heat exchanger, either on the primary or on the secondary side, which required more mass flow in order to have the same power consumption. This sudden change is observed at the end of the week long simulation, which means there could be a weekend setting on a local controller that affected the system. Based on the behavior of consumer A and E, it is evident that each consumer has their distinct setup in the heat exchanger which a linear correlation struggles to describe completely.

The deviation in mass flow during hours of peak consumption, were also observed when comparing the modeled total mass flow at the plant with the measurements. An overall larger deviation was however observed compared to each consumer. This deviation can be explained from figure 5.21, where the mass flow measured at the plant was clearly larger than the summed up flow measured at each consumer. This shows that there could be errors in the measurements either at the plant or at the consumers. These errors could be direct errors in the measurement equipment, and/or it could be errors when saving these data to the database. After comparing the measured power, mass flow and delta temperature with the energy balance, there was observed round-off errors when calculating the power consumption. This could be due to truncation of data when it was saved at Statkraft's database. The error could also origin from left out consumers, that the historical data did not include.

Two separate parameter estimations were performed in Modelfit. When estimating the

specific heat coefficient at each consumer, the SQP algorithm was observed to have relative small impact. From the modeled delta temperature, this could be explained by the observed low sensitivity at several of the consumers. It was observed that the low sensitivity was associated with primarily the large consumers in the network, including consumer E. The SQP were therefore not able to better fit the delta temperature at these consumers with only the specific heat coefficient to adjust on.

This low sensitivity caused the delta temperature at the large consumers to experience significant deviations. This deviation has to be seen in context with the linear correlation at each consumer. The correlation ultimately creates different characteristics in the heat exchanger at each consumer. As a result it was observed that the large consumers had significant lower sensitivity in the return temperature, when a step in consumption was performed. The correlation therefore appears to not catch the characteristics of large consumers accurately enough. This was partly because the majority of the large consumers had close to no correlation between the power consumption and delta temperature, while some of the smaller consumers had to some extent a correlation. Apart from the deviations experienced at the large consumers, the modeled delta temperature matched the measurements relatively well. The major deviations appeared during peak consumption, which is relatable to the deviations in the mass flow.

5.5 Conclusion

The process model describing the DHS at Stjørdal, with estimated parameters, has been validated with one week of historical data and with promising results. Apart from minor deviations during peak consumption, the model matched the measurements relatively well in both mass flow and return temperatures. However the characteristics of the heat exchanger at the large consumers, were observed to deviate from the historical measurements. More specifically had the modeled return temperature a significantly lower sensitivity. Consequently the model was able to display the consumption of the smaller consumers more accurately than the larger ones. This was because the model relied heavily on a linear correlation between the power consumption and mass flow, which further had low correlation to the return temperature at several of the large consumers. Since the model utilized the energy balance to calculate the return temperature, a deviation was inevitable.

Moreover was a distinct consumer-specific behavior observed in several of the historical measurements, although the majority of the datapoints at the smaller consumers were more unambiguous. Based on these results would a more personalized correlation, based on the distinct characteristics at each consumer, better display the consumers in the network.

Further testing is required to observe if the model can handle longer simulations, e.g., through a month or a year. Especially the modelling approach of the consumer substation could prove insufficient since it was developed based on a week of measurements, and contained inaccurate characteristics of several consumers. By having more datapoints the effect of these errors could perhaps be reduced, in addition to the deviation between the two separate measurements of the total mass flow.

Chapter 6

Predictive Optimization

This chapter starts by describing how Statkraft currently controls the DHS at Stjørdal. Further has a controller been designed and implemented together with the developed process model. The chapter then presents the results, followed by a discussion and conclusion.

6.1 Control design

With the current setup, the plant at Stjørdal is operated by automatically updating the supply pressure and temperature values. The supply temperature is controlled according to the ambient temperature. For instance if the ambient temperature is reduced, the supply temperature at the plant is automatically increased by a certain amount. If the current temperature can not provide the requested power by the consumers, they have to contact Statkraft so that an operator at the plant can increase it. A constant delta pressure of 3.5 bar is kept between the supply and return line. If a consumer changes their valve position, it will be measured in the return line and the supply pressure is then automatically adjusted.

The following DRTO problem has been solved by utilization of Nonlinear Model Predictive Control, including both economic and regulatory objectives in the cost function. The controller has been tested on the plant replacement model that was developed and validated in chapter 5. Due to the modelling approach in the process model, the control principle has been adjusted accordingly so it can be solved with a NMPC. Especially the approach of modelling the delta pressure and mass flow at the consumer, made the supply pressure not comparable with the historical data. Additionally have certain assumptions been made:

- The requested power from each consumer has been assumed available either beforehand or real time. The consumption has been implemented as measured disturbance (DV) that is fed forward into the model.
- There exists equipment to measure temperature and mass flow at each consumer at Stjørdal today, but it is only used for historical analysis. It is assumed that these measurements are available real time or beforehand.

- It is assumed that the cost of incinerating bio-fuel is higher than operating the pump. Additionally is it assumed that it takes more time to adjust the supply temperature than the pressure.
- As mentioned in chapter 5, the return pressure have been assumed constant. This enables a detectable change in pressure difference at the consumer, if the supply pressure at the plant is changed.
- As described in chapter 5.1.2 is the inlet temperature on the secondary side of the heat exchanger, assumed to not be lower than $^{\circ}22$ C. Additionally is it assumed that the heat transfer area and coefficient in the heat exchanger is of such value that the modeled temperature difference is physically possible.
- The plant at Stjørdal operates with three pumps in parallel. By having three pumps available the pressure limit is close to the same, but the mass flow can be significantly increased. In order to create (and evaluate) a cross connection between the supply pressure and temperature in the controller, it was however necessary to assume that only one pump was available. Consequently a maximum pressure limit would be reached, without the possibility of increasing the mass flow further.
- From Grundfos (2019) has the pump an upper limit of 16 bar. It has however been assumed that this is the absolute maximum pressure that the pump can operate on, which is not viable during a long period of time. In reality would perhaps pump number two be turned on in order to reduce the load on the first pump. Therefore has an upper limit of 15 bar been assumed.

In table 6.1 are the MVs and DV, associated to the optimization problem, displayed. The plant controls the supply pressure and temperature, and are therefore defined to be manipulated variables. By using these two variables, the algorithm is expected to find a optimal combination that provides the requested power from the network at all times. In addition are the power consumption implemented as measurable disturbances to the network, which is updated every hour. Their respective power consumption can therefore be fed forward into system.

	Variable	**Unit**	**Abbreviation**
MV	Supply Pressure	Bar	P_s
	Supply Temperature	K	T_s
DV	Power consumption from consumer	kW	Q_i i = 1,2..16

Table 6.1: Overview of manipulated variables and disturbance variables

In table 6.2 the controlled variables are shown. They are implemented to measure the output of the system, so that the regulatory and economic objectives can be reached. Regarding the current setup at Stjørdal, the CV would be the ambient temperature. Since there is a connection between the power consumption and the ambient temperature, the plant will presumably deliver the required supply temperature based on its cycle. A different approach is to measure the return temperature, $Tr_{consumer}$, at each consumer, and then determine the supply temperature based on a lower constraint on the return temperature. In chapter 5.1.2 was the modeled constraint on the return temperature, described and implemented. This was performed in order to prevent it from reaching unphysical levels. However in the transition between the original function and the constant 295 K, the CV will be highly nonlinear even when using the softmax function. This could be difficult for the NMPC when performing a linearization and line search to find the optimum. The controller could get stuck or be flickering between solutions. Due to these issues has a constraint of 298 K (about 25 °C) been implemented in the controller. By using a slightly higher value on the controller, the highly nonlinear area can be somewhat avoided. Additionally is this performed in order to have the constraint included in the objective function of the DRTO.

The controlled variable, q_{diff}, includes the requested mass flow at each consumer, q, subtracted the maximum deliverable mass flow, q_{max}. As described in chapter 5.1.2, has the pressure been connected with the mass flow, by using the pressure difference at each consumer to calculate a maximum deliverable mass flow. By using q_{diff} as an output, the supply pressure can be adjusted accordingly so that the difference stays close to zero Bar. A value above zero would indicate that the consumer is using more water than the plant can deliver, which would be unphysical. Therefore has a high cost been put on breaking this constraint. A value below zero would indicate that there is more than necessary pressure in the system. Additionally if the pump can not deliver a higher pressure, the requested mass flow at the consumer simply has to be reduced down to the deliverable flow. After such cut in mass flow, the consumer would still be receiving his requested power consumption due to the energy balance in equation 2.14

Variable	**Unit**	**Abbreviation**
Mass flow subtracted maximum potensial mass flow at consumer i	kg/s	$q_{diff,i}$, i = 1,2...16
Return temperature at consumer i	K	$Tr_{consumer,i}$, i = 1,2...16
Supply temperature at plant	K	T_s
Supply pressure at plant	Bar	P_s

Table 6.2: Overview of controlled variables in the optimization problem

The supply temperature and pressure are also included as controlled variables, since they form the economic objectives. There is a cost of operating the pump since it requires energy in order to produce the pressure. Similarly there is a cost associated to incineration

of bio-fuel. A higher supply temperature requires more fuel, and should therefore be kept at a minimum. However the plant model has not been included in this thesis, and the exact cost in norwegian kroner of supplying temperature or pressure is not known. An alternative approach is to reduce the temperature and pressure as much as possible, knowing it will ultimately reduce the cost. The methods unreachable setpoint and infeasible soft-constraint, has been utilized for this purpose.

As an overview, the controller has been designed so that there is a cost related to not fulfilling the requested power consumption by the consumers. At the same time there exists a smaller cost related to producing this energy at the plant. Since the mass flow is calculated directly from the power consumption, the pump has to provide the necessary pressure (which produces the necessary q_{max}) in order to satisfy the consumer. The pump has an assumed upper limit of 15 bar. If the requested mass flow, q, requires a higher pressure, the flow will be reduced to the maximum deliverable flow, q_{max}. In order to preserve the energy balance in equation 2.14, the return temperature then drops. By constraining the return temperature from dropping below 298 K at each consumer, the plant has to provide the necessary supply temperature. This way a cross connection between the pressure and temperature is established.

The economic and regulatory objectives are further implemented in the cost function displayed as a matrix formulation in equation 6.1, where Z is the measured output. The regulative objectives have been implemented by using soft constraints with a slack variables. Based on the CVs are exact penalty desirable, and therefore are linear terms utilized. The slack variable, $\mathcal{E}$, then defines the largest value the constraint is broken with. The regulative objectives can be further described as follows:

- The requested mass flow should not be greater than the deliverable flow and therefore is an upper constraint, on q_{diff} at 0 Bar, implemented at each consumer. The soft constraint then produces a linear cost with the term $r^T\mathcal{E}$ in equation 6.1. The slack variable is required to be zero at all times in order to prevent unphysical flow values, and therefore has the highest cost been set to this constraint. In equation 6.2 the constraint is displayed with the corresponding slack variable, where P1 is the number of evaluation points, and i are the number of consumers.

- The return temperature at each consumer should not go below 298 K. A minimum value of 298 is therefore implemented as a soft constraint, by including a linear cost with the term $r^T\mathcal{E}$, in equation 6.1. The output should not break the constraint, but it would not be as critical as the constraint on q_{diff}. The decided value ultimately depends on the assumed inlet temperature on the secondary side of the heat exchanger. The cost has therefore been set lower than the cost on q_{diff}. The constraint is also displayed in equation 6.2, where P2 is the number of evaluation points, and i are the number of consumers.

Both methods of unreachable setpoint and infeasible soft constraint has been experimented with in this thesis. The unreachable setpoint is implemented by a quadratic cost in equation 6.1, with the term $(Z - Z_{opt})^T Q(Z - Z_{opt})$. The constant Z_{opt} will then represent

the unreachable setpoint value. An unreachable setpoint on the supply pressure would naturally be 0 Bar, since it would not be physically possible to reach while the consumers have a requested consumption. The unreachable setpoint on the temperature has been set to 300 K, which is slightly above the regulatory constraint on the return temperature. Seen in context with the heat loss to the surroundings, it is set relatively close to the regulatory constraint which can be defined as a unreachable value.

The infeasible soft constraints are utilized similarly to the regulatory objectives as a linear cost with the term $r^T\mathcal{E}$ in equation 6.1. In equation 6.3 the constraint for both objectives are shown, where j is the number of block intervals. Both 0 bar and 298 K, respectively the unreachable pressure and temperature values, has been used as a infeasible constraint. Their respective value is implemented as a upper limit on the constraint. The supply pressure then has a upper constraint at zero bar, and a lower constraint at a negative value. The supply temperature has a upper constraint on 300 K, and a lower constraint at for instance 273 K.

Additionally is the change in input penalized with weights in the matrix R, in order to prevent unrealistic control moves performed by the controller. The cost on the pressure was set slightly lower than the temperature, since the pump naturally will be able to change its state much faster than the incineration.

Since the regulatory objectives had a significant higher importance than the economic, the weighting was set much higher on the former. Between the pressure and temperature, was the latter MV the primary focus of reduction, and therefore was a slightly higher weight set on the temperature in the economic objectives. This was done to express the assumed higher cost on bio-fuel than electricity. Since the regulatory objectives were implemented with a linear cost, it became more difficult to tune the controller after the unreachable setpoint was implemented. This was likely due to the pure quadratic cost, which could be less intuitive to tune in combination with the linear terms.

$$\underset{z\in\mathbb{R}^n}{\text{minimize}} \quad J = \frac{1}{2}(Z - Z_{opt})^T Q(Z - Z_{opt}) + \frac{1}{2}\Delta U^T R \Delta U + r^T\mathcal{E} + \frac{1}{2}\mathcal{E}^T S\mathcal{E} \tag{6.1}$$

CV constraints:

$$\begin{aligned}(q_{diff})_{min_i} - \mathcal{E} \leq (q_{max})_{k+j,i} \leq (q_{diff})_{max_i} + \mathcal{E}, \quad j = 1, 2...P1, i = 1, 2..16 \\ T_{return_{min_i}} - \mathcal{E} \leq T_{return_{k+j,i}} \leq T_{return_{max_i}} + \mathcal{E}, \quad j = 1, 2...P2, i = 1, 2..16\end{aligned} \tag{6.2}$$

MV constraints:

$$\begin{aligned}T_{s_{min}} - \mathcal{E} \leq T_{s_{k+j}} \leq T_{s_{max}} + \mathcal{E}, \quad j = 1, 2...6 \\ P_{s_{min}} - \mathcal{E} \leq P_{s_{k+j,i}} \leq P_{s_{max}} + \mathcal{E}, \quad j = 1, 2, 3, 4 \\ \Delta T_{s_{min}} \leq \Delta T_{s_{k+j}} \leq \Delta T_{s_{max}}, \quad j = 1, 2..6, \\ \Delta P_{s_{min}} \leq \Delta P_{s_{k+j}} \leq \Delta P_{s_{max}}, \quad j = 1, 2, 3, 4\end{aligned} \tag{6.3}$$

In order to display the effect of using a NMPC to control a DHS, two cases of the optimization problem has been investigated. In the first case the controller had full information about the disturbance, meaning it was provided throughout the prediction horizon. In the second case the controller had limited information, i.e., the disturbances were only given at the current sample. The NMPC then had to figure out an optimal combination of the MVs, while minimizing the break of the regulative constraints. By comparing these two cases, the effect of having information beforehand was displayed. In reality the information provided would be something in between, were the plant has historical information available, but the real-time disturbance would slightly deviate from it. As a result has the two cases been compared to the measurements, to observe if the NMPC were able reduce the supply temperature.

By using the provided software from Cybernetica, these two cases has been simulated with disturbances from the first week of February 2019. The sampling frequency was kept the same as during the validation, more specifically 10 minutes. By using CENIT MMI, the history, current value and optimal trajectory of the MVs and CVs were displayed while tuning. This also enabled the possibility of online adjustments of parameters, constants and disturbances. An example is displayed in figure 6.1, where the supply temperature and power consumption [kW] of consumer C, J and O are displayed. The historical value is shown to the left with negative time values, the predicted trajectory to the right with positive time values through the horizon, and finally the current value at time zero. The supply temperature can be observed to increase, while the MV block trajectory shows further increases are planned. The increase is planned due to a predicted future increase in power consumption 15 to 25 hours into the horizon, which the controller has to compensate for early due to the heat delays.

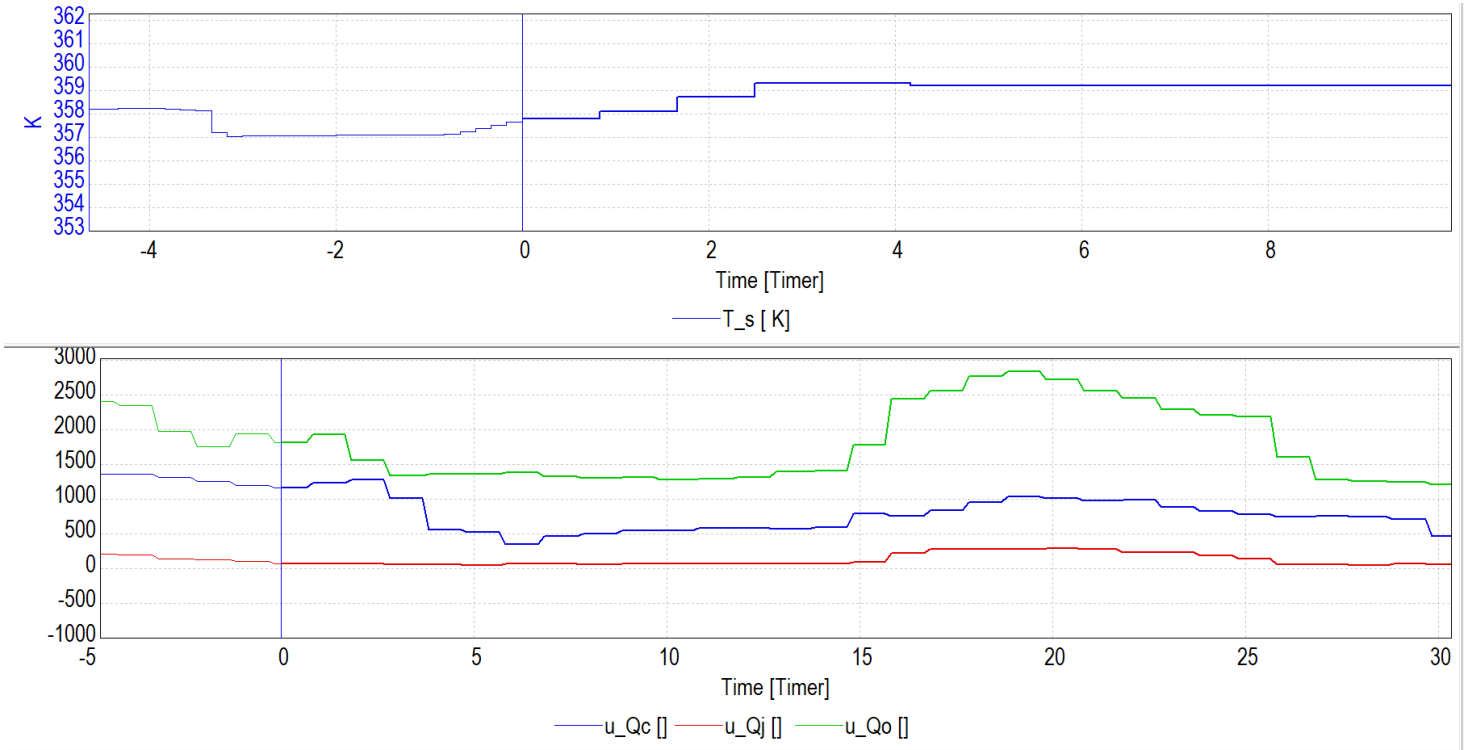

Figure 6.1: Displaying the Cenit MMI

The length of the receding horizon was determined based on the longest time delay in the model. Since the heat propagation has the slowest dynamics, the time delay of the return temperature at each consumer was investigated. The model was therefore simulated with the lowest disturbances from each consumer(causing the lowest mass flows), and with a step in supply temperature. In the setup of the controller, the supply temperature was restrained from increasing more than 1 °C per sample. However in order to have a buffer, a step of 5 °C was performed in order to test the time delay. The horizon length was further determined by the consumer with the longest time delay in the return temperature.

In figure 6.2 and 6.3 the delay of each consumer are shown. It can be observed that consumer J has a distinct longer delay than other consumers, and are therefore the one deciding the horizon length. A step in supply temperature is observed to take about 40 hours to reach steady state at consumer J. Additionally must the effect of last input block be observable by the MPC. The last block in the supply temperature has been set to 250 minutes, which is slightly above 4 hours. The resulting horizon length has therefore been set to 45 hours.

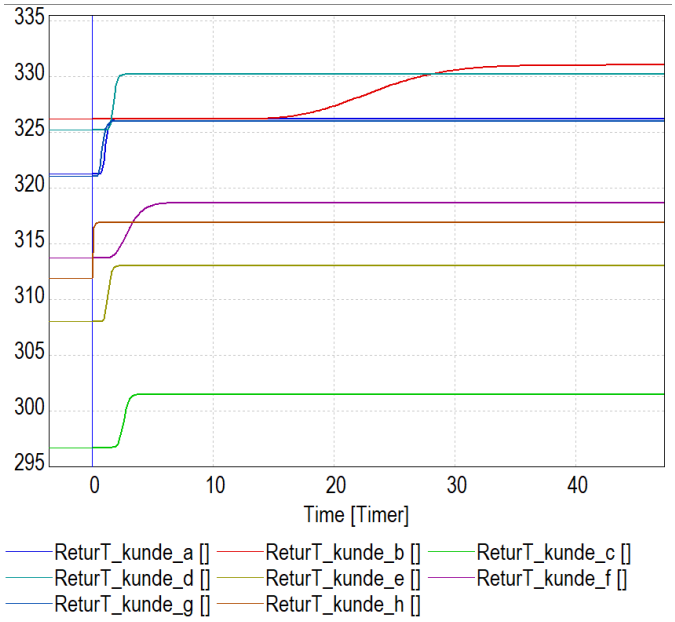

Figure 6.2: Heat delay at consumer A - H after a step in the supply temperature, with low consumption

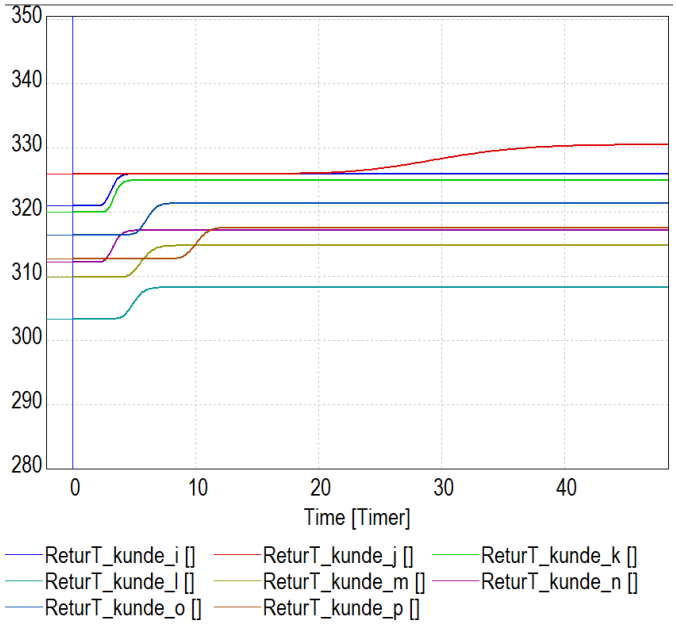

Figure 6.3: Heat delay at consumer I - P after a step in the supply temperature, with low consumption

Moreover must the evaluation points where the MPC can not detect any effect of a perturbation, be removed. This means that all points before the effect of the step must be removed respectively at each consumer. However this process is not straight forward since the time delay will change throughout the simulation. In figure 6.4 and 6.5 the same step in supply temperature is performed, but this time the max power consumption is used at each consumer. On several consumers it can be observed a significantly reduction in delay. This ultimately becomes a trade-off between how the regulatory constraint will be broken. If the evaluation points are set according to the longest delay, there will be occasions where the controller does not evaluate a break in constraint since it is happening to early in the horizon. Opposite if the evaluation points are set according to the shortest delay, there will be occasions where the controller can not detect a change in the CV from the perturbation. This could further cause undesirable behavior from the controller, since it will predict a different model-behavior than what will actual happen.

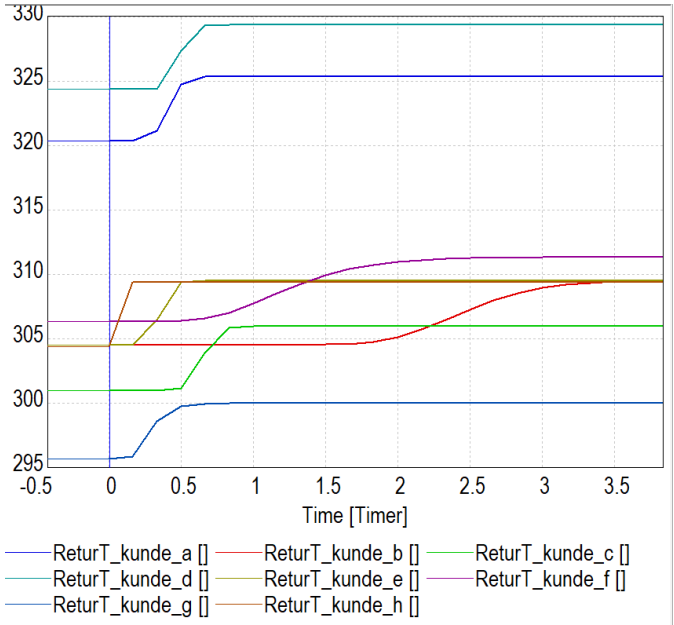

Figure 6.4: Heat delay at consumer A - H after a step in the supply temperature, with high consumption

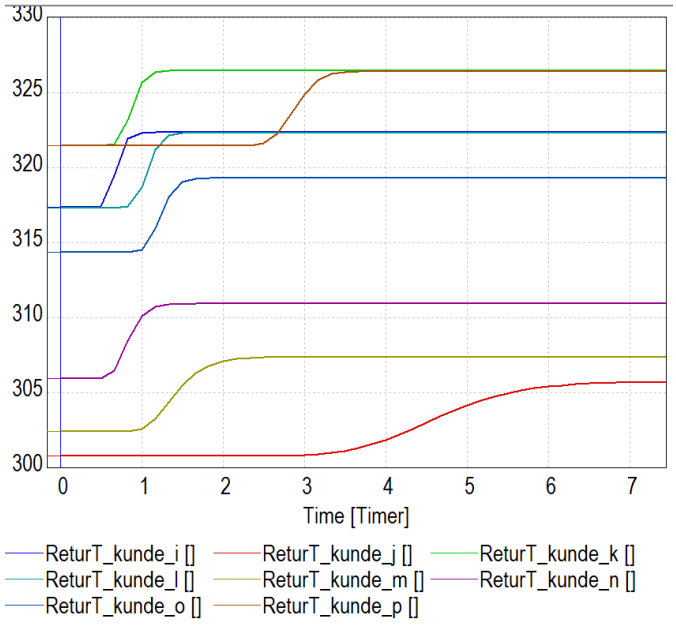

Figure 6.5: Heat delay at consumer I - P after a step in the supply temperature, with high consumption

The best solution would be to change the number of evaluation points dynamically. This way the optimal number of points could be changed in each sample. However this feature was unfortunately not supported in Cenit version 6.9. Instead has an averaged value been used at the consumers where there is a significant difference between the longest and shortest delay. By comparing the four graphs, it can be observed that consumer A, G and H does not have a significant difference in delay. The starting evaluation point at each remaining consumer have further been moved according to the displayed value in table 6.3. The second column displays the largest and then the shortest time delay at the respective consumer. The third column displays the averaged value that will be used to determine the first evaluation point at the consumer.

Consumer	Detectable change [hours]	Averaged value [hours]
B	14-1.5	7.8
C	2.5 - 0.5	1.5
D	2 - 0.2	1.1
E	2 - 0.2	1.1
F	2.5 - 0.4	1.5
I	2.5 - 0.5	1.5
J	18-3.5	10.8
K	2.5 - 0.5	1.5
L	4 - 1	2.5
M	4 - 1	2.5
N	2.5 - 0.5	1.5
O	4 - 1	2.5
P	8-2.5	5.3

Table 6.3: Average heat delay to each consumer

A large amount of time was spent on experimenting and tuning the controller in order to reach the objectives. This included adjusting weights, input blocks and evaluation points based on observed behavior. After an adequate setting was found, the simulation of one week was performed without any changes in the controller.

The tuning was performed with the intentions of having a controller that changed the supply temperature and pressure in a proper manner (e.i., no possible damaging or unphysical control moves), at the expense of spending longer time steering the system to a economic optimum. Due to the lack of specific information regarding the delays of the incineration and pump, the tuning was performed based on the authors subjective opinion of a unphysical behavior.

As described in chapter 3 can limited number of evaluation points be used to decrease the amount of decision variables in the horizon. The temperature related CVs were originally evaluated from 20 minutes, and then every other sample. However were several of the starting points adjusted according to the averaged time delay at each consumer. Since the network pressure were able to change instantaneously, the related CVs were evaluated

from the first sample. Further were evaluation performed every sample the first hour, and then every 20 minutes.

Input blocking were also utilized in order to further reduce the number of decision variables. The pressure propagation was expected to happen instantly and therefore was the input blocks set close in the beginning, and then constant throughout the rest of the horizon. The temperature propagation has the opposite characteristics, and therefore were the blocks more spread out in addition to be set slightly further in the horizon.

Moreover was an upper and lower limit added to both MVs. These constraints were not included in the objective function, but operated as a hard physical constraint at the plant. The upper limit on the supply temperature was set to 400 K, and the lower limit was set to 300 K. The upper limit on the supply pressure was set to 16 bar. Additionally was the maximum pressure before the mass flow got reduced, set to 15 bar (Implemented as a constant third MV). This way the pressure did not go to 16 bar, unless absolutely necessary. The lower limit in the supply pressure was set to 0. A final limit was set on the possible change in each MV per sample. This was implemented in order to prevent possibly damaging control moves. The temperature was restrained to 1 °C per sample, while the pressure was set to 10 bar per sample.

6.2 Result

The two optimization cases are detailed below in their respective subsection. Through the tuning process it was observed that using both unreachable setpoint and infeasible soft constraints gave the best results. Therefore has both been used together during the simulations. The final tuning values on the MVs and CVs are further shown below:

Objective: Produce an adequate return temperature and maximum deliverable mass flow at each consumer, while keeping the supply pressure and temperature at a minimum.

Horizon length: 45 hours

MV input blocking (minutes):
T_s: [50, 100, 150, 250] Weight on ΔT_s: 200
P_s: [10, 20, 50, 200] Weight on ΔP_s: 15

CV setpoints:
T_s = 300, weight: 1
P_s: 0, weight: 0.7

CV constraint:
$Tr_{consumer_i}$ = [298,400], i = 1,2...16, weight: 1000
$q_{diff,i}$ = [-100,0], i = 1,2...16, weight: 10 000
T_s = [-100,300], weight: 10
P_s: [-100,0], weight: 7

CV evaluation points:
$q_{diff,i}$ = Every 10 minutes for one hour into the horizon, then every 20 minutes. i = 1,2...16.
T_s = From 20 minutes into the horizon, then every 20 minutes
$Tr_{consumer_{A,G,H}}$ = From 20 minutes, then every 20 minutes
$Tr_{consumer_B}$ = From 470 minutes, then every 20 minutes
$Tr_{consumer_{D,E}}$ = From 70 minutes, then every 20 minutes
$Tr_{consumer_{C,F,I,K,N}}$ = From 90 minutes, then every 20 mintues
$Tr_{consumer_J}$ = From 650 minutes, then every 20 minutes.
$Tr_{consumer_{L,M,O}}$ = From 150 minutes, then every 20 minutes
$Tr_{consumer_P}$ = From 320 minutes, then every 20 minutes

6.2.1 Dynamic Optimization with full information

In the first case the disturbances are included in the prediction horizon, meaning that the MPC receives information about the disturbance in advance. This gives the MPC an enormous advantage, considering the large time delays in the network, to prepare for future changes in the power consumption.

In figure 6.6 are the mass flow difference, q_{diff}, for consumer A, C, D and O are plotted. The rest of the consumers are displayed in appendix B.19 - B.21. The purpose of the graph is to display the consumers that had their respective regulative constraint on q_{diff} active at some point in the simulation. The most important part of the graph is therefore at the upper part of the y-axis. It shows that there are no consumers that are receiving a higher flow than physically possible from the pump. It can be observed that the flow difference drops to negative values three times when consumer O has the constraint active, before stabilizing close to zero relatively fast. During this short amount of time there are no consumers that has their constraint active, which means there are more pressure than required in the system. However during major part of the simulation, there are always one or several consumers having their respective constraint active. An additional observation can be made on the consumers that does not have the constraint active at some point. Their q_{diff} are then negative, since q_{max} at their respective substation is larger than the required mass flow.

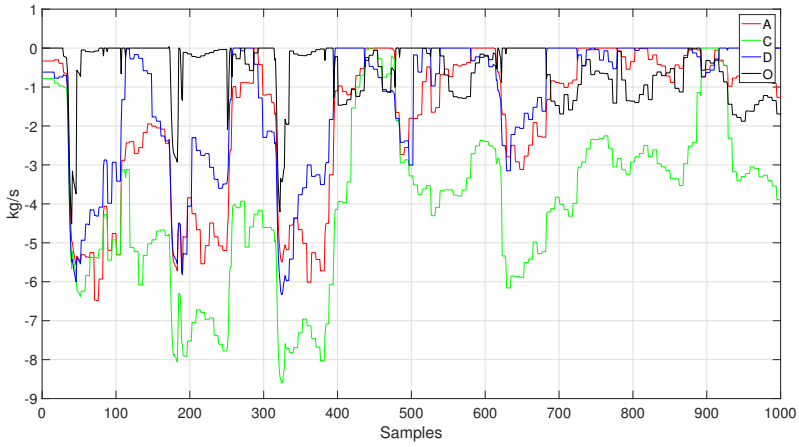

Figure 6.6: Mass flow difference at consumer A, C, D and O

Moreover is the supply pressure displayed in figure 6.7. It can be observed to have a cyclical change, especially in the first part of the week, which corresponds to the days in the simulation. The pressure is observed to vary between 15 and 8 bar during the first part of the week. At three instances the pressure reaches the maximum allowed pressure of 15 bar, with smaller oscillations right before or after. During the rest of the week the pressure varies between 8.5 and 4.2 Bar.

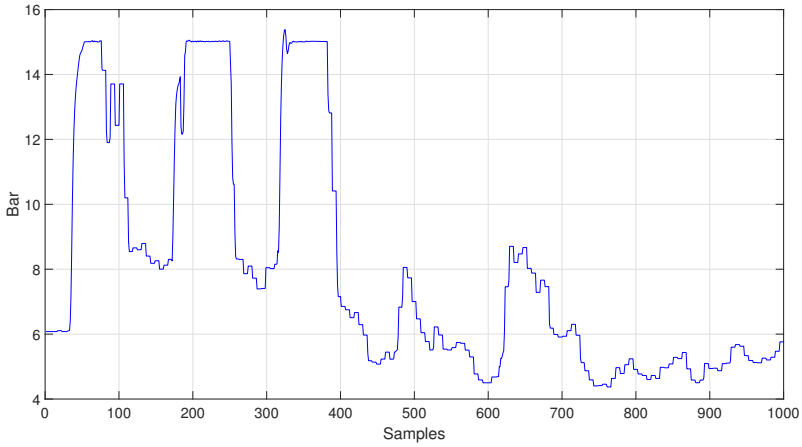

Figure 6.7: Supply pressure at the plant

In figure 6.8 the modeled mass flow is compared to the measurement. Apart from the similar deviations as described in chapter 5, it can be observed a lower modeled flow at the two peaks of consumption at sample 210 and 340. At the lower peak at sample 50, the model appears to somewhat match the measurement. These results indicates the cut in mass flow.

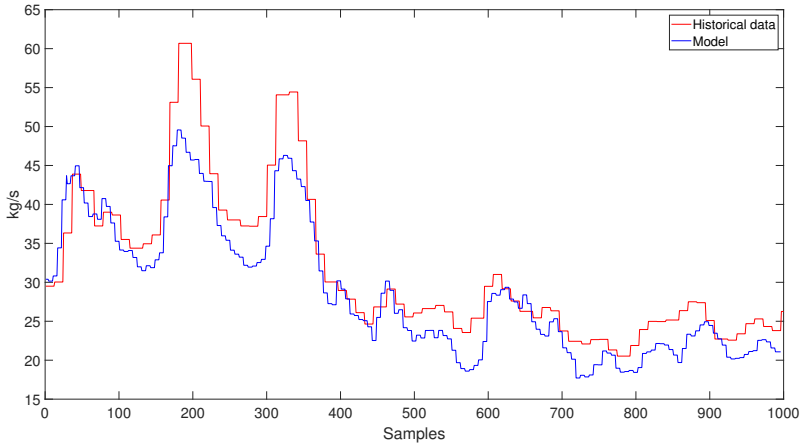

Figure 6.8: Comparison between the measured and modeled total mass flow

In figure 6.9 the supply temperature at the plant is displayed. The temperature is observed to vary between 91 and 84 °Celsius the first part of the week. Two occasions of oscillation can be observed at sample 260 and 450, although they only last for a couple of samples. Additionally can a large spike be observed between sample 400 and 415. During the second part of the week the supply temperature is observed to vary between about 87 and 84 °C. The temperature appears more stable, with only one major drop at around 870 samples. As an overall observation are the average supply temperature increased during the second part of the week, while the ambient temperature and consumption decreased during this period.

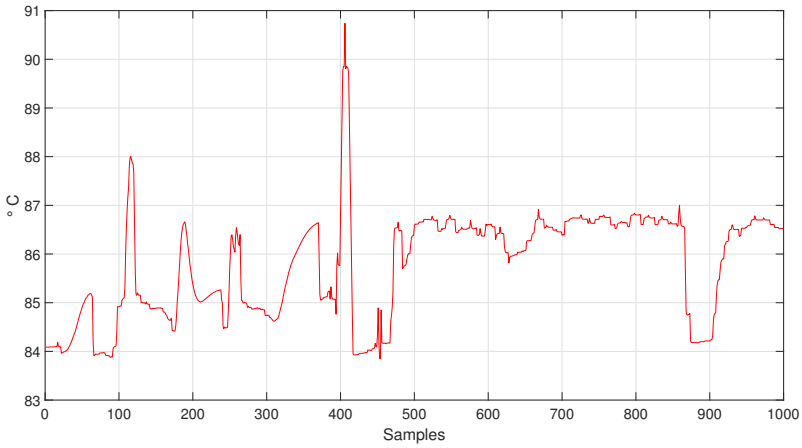

Figure 6.9: Supply temperature at the plant

The measured supply temperature can be observed in Appendix B.1. When subtracting the measurement from the optimized modeled temperature, the difference can be plotted as shown in figure 6.10. During the first part of the week, the mean temperature difference is 12.88 °C, where a positive number indicates that the measurements are larger than the model. During the second part of the week the average difference is about 8.33 °C. The plot contains some oscillations as well, but they are likely to originate from the oscillations in the modeled supply temperature.

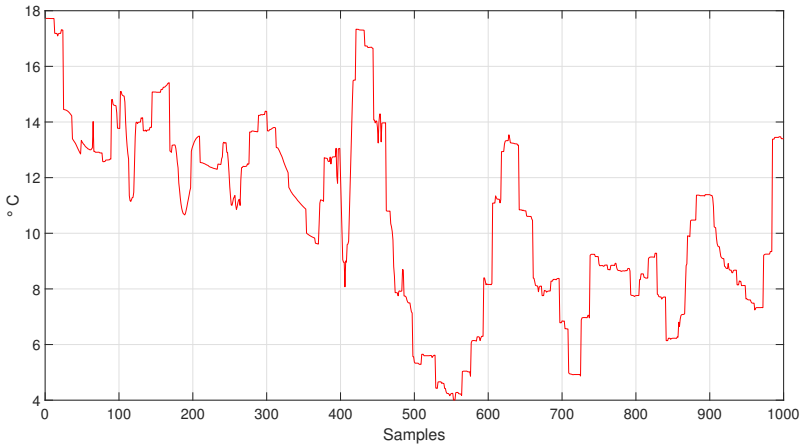

Figure 6.10: Measured supply temperature subtracted the optimized modeled supply temperature

In figure 6.11 and 6.12 are the return temperature of consumers C, G, J and O displayed. The rest of the consumers are displayed in appendix B.22 - B.26. The purpose is to display the consumers that at some point had the regulative constraint on the return temperature either active or were breaking it. The most important part of the graph is therefore at the lower part of the y-axis. It can be observed during a large part of the simulation, that at least one of the consumers are having either the constraint active at 25 °C, or they were breaking it.

During the first part of the week all consumers have their respective constraint active at some point. Consumer C is active for the majority of the time, while consumer J, G and O only touches the constraint for a short amount of time during large drops in temperature. It can be observed that the return temperature of consumer C increases repeatedly when the return temperature at other consumers are predicted to drop. Consumer O is the only consumer to break the constraint, which happens between sample 200 and 220 by about 1.5 °C. During the second part of the week, consumer C has more or less its constraint active the whole period. The return temperature appears to not settle completely, but with smaller oscillations through the rest of the simulations. As a side note can the return temperature of consumer J and G be observed to stutter, with relatively abrupt movements, compared to consumer C and O throughout the simulation. This is simply because the implemented disturbances are not filtered. Instead they are constant for one hour, and then

changes instantly to the next.

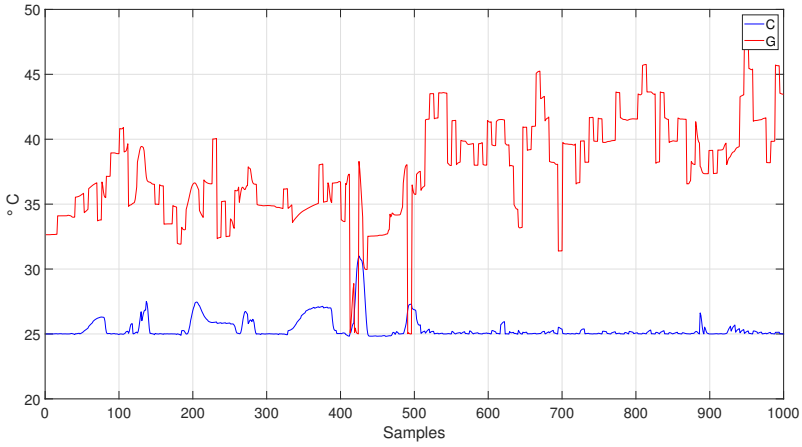

Figure 6.11: Return temperature of consumer J and O

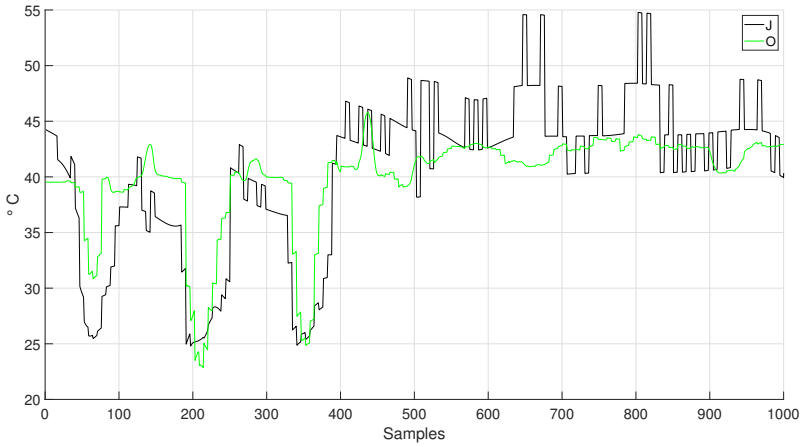

Figure 6.12: Return temperature of consumer C and G

Furthermore are the return temperature at the plant displayed in figure 6.13. The temperature is observed to vary between 39 and 44 °C during the first part of the week. Apart from the transient period the first 100 samples, three distinct days can be spotted out. At sample 110, 270 and 400 the returning water from hours of high consumption is observed. The average temperature is observed to be higher during the second part of the week. Apart from a large drop at around sample 900, the temperature is varying between 44.5 and 40.5 °C.

Similarly as performed with the supply temperature, can the modeled return temperature be subtracted from the measured in order to compare the two values. In figure 6.14 it can be observed during the first part of the week a 10.71 °C lower return temperature in the modeled return temperature compared to the measurement. During the second part of the week the average difference is reduced to 8.55 °C.

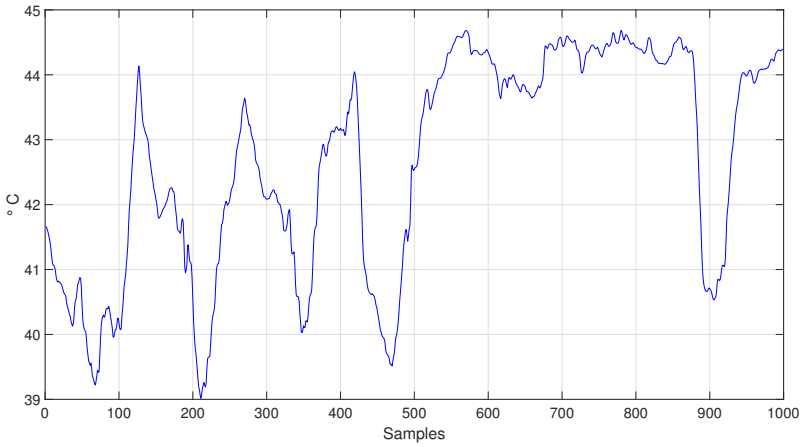

Figure 6.13: Return temperature at plant

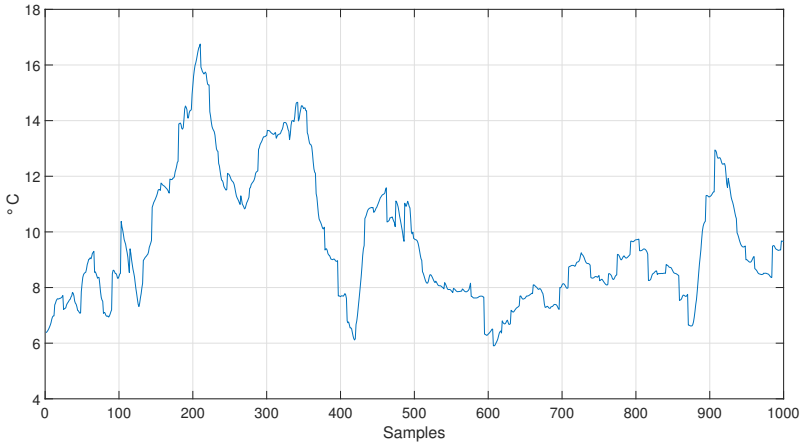

Figure 6.14: Measured return temperature subtracted the optimized modeled return temperature

6.2.2 Dynamic Optimization with limited information

In the second case the same set of disturbances were fed to the model and controller, but the controller did not have information about the disturbance in the predicted horizon. The case therefore represents a situation more similar to the current setup at Stjørdal where the plant only reacts to changes at the current sample. The controller then has to produce the required supply pressure and temperature in a reactive manner. The setup in the controller was kept unchanged, and therefore were larger oscillations expected. This was performed in order to more easily be able to compare the two cases. An alternative way would have been to made the controller slower, by increasing the penalty on input changes. This would ultimately caused less oscillations, but the breaking of the regulative constraints would have been much more comprehensive.

In this second case only the results displayed in this chapter, has been included. The was done in order to decrease the length of the appendix, and since the remaining of plots were not relevant for discussion. In figure 6.15 the mass flow difference, q_{diff}, is plotted of consumer A, C, D and O. These consumers had at some point the constraint either active or were breaking it through the simulation. Several positive spikes can be spotted at all consumers during the hours of having their respective constraint active. Especially the largest consumer, O, has the largest spikes at samples 40, 190 and 340 of approximately 3 kg/s. During these hours the actual delivered mass flow is larger than the deliverable flow, which is unphysical behavior of the model. Since the pressure is able to change quickly, it is however able to compensate for the immediate changes after a few samples. This brings the pressure to sufficient levels and cuts the mass flow if necessary.

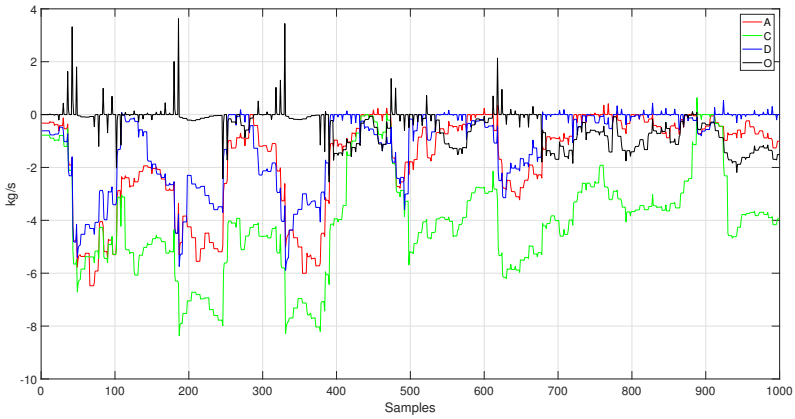

Figure 6.15: Mass flow difference at consumer A, C, D and O

Furthermore in figure 6.16 are the supply pressure at the plant displayed. During the first part of the week it can be observed to have a cyclical change, which corresponds to the three first days in the simulation. The pressure is observed to vary between 15 and 8 bar, with three spikes at appearing right after a large increase. The spikes reaches the physically maximum allowed pressure of 16 bar, then quickly settles to the maximum pressure of 15 bar. During the rest of the week the pressure varies between 8.5 and 4.2 Bar.

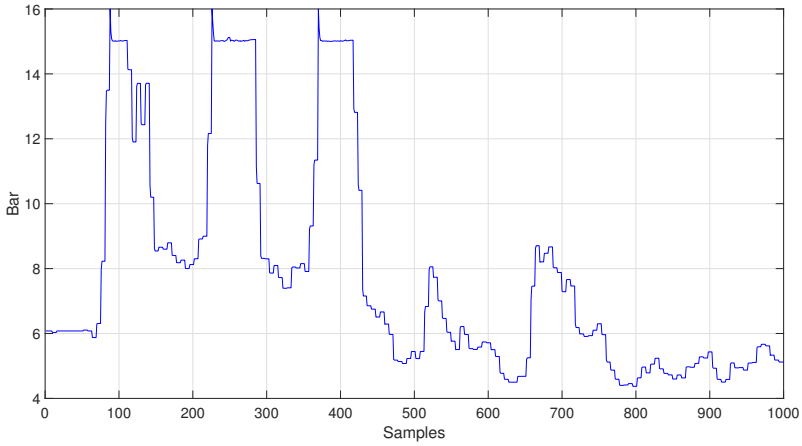

Figure 6.16: Supply pressure

The supply temperature at the plant is displayed in figure 6.17. The immediate observation is that the controller had to make significantly more aggressive changes to the temperature. Especially during the second part of the simulation there are large oscillations occurring, and the temperature is barley stable from one hour to the next. However can there be observed hours with significantly reduced oscillations between sample 840 and 950. The temperature is ranging between 91 and 84 °C during the simulation, with distinctively lower temperatures during the first 400 samples.

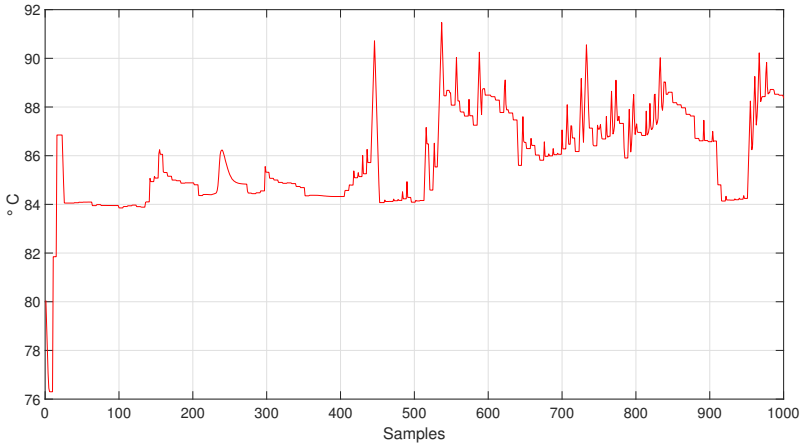

Figure 6.17: Supply temperature

Furthermore is the return temperature of consumer C, G, J, and O displayed in figure 6.18 and 6.19. These are the consumers that had active constraints on their respective return temperatures during the simulation. During the first part of the week all four consumers are at some point breaking the constraint of 25 °C. Consumer O has the largest deviation at sample 240 of approximately 2.5 °C, which is close to reach the hard constraint at 22 °C. At consumer G, J and O the breaking of constraint appears due to large but briefly drops in return temperature. Since they quickly increase after the drop, the amount of time below 25 °C is relatively short. In contrast is consumer C close to the constraint during the majority of time. During the second part of the simulation, consumer C is the only one with the constraint active. The return temperature can however be observed to oscillate far more compared to the first part of the week, and more samples are observed below the constraint. However the oscillations appears to slow down from sample 840.

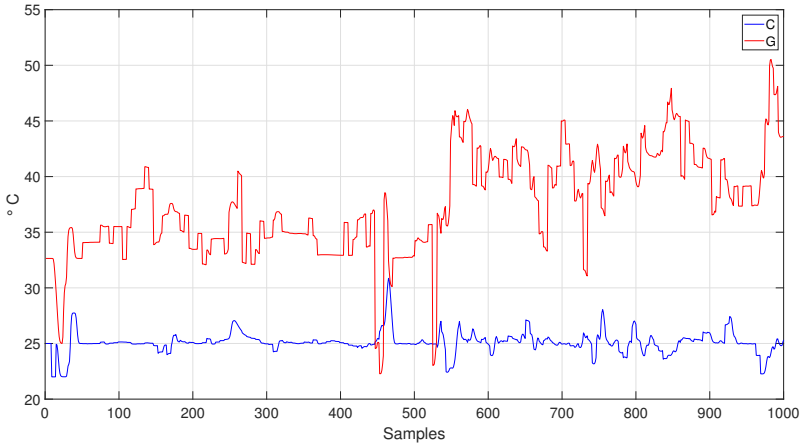

Figure 6.18: Return temperature of consumer C and G

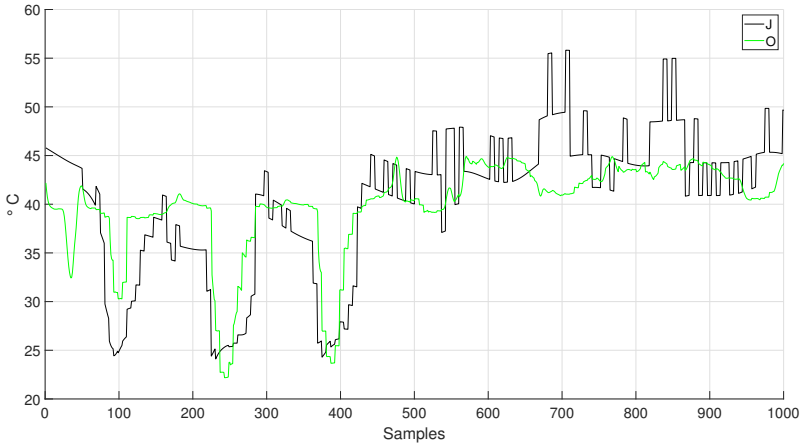

Figure 6.19: Return temperature of consumer J and O

In figure 6.20 are the return temperature at the plant displayed. During the first part of the week the temperature is ranging between 42.5 and 38.5 °C. The cyclic pattern of three days can be observed between sample 100 and 500. Through the second part of the week the return temperature is ranging between 46.5 and 41 °C. It can also be observed an increase in the average temperature compared to the first part of the week.

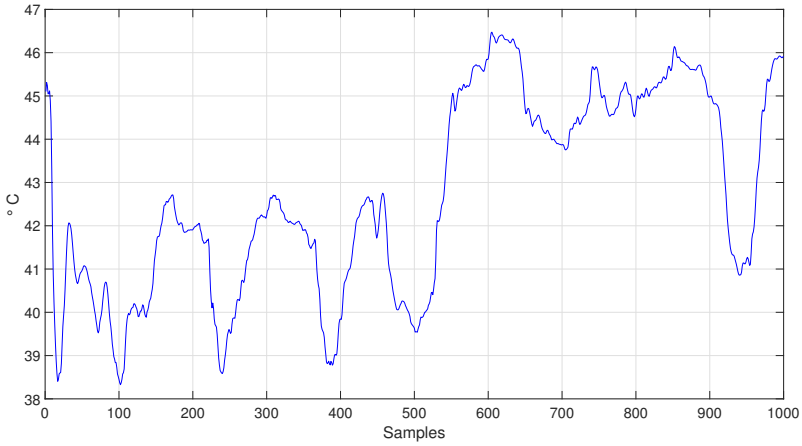

Figure 6.20: Return temperature at the plant

6.3 Discussion

6.3.1 Full information of the disturbance

The utilization of a predictive controller can be an important tool in order to optimize a DHS in regards of economic and regulatory objectives. The availability of the power consumption beforehand can be a crucial factor in the performance of the controller. The results showed an economic minimization as well as fulfilling the regulatory objectives, when full information about the consumption was present. The modeled supply temperature was significantly reduced compared to the historical measurements. The consumers were therefore able to extract the same amount of energy with a reduced inlet temperature, while the heat loss to the surroundings were reduced. Less unused energy was therefore transported back to the plant, and were instead being utilized by the consumers. The supplied pressure from the simulation was not comparable with the historical data due to the modelling approach in chapter 5. Instead was the output used to support the explanations of other controlled variables.

During the first part of the week the overall consumption was both larger and fluctuated more due to the colder weather. This further required large adjustments in pressure in order to satisfy the required power consumption. As a result did the pressure reach the maximum limit at three occasions during the first part of the week. The mass flow was therefore cut in order to prevent unphysical behavior, and can be observed when compar-

ing figure 5.20 and 6.8 where the latter modeled mass flow appears lower at the respective time instances. When comparing the supply pressure with the regulative constraint on q_{diff}, it can be observed that consumer O caused the need to maximize the pressure since it has the constraint active through those samples. This can additionally be observed in appendix B.28, were the mass flow of consumer O are seen close to constant during these samples, while the consumption increases as displayed in appendix B.8. The increase was of such magnitude that the controller chose to increase the pressure slightly beforehand in each occasion, in order to prevent a break in the regulative constraint.

The reduction in mass flow further caused the return temperature to drop significantly but briefly during these samples. However the chosen evaluations points, based on the average time delay at each consumer, led to consumer O breaking the constraint during a few hours. Since consumer O only had the constraint active during hours of large consumption, the controller did not consider the break in constraint since it happened before the CV was evaluated. This type of deviation could have happened at any of the consumers close to the constraint, depending on the delay and network temperature. As a solution would perhaps a dynamic number of evaluation solve this issue. At the same time are consumer C, J and G observed to only touch the constraint but not breaking it, while having a large power consumption. There are different reasons for this behavior, and therefore will each consumer be described separately in more detail:

- Consumer J has a large time delay due to the geographical distance from the plant. Compared to the second case where the controller had no information about the disturbances beforehand, the return temperature were observed to only slightly break the constraint during the first part of the week. In this case the controller has no possibility to immediately influence the breaking of the constraint, due to the delay in the network. This shows that in the first case, the controller was only preventing a slight deviation and it could have been much larger if the consumption had been higher. An example can be shown at sample 350 in figure 6.12, were both consumer J and O are touching the constraint. In figure 6.19 at the same sample, the same return temperatures can be observed to only slightly break the constraint.
- Consumer G has in contrast close to no difference in time delay, since it is geographically close to the plant. Therefore could the evaluation points be set close to zero, and as a result was the controller able to adjust the temperature in order to prevent a break in constraint.
- Consumer C had a medium time delay, and could therefore be assumed to have smaller deviations from the constraint. However consumer C are during major parts of the simulation the only one with active constraint on the return temperature. Therefore would the break in constraint only happen for a brief sample, before returning back to the constraint due to the next evaluation point in the horizon. However due to other consumers having their constraint active regularly, the deviations are not easily spotted. These smaller constraint breaks are visible when significantly zoomed in as shown in appendix B.27.

Due to the large and brief drops in return temperature observed at consumer G, J and O, are the supply temperature also observed to fluctuate in order to fulfill both the regulatory

and economic objectives. The largest reduction in supply temperature, compared to historical data, was however observed during these first three days by approximately 13 °C. This indicates that the plant increases the network temperature buffer during colder days, in order to satisfy the required energy from the consumers. The controller can however predict exactly when a increased temperature is required, and therefore does not require such a buffer. Therefore are perhaps the largest reductions possible during colder days, when the biggest buffer is present with the current setup. However if the controller were to be implemented in a real plant, a small buffer would be recommended in order to ensure a high enough temperature.

Between sample 390 and 450, were several spikes and oscillations observed in the supply temperature. They can be connected with the two large reductions in return temperature at consumer G. Due to the geographical closeness to the plant, the controller waits as long as it can before then increasing the supply temperature relatively fast. The oscillations occurs because of the square waved return temperatures of consumer G, which are further a result of the unfiltered disturbance and a low mass flow. Since the evaluation points are set every 20 mintues, the ”kinks” could drop below the constraint in the horizon between these points. The same effect can be observed around sample 250, where consumer J causes brief oscillations. However at sample 200, the mass flow is large enough to smooth out the temperature. A solution would be to filter the disturbance in order to smooth the curve, or evaluate the the output in every sample in the horizon. These movements in the supply temperature were not observed as unphysical since they took several hours to perform. However could a different approach been taken if it was desirable to have slower changes on the input, by starting to increase the temperature earlier.

During the second part of the week the consumption is reduced due to higher ambient temperatures. The pressure is therefore significantly reduced, and less aggressive adjustments had to be made. This can be seen in figure 6.6 where q_{max} has close to no oscillations. As a result are there no instances where the mass flow is cut, and only the deviation observed during the validation in chapter 5 causes the deviations in figure 6.8.

The warmer weather causes the consumption do reduce, which typically would increases the return temperature at the consumer. A natural control move would therefore be to reduce the supply temperature. However this is not the case during the second part of the simulation due to the characteristics of consumer C. As displayed in chapter 5, are the sensitivity in the return temperature relatively low when a step in consumption is made. Additionally are the return temperature observed to reduce when the consumption is reduced. This restrains the controller from lowering the supply temperature, and instead it must be increased. As a result has consumer C the regulative constraint active through the rest of the simulation, since no other consumer is close to reach 25 °C. This also causes the difference between the modeled supply temperature and the measurement to reduce, since they move in different directions.

Due to the low sensitivity at consumer C, are the supply temperature observed to be more stable and with only smaller fluctuations. Apart from a larger adjustment at 880 samples, it barley moves one degree through the rest of the simulation. At the same time are the return temperature at consumer C observed to slightly oscillate at the constraint through the rest of the simulation. This is again because of the placing of the evaluation points.

An average time delay was chosen, and therefore will the first number of points have no sensitivity when the power consumption is low. Additionally are the consumption changing every hour, with a low water consumption. Therefore will also the squared waved consumption affect the result. Together this causes smaller oscillations in the predictions, and the MPC were observed to regularly switch between optimal trajectories. However at about sample 900 the oscillations are almost gone. This is because of a large increase in consumption at consumer C, which further causes the the supply temperature to rapidly decrease. Due to the large increase, the evaluation points match the delay better during these samples.

6.3.2 Limited information of the disturbance

In the second case the controller did not have information about the disturbances in the prediction horizon. Overall this forced the controller with reactive behavior, since the disturbance had to occur before the controller could compensate for the effect.

In the first part of the week, the large increase in consumption can be observed to break the constraint on q_{diff} at several occasions. The large increase in consumption at consumer O causes unhpysical behavior in the model, where the delivered mass flow is observed to be lower than the received flow at the consumer. However the break of the constraint were quickly removed by relatively aggressive adjustments in the pressure. These large increases caused the pressure to spike up to the maximum allowed pressure of 16 bar, before quickly settling down to 15 bar. This is because the controller is using any means necessary to keep the regulative constraint on q_{diff} at zero or lower. It can also be observed that the pressure is increased more slowly in the beginning compared to in case one, which is simply because the controller does not know about the incoming large increase in consumption.

The supply temperature is also increased in order to compensate for the increased consumption, but several of the return temperatures break their respective constraint due to the large delays in the network. However, as already discussed above, are the amount of deviation from the regulative constraint relatively low. Consumer J and C goes barely below the constraint, while consumer G and O breaks it by a couple of degrees. This shows that the majority of reductions in return temperature can be handled without knowing about the consumption beforehand. However this result has to be seen in context with the low sensitivity at the return temperature of consumer C. Since the return temperature changes relatively little during the whole simulation, the consumer keeps the supply temperature from reducing further. When the overall consumption increases, the network has sort of a buffer because of consumer C, which are further used by the other consumers. If there had been larger sensitivity at consumer C, there would have been a larger differences between case one and two. Since the low sensitivity was observed to be a deviation in chapter 5, this result should be further tested. The solution to the breaking of the regulative constraints, would be to have a larger buffer, of both heat and pressure, in the network. By increasing the lower constraint on the return temperature at each consumer and reducing the upper constraint on q_{diff}, there would be a larger energy buffer in the network.

During the second part of the week The pressure is able to handle the variation in consump-

tion adequately. Due to the warmer weather, there are only small occasions of breaks in the regulative constraint on q_{diff}. The supply temperature was however observed to oscillate far more during the second part of the week, as well as the return temperature at consumer C. This is because of the issues explained earlier regarding consumer C. Due to several evaluation points having no sensitivity and a square waved disturbance that changes every hour, larger oscillations in the temperature were unavoidable. However the oscillations are observed to significantly reduce from sample 850. When seen in context with the consumption, it can be observed to have relatively small changes from sample 850 to 930, before it increases drastically. It is therefore safe to say that reduced changes from hour to hour in the disturbance or a large enough flow rate, contributes to less oscillations in the supply temperature.

As a final note would the scenario of increasing the penalty on the change in supply temperature, making the controller slower, most likely only have affected the return temperature of consumer C and G. Consumer J and O would probably have been close the same due to the behavior already discussed.

6.4 Conclusion

In this chapter the use of DRTO in order to find the optimal solution based on both regulatory and economic objectives, has been studied. In the first case the disturbances were implemented in the prediction horizon, while in the second case the disturbances were unpredicted. Both cases utilized the same setup in the controller.

In the first case the controller was found to perform well to the predicted power consumption. Compared to historical data, the supply temperature was on average reduced by approximately 13 °C during cold days, and by approximately 8 °C during days with higher ambient temperatures. This shows that the biggest potential of reducing the network temperature, is during colder days when the largest temperature buffer is present with the current setup. Only at one occasion was a regulative constraint broken. This was because of a fixed number of evaluation points on the return temperature at each consumer, which were based on a average time delay. Ultimately this became a trade-off between breaking the regulatory constraints or having oscillations in the supply temperature. A possible solution would be to implement dynamic number of evaluation points that can change from sample to sample. This way the changing time delays in the network can be accounted for.

Moreover was the supply temperature observed to increase during days with warmer ambient temperatures. This was because of the characteristics of the heat exchanger at one of the large consumers. The return temperature was observed to reduce when the consumption reduced. Together with low sensitivity, this forced the controller to slightly increase the supply temperature when the ambient temperature increased.

In the second case the controller was required to act reactively to the disturbances, which ultimately required more aggressive control on both the supply pressure and temperature. This increased the amount of oscillations in the temperature, especially when the consumption was low. This was again due to the fixed number of evaluation points. Addi-

tionally was the constraint on the return temperature observed to be broken by a relatively small amount, although the time delays to several of the consumers were large. It was discovered that the low sensitivity in the return temperature at consumer C, and the fact that consumer C had its respective constraint active during the majority of the simulation, saved several of the other consumers. This was because the controller could not lower the supply temperature significantly during low consumption, and consumer C therefore created a temperature buffer for the other consumers. If the sensitivity had been larger, there would have been a larger difference between these two cases.

Chapter 7

Overall Conclusions

In this thesis, a plant replacement model of the DHS at Stjørdal has been developed. The model includes the heat and pressure propagation through the network, together with a consumer substation for each aggregated consumer. Moreover has a DRTO been utilized in order to find the optimal combination of supply temperature and pressure based on both regulatory and economic objectives.

Apart from minor deviations during peak consumption, the modeled mass flow and return temperature at the consumer matched the measurements relatively well when validated. However the return temperature at large consumers were observed to have low sensitivity compared to the measurements. This was because the model relied heavily on a linear correlation between the power consumption and mass flow, which did not catch the characteristics of the larger consumers accurately enough. As a consequence the controller became relatively restrained from adjusting the temperature during optimization, since one of the large consumers had in general a low return temperature throughout the simulation. Only occasional large reductions in return temperature at the smaller consumers, required a reaction in advance. During warmer weather, were the controller required to increase the network temperature, due to these challenges. The effect of the low sensitivity, became particularly evident when the NMPC was tested in the second case. Without any information about the power consumption in the prediction, the breakage of the regulative constraints only increased slightly. The difference between these two cases could have been quite different if the sensitivity at the large consumer had been more accurate.

Moreover were the controller able to reduce the supply temperature on average between 8 and 13 °C, with one occasion were a regulative constraint were broken. Additionally were oscillations observed in the temperature during low flow rates. Both of these challenges were a result of using a fixed amount of evaluation points on the return temperature. This is because the delay in the heat propagation changes according to the mass flow of each respective consumer. By using a fixed amount of evaluation points it ultimately became a trade-off between breaking the regulatory constraint, or having oscillations in the supply temperature. In other words there were always points either with no sensitivity (large de-

lay), or points that should have been included because it had sensitivity (short delay).

The modelling approach of the mass flow distribution made the pressure incomparable during validation and optimization. However the results showed that the pressure was kept at adequate levels in order to provide the consumer with the requested flow. If the requested flow was predicted to become larger than the deliverable mass flow, a cut was performed.

Due to these challenges should further investigations be performed. More specifically should the model be simulated during longer periods of time (e.g, a month or a year), in order to observe how it handles different combinations of disturbances. In addition should the modelling approach of the consumer substation be investigated, in order to further test the challenges with the heat exchanger at large consumers.

Chapter 8

Future work

From the results and discussions in chapter 5 and 6, has several further experiments been suggested. Some of these will be repeated in this chapter, while additional will be added. The measurements from the first week of February 2019 has been used for all simulations in this thesis. This includes a linear correlation between power consumption and mass flow, which became the basis to calculate the mass flow through each consumer. The correlation was observed to be somewhat inaccurate during hours of peak or close to zero consumption. Inclusion of different correlations depending on the consumption level may be further investigated to increase the coefficient of determination.

Based on the deviations during validation, and possible measurement errors, it would be advisable to further test the process model and controller with measurements over a longer time period (or just a different time period). This way the correlation can be further tested, and possibly updated to include a larger span of measured consumption. Especially the time delay at each consumer could prove to vary on a larger scale than observed in this thesis, which needs to be investigated. As described in chapter 5 was a correlation between the measured power consumption and return temperature observed at some of the consumers, but others had too large spread on the datapoints. If a larger span of measurements were investigated, a correlation could perhaps be found at all consumers. This way the mass flow and return temperature could be found with a different correlation. This could possibly be used to overcome the lack of sensitivity observed on the return temperature at large consumers. A final addition to the use of larger span of measurements, is that the observed possible errors in the measurements can be further investigated. These deviations could truly be errors, or the water consumption could actually be larger due to for instance left out consumers in the network.

Moreover was the delay at each consumer used to determine the cut in evaluation points. However this solution is not optimal due to the issues described in chapter 6. A better solution would be to use a dynamic number of evaluation points, that could change from sample to sample. This could however increase the computation time. In case one was the average computation time of each sample about 19 seconds, and therefore are there sig-

nificant possibilities of adding extra features. The resulting evaluation points could then be adjusted according to the time delay, and therefore prevent the issues described in this thesis. According to Svein Olav Hauger, Senior Specialist at Cybernetica, should this solution be possible with newer versions of Cenit.

By using the correlation to calculate the mass flow at each consumer, the optimal combination between supply pressure and temperature becomes significantly reduced. This is because there are many combinations of mass flow and delta temperature at the consumer, that could produce the same amount of power. By restricting the mass flow based on the historically observed correlation with the power, several combinations are not considered. The new local optimum could therefore be different from the one achieved in this thesis. However in order to include this possibility, the mass flow at the consumer has to be calculated with a different approach. For instance measuring the valve position, mass flow or temperature on the secondary side of the heat exchanger, could open the possibility of using different approaches. Additionally has global analysis of the optimization problem not been performed, and further investigation could be attempted to test if the discovered local optimum also is a global optimum.

Furthermore could perhaps an even better result be obtained if the disturbances were filtered beforehand. In a real world would the consumer not have a constant power consumption for one hour, and then immediately change it to a new constant value the next hour. By filtering the disturbance, some of the oscillations in the MVs and ”kinks” in the CVs could possibly have been avoided.

As mentioned in chapter 2 was the plant model not included in this thesis. Instead was the plant assumed to be able to produce the required setpoints from the MPC at all times. By including a plant model, the constraints in the supply temperature and pressure could be more accurately set. Additionally could the economic objectives be set more accurately.

Appendix A

Tables

Number	D1 [m]	D2 [m]	D3 [m]
1	0.1	0.114	0.16
2	0.1	0.114	0.180
3	0.1	0.114	0.225
4	0.125	0.139	0.25
5	0.125	0.139	0.225
6	0.15	0.168	0.25
7	0.15	0.168	0.5
8	0.2	0.219	0.315
9	0.2	0.219	0.355
10	0.25	0.273	0.4

Table A.1: Combinations of pipe and insulation diameters in the network

Day	Lowest Temperature	Highest Temperature
1	-13.3	-2.8
2	-18.5	-8.5
3	-14.1	0.2
4	-2.9	4.9
5	-2	3
6	-4	4.8
7	-3.3	2.6

Table A.2: Ambient temperature at Stjørdal

Appendix B

Figures

B.1 Historical Data

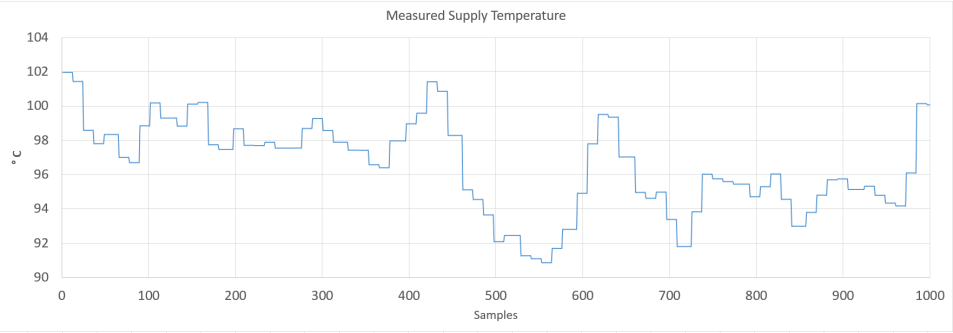

Figure B.1: Measured Supply Temperature

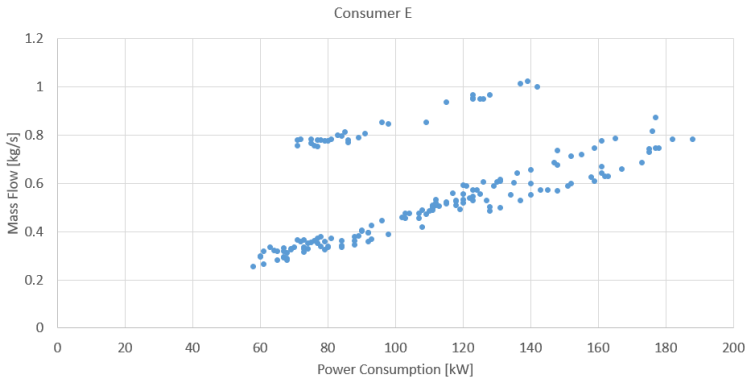

Figure B.2: correlation between mass flow and power consumption of consumer E

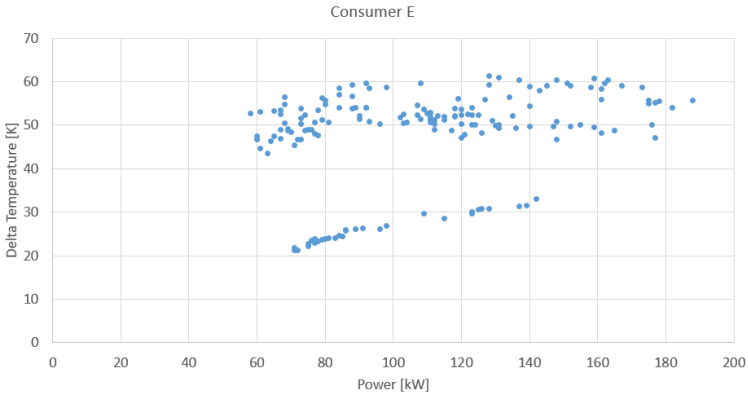

Figure B.3: correlation between return temperature and power consumption of consumer E

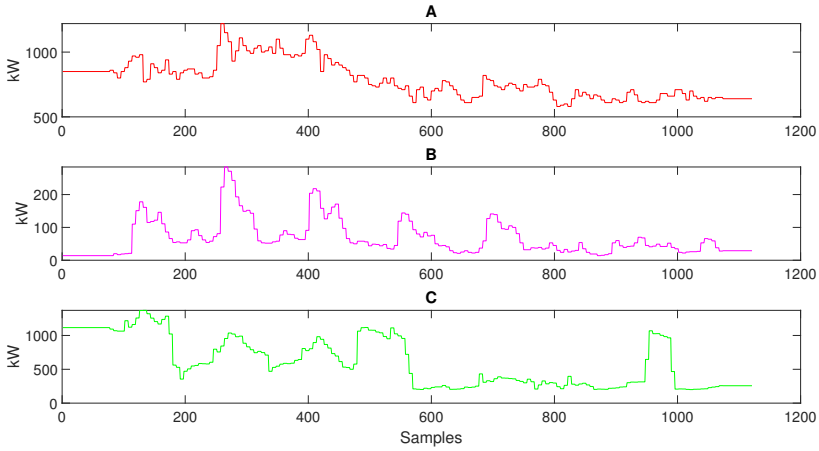

Figure B.4: Power consumption at consumer A - C, 1st week of February 2019

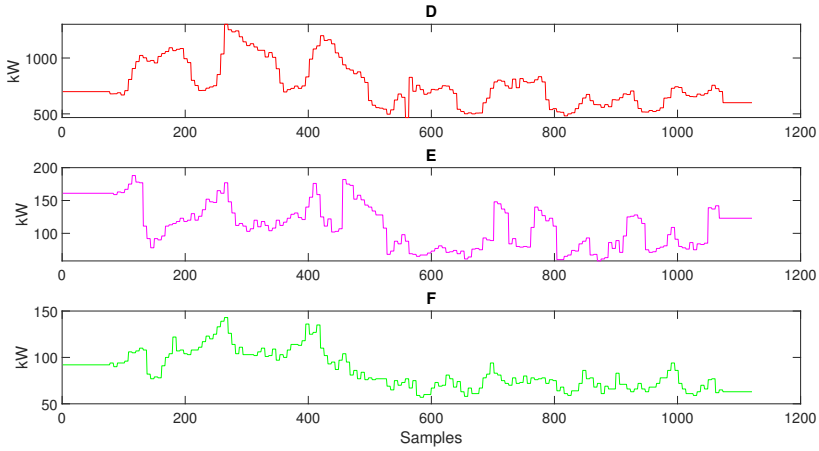

Figure B.5: Power consumption at consumer D - F, 1st week of February 2019

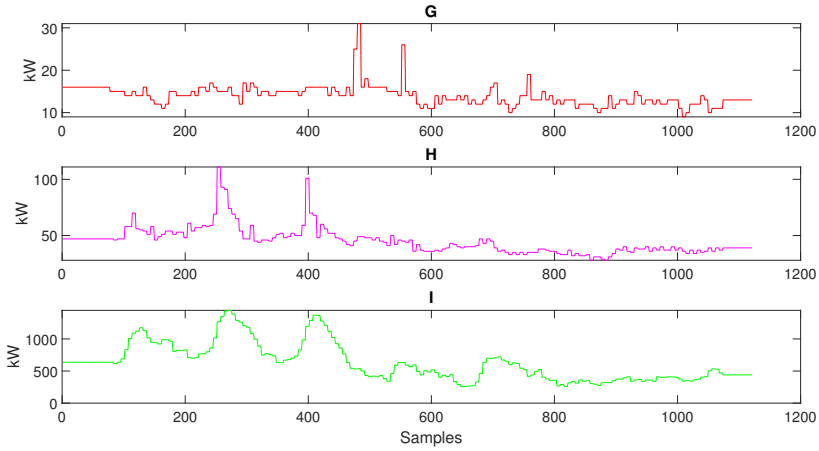

Figure B.6: Power consumption at consumer G - I, 1st week of February 2019

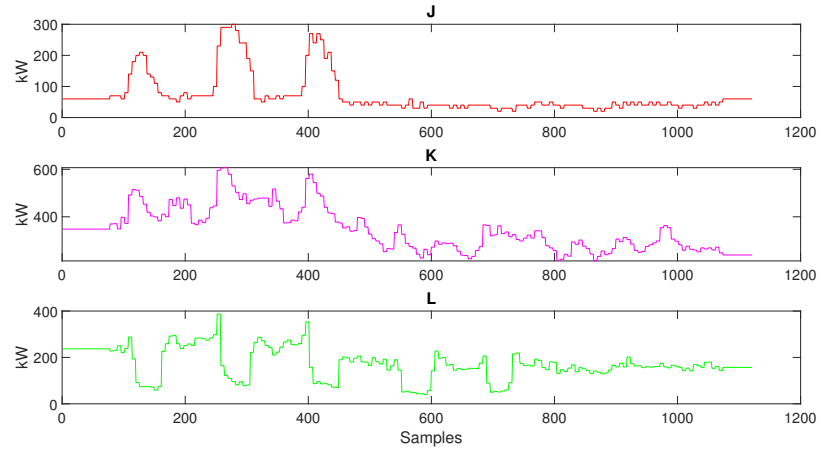

Figure B.7: Power consumption at consumer J - L, 1st week of February 2019

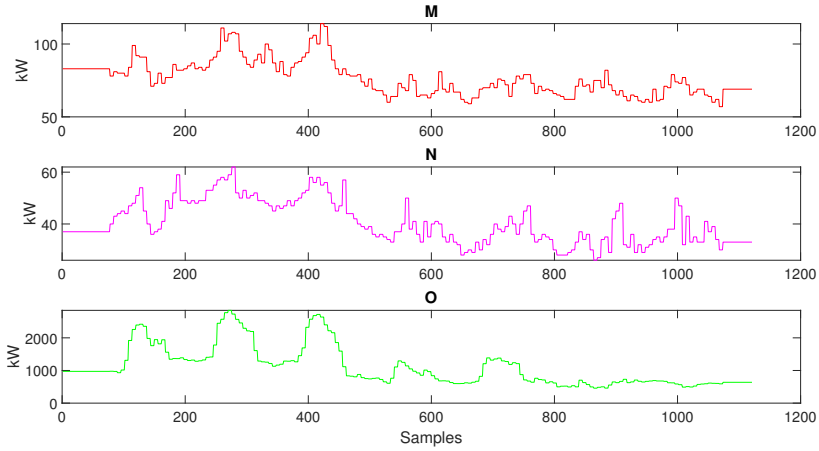

Figure B.8: Power consumption at consumer M - O, 1st week of February 2019

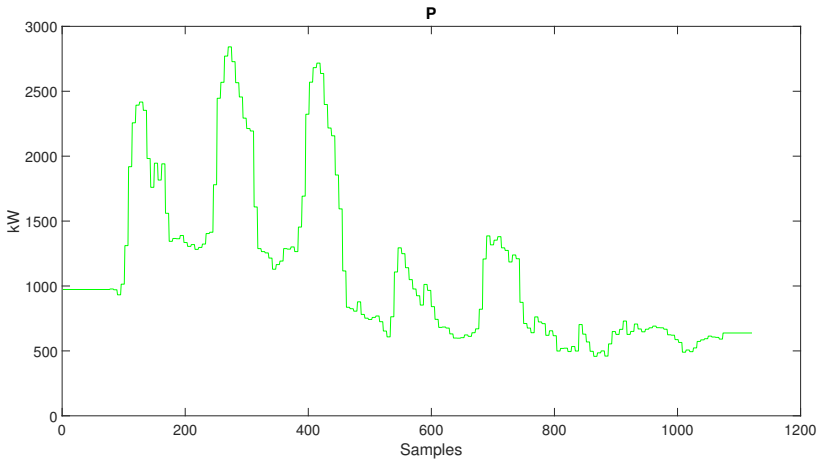

Figure B.9: Power consumption at consumer P, 1st week of February 2019

B.2 Result from Validation

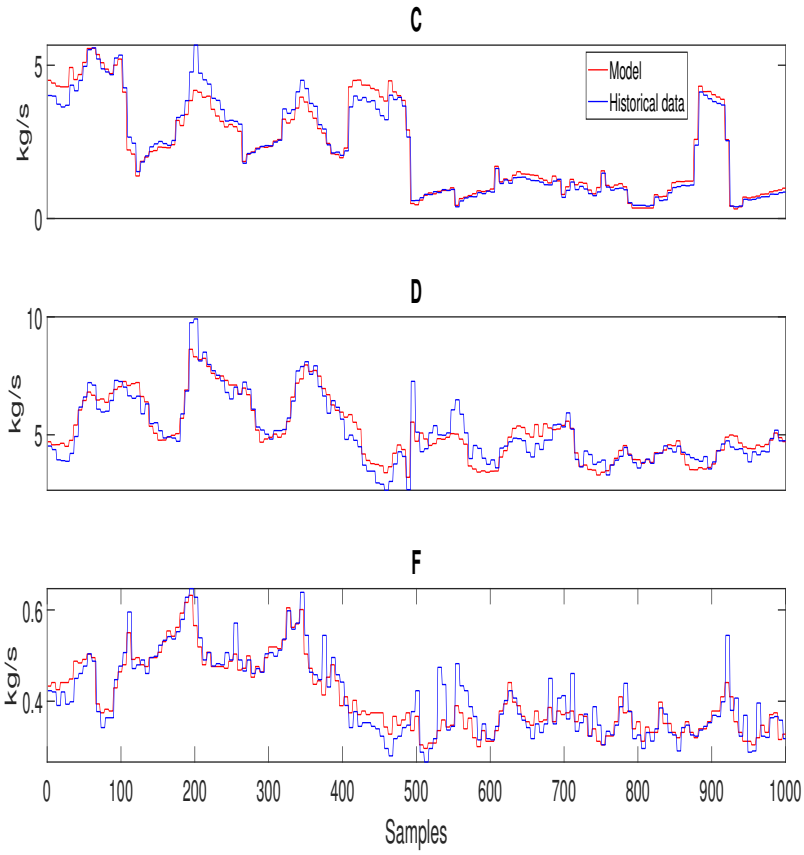

Figure B.10: Flow of consumer C, D and F

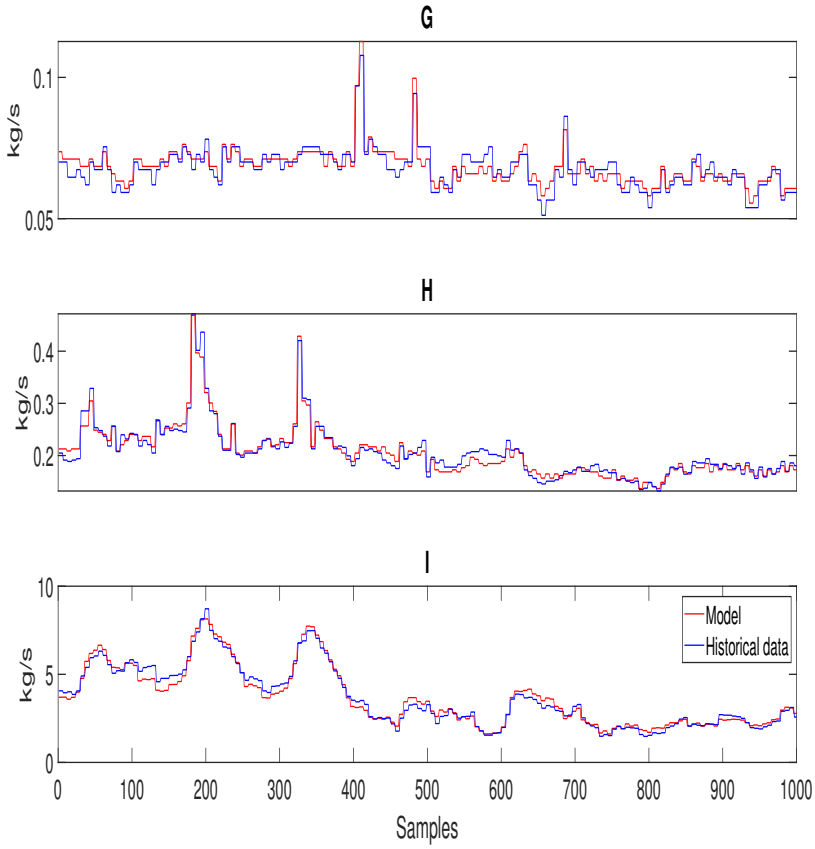

Figure B.11: Flow of consumer G-I

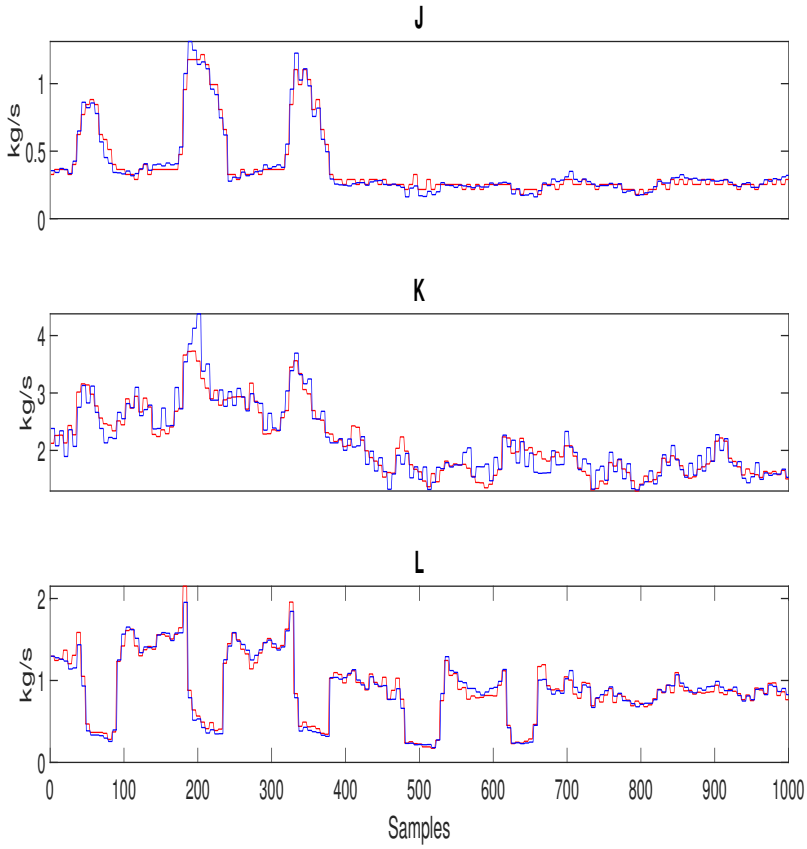

Figure B.12: Flow of consumer J-L

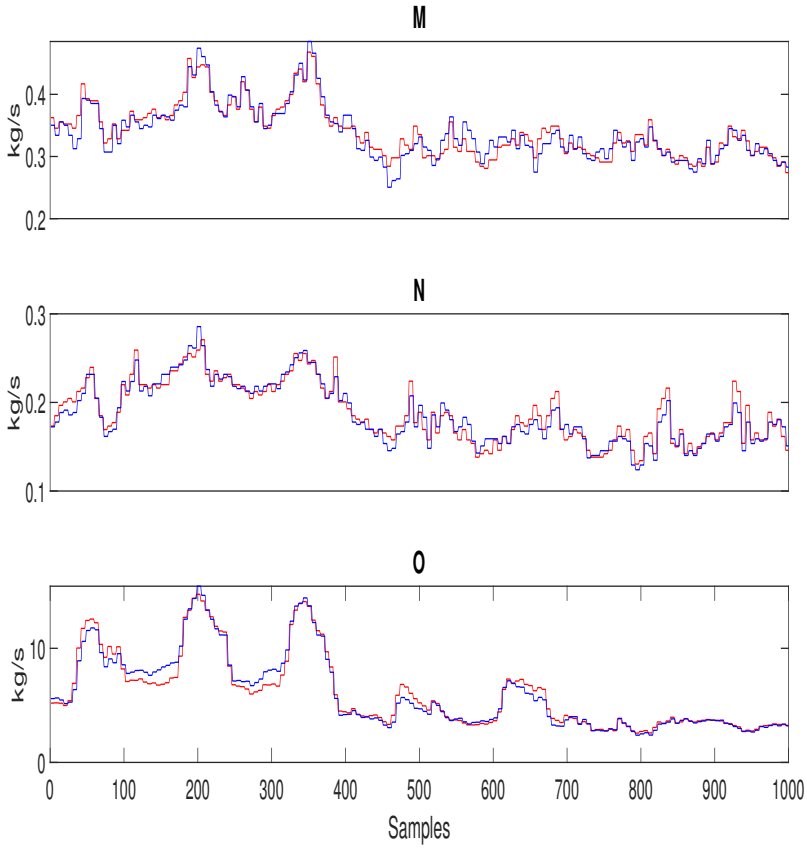

Figure B.13: Flow of consumer M-O

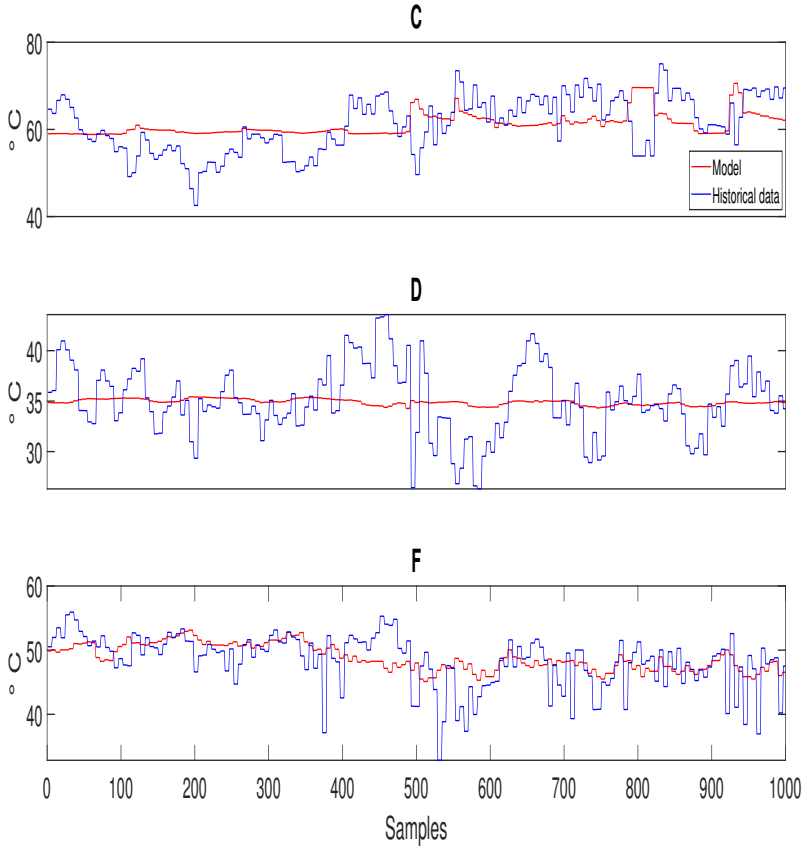

Figure B.14: Delta temperature of consumer C, D and F

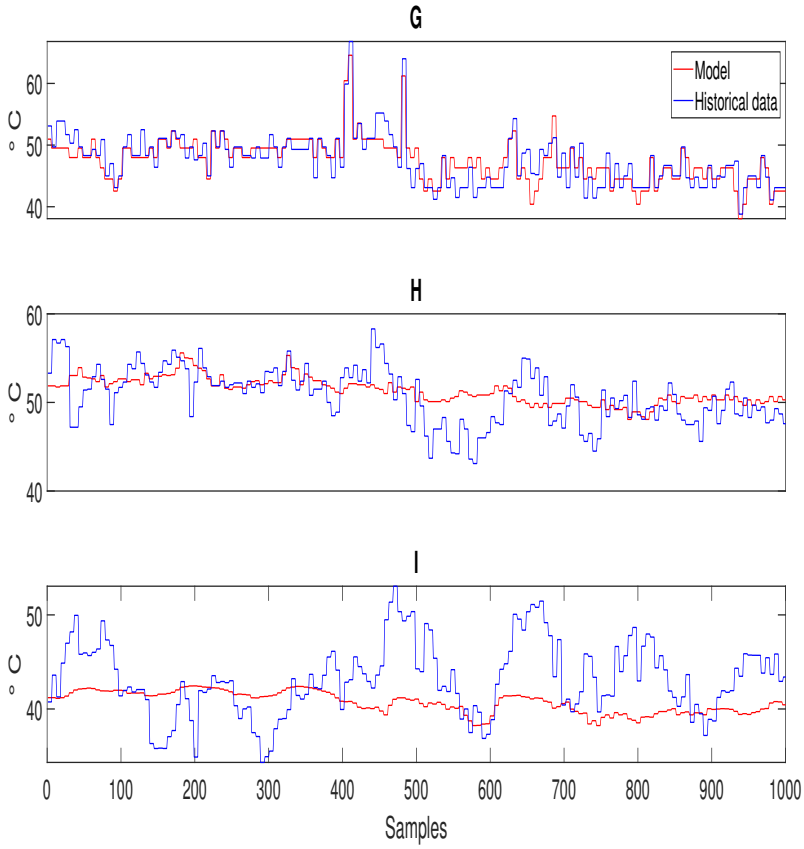

Figure B.15: Delta temperature of consumer G-I

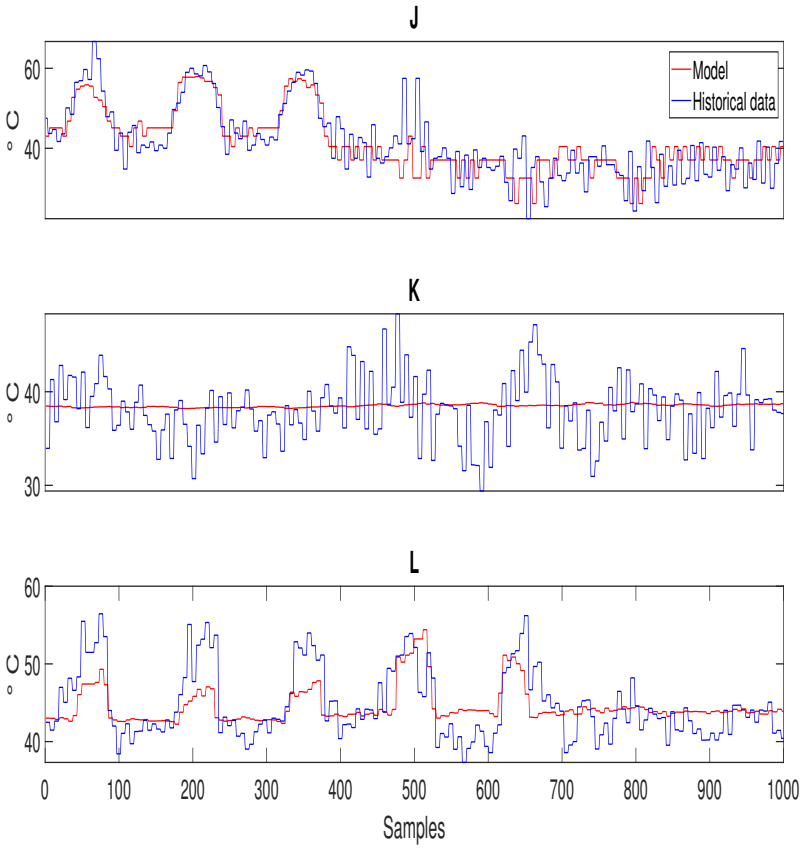

Figure B.16: Delta temperature of consumer J-L

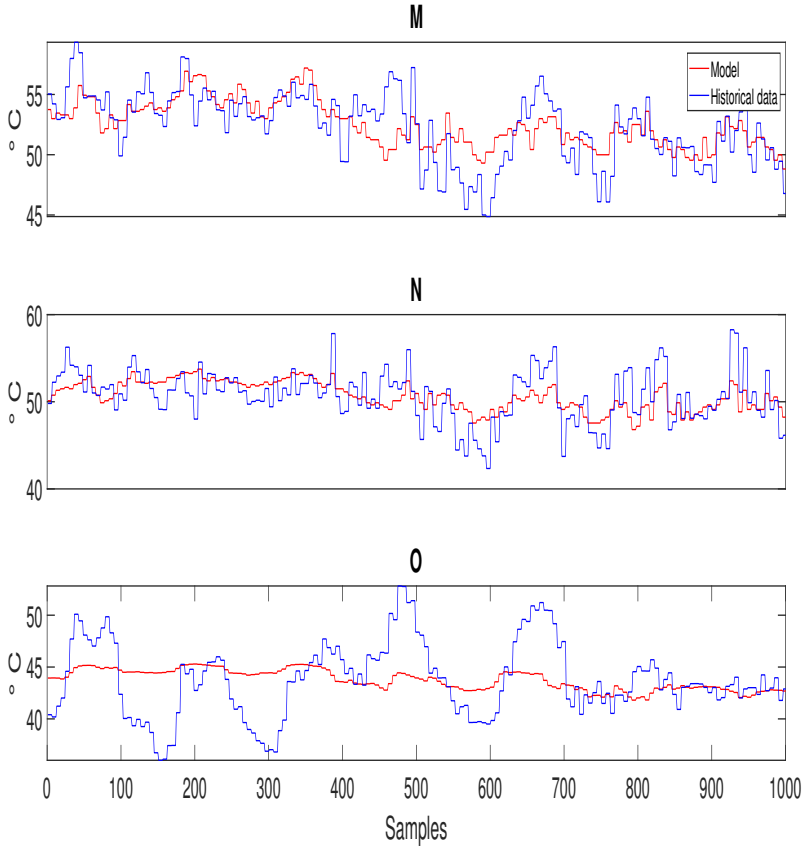

Figure B.17: Delta temperature of consumer M-O

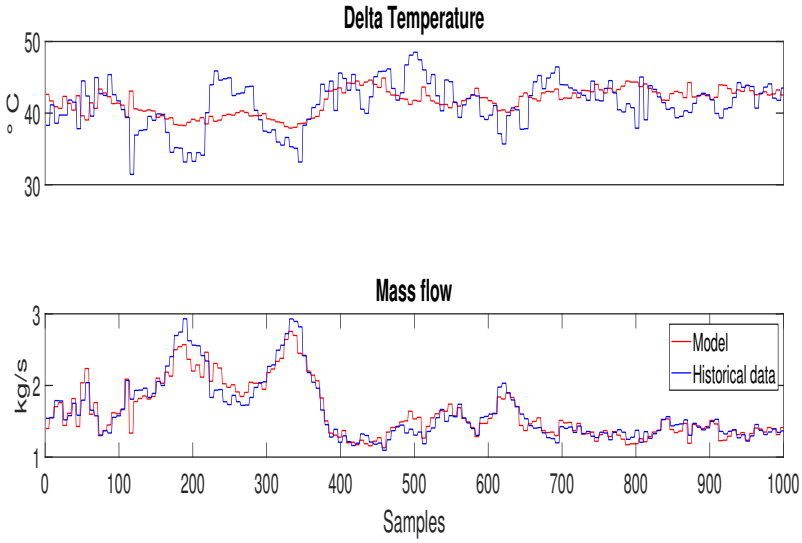

Figure B.18: Delta temperature and mass flow of consumer P

B.3 Results from Optimization with full information

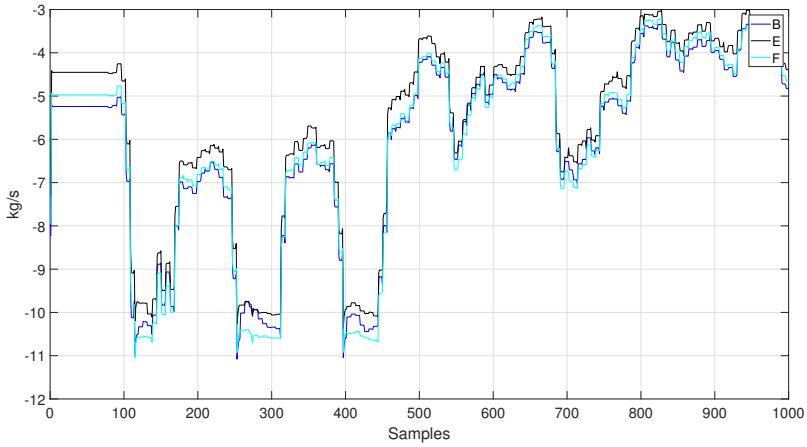

Figure B.19: Mass flow difference at consumer B, E, F

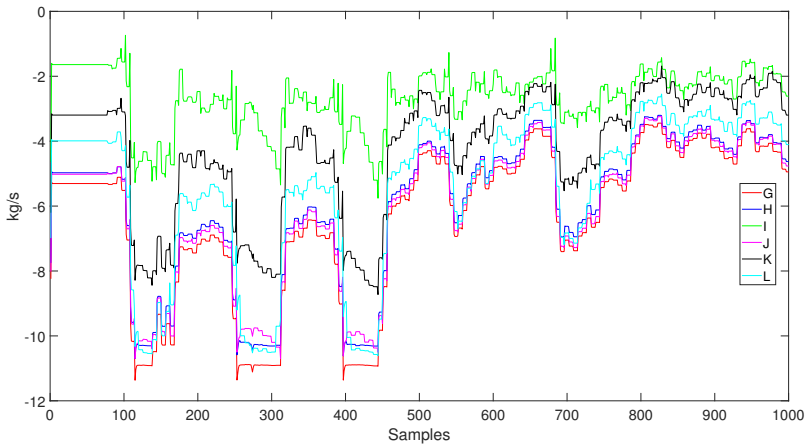

Figure B.20: Mass flow difference at consumer G, H, I, J, K and L .

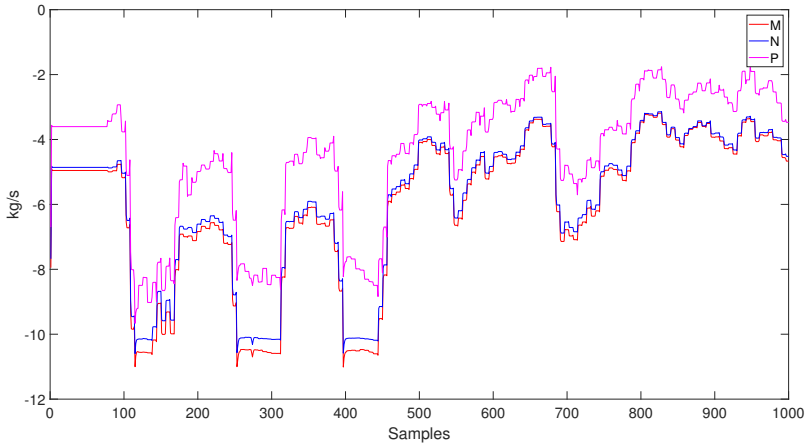

Figure B.21: Mass flow difference at consumer M, N and P .

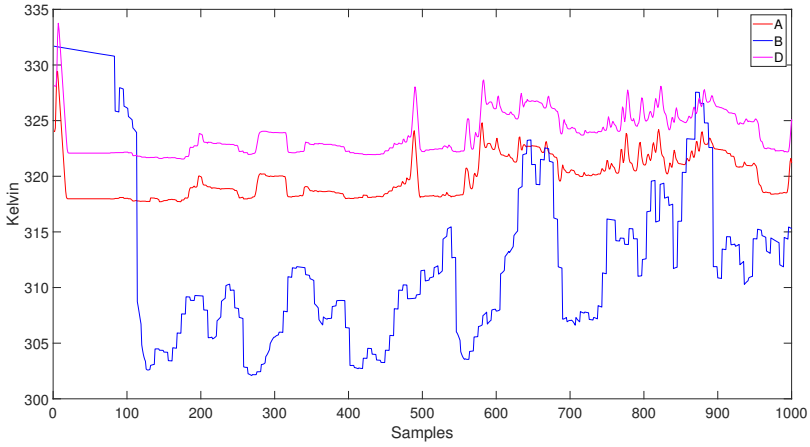

Figure B.22: Return temperature at consumer A, B, D

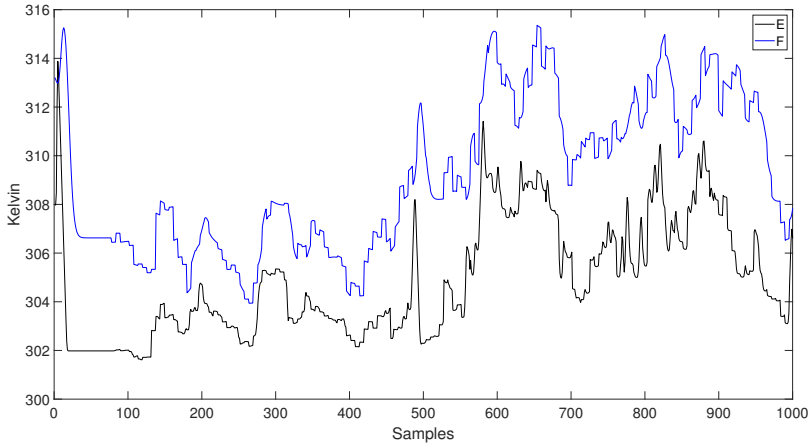

Figure B.23: Return temperature at consumer E and F

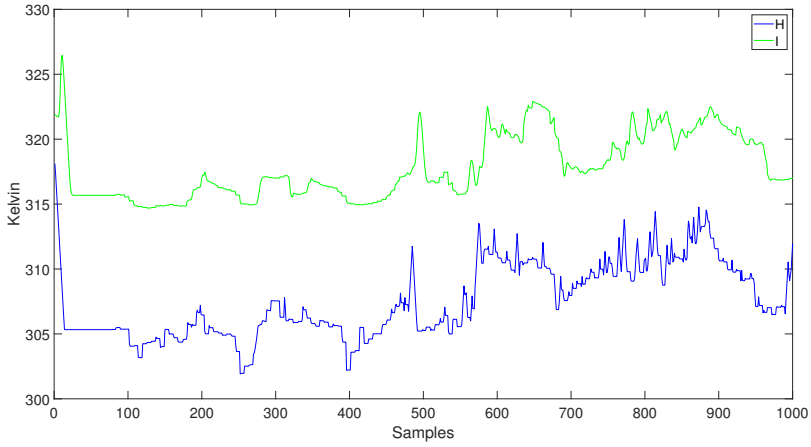

Figure B.24: Return temperature at consumer H and I

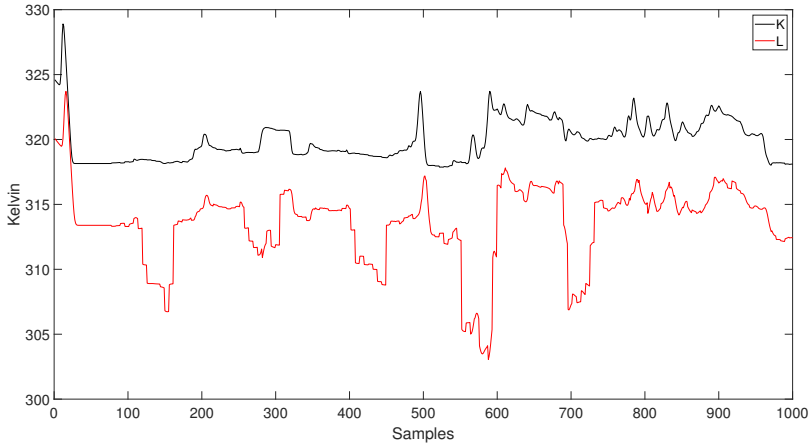

Figure B.25: Return temperature at consumer K and L

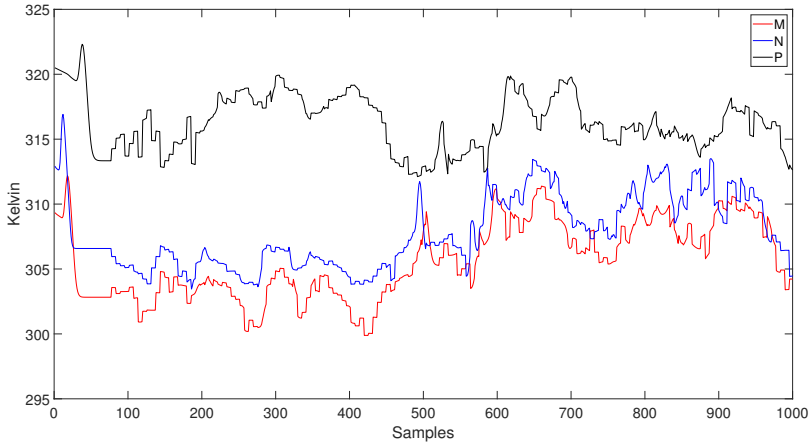

Figure B.26: Return temperature at consumer M, N and P

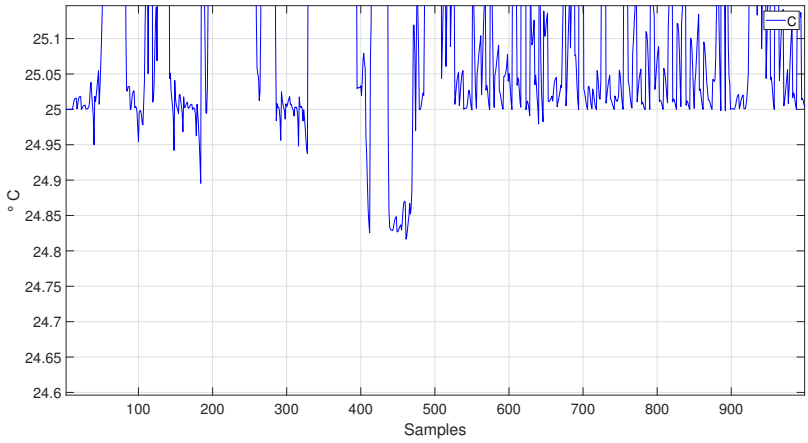

Figure B.27: Return temperature at consumer C zoomed in at the constraint

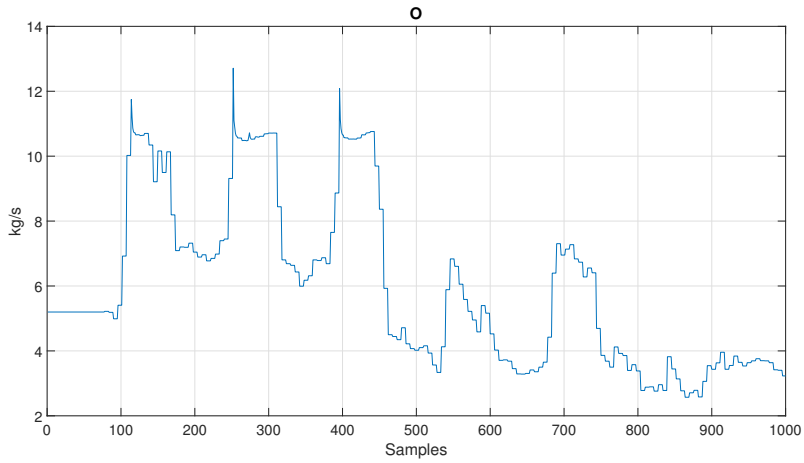

Figure B.28: Mass flow at consumer O. Full information in the controller

B.4 Miscellaneous

Heat exchanger: B25Tx70

Side 1 : Inner circuit
Side 2 : Outer circuit

DUTY REQUIREMENTS	Unit	Side 1		Side 2
Heat load	kW		150,0	
Inlet temperature	°C	70,00		5,00
Outlet temperature	°C	24,80		65,00
Flow rate	kg/s	0,7939		0,5983
Thermal length		4,203		5,579

PLATE HEAT EXCHANGER	Unit	Side 1		Side 2
Total heat transfer area	m²		4,28	
Heat flux	kW/m²		35,0	
Mean temperature difference	K		10,75	
O.H.T.C. (available/required)	W/m²,°C		3260/3260	
Pressure drop -total*	kPa	6,98		3,85
- in ports	kPa	1,50		0,848
Port diameter	mm	24,0/24,0 (up/down)		24,0/24,0 (up/down)
Number of channels per pass		34		35
Number of plates			70	
Oversurfacing	%		0	
Fouling factor	m²,°C/kW		0,000	
Reynolds number		722,5		420,2
Port velocity	m/s	1,77/1,77 (up/down)		1,33/1,33 (up/down)

PHYSICAL PROPERTIES	Unit	Side 1		Side 2
Reference temperature	°C	47,40		35,00
Dynamic viscosity	cP	0,572		0,720
Dynamic viscosity - wall	cP	0,626		0,633
Density	kg/m³	989,2		994,1
Heat capacity	kJ/kg,°C	4,180		4,178
Thermal conductivity	W/m,°C	0,6404		0,6233
Largest wall temperature difference	K		1,26	
Minimum wall temperature	°C	16,79		15,54
Maximum wall temperature	°C	67,98		67,66
Film coefficient	W/m²,°C	8050		6110
Average wall temperature	°C	42,32		41,69
Channel velocity	m/s	0,104		0,0761
Shear stress	Pa	11,5		6,28

*Excluding pressure drop in connections.

Figure B.29: Heat exchanger B25

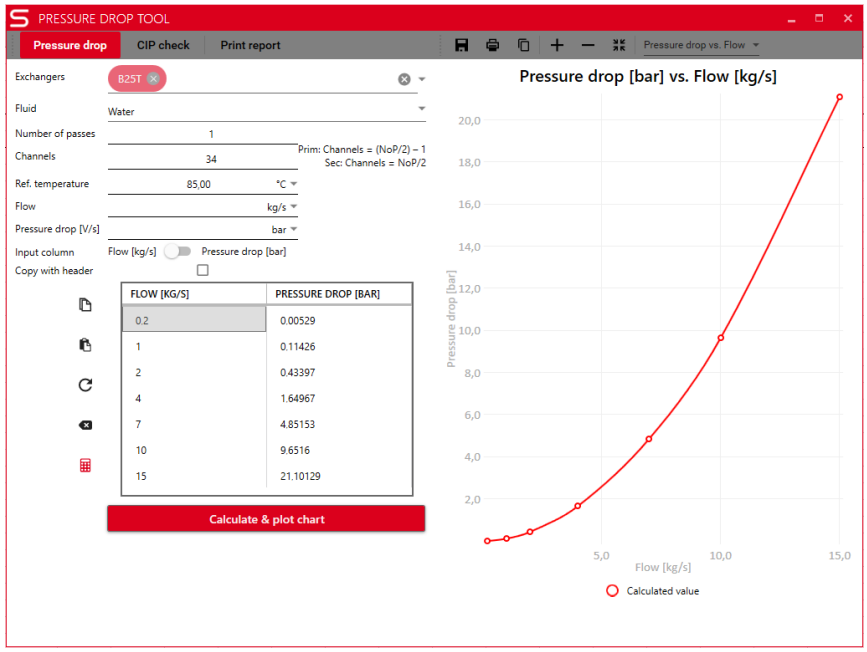

Figure B.30: Pressure loss in pipes at consumer

SWEP International AB
Box 105, Hjalmar Brantings väg 5
SE-26122 Landskrona, Sweden
Phone: +46-418 400 400
Fax: +46-418 292 95
www.swep.net

FJÄRRVÄRMECENTRAL

Kund:	Stjördal Fjernvarme	**Offertnr:**	**HQLADI-231.1M**
Er Referens:	Torbjörn Landsem	**Datum:**	2016-09-26
Projekt:	Nye SARA	**Vår Referens:**	David Ingvarsson
Adress:	Sutterøgata 21	**Uppvärmd Yta, m²:**	Okänt
Dim. Differenstryck, kPa:	Min 70	**Antal Lägenheter:**	Okänt
Fjärrvärmenät:	Statkraft_70_95-70	Max	70
Modell:	ISAC 2	Konfigurationstyp:	Parallell

		VS1		**VV**	
Värmeväxlare		SWEP		SWEP	
Modell		B35TH0/1P		B25T/1P	
Antal Plattor		90		70	
Effekt	kW	**430**		**150**	
Krets		**VP**	**VS1**	**VP**	**VV**
Temperatur in	˚C	95	30	70	5
Temperatur ut	˚C	32.4	50	24.8	65
Flöde	l/s	1.64	5.14	0.79	0.6
Tryckfall Sommar/(Vinter)	kPa	2.9	25.2	7	3.8
Rördim. (Intern)	DN	50 (40)	65	50 (32)	25
VVC-dimension	DN				25
Tryckklass PN	bar	16	6	16	10
Provtryck	bar	23	9	23	15
Säkerhetsventil	bar		6		10
Regulator		KTC		KTC	
Modell		Statkraft **AS1**		Statkraft **AS1**	
Styrventil		ESBE VLC125		ESBE VLC125	
Dimension	DN	25		15	
K_{vs}-värde	m³/h	10		4	
Ställdon		ESBE ALB144		Schneider MG900 SRU	
Cirkulationspump		-		-	
Modell		-		-	
Flöde (Dim)	l/s	-		-	
Lyfthöjd (Dim)	kPa	-		-	
Spänning/Fas/Frekv.	V/ø/Hz	-		-	
Effekt/Ström	W/A	-		-	
Temperaturgivare		KTC		KTC	
Primär retur		- / ITS 120P		- / ITS 120P	
Sekundär fram/retur		ITS 120P / ITS 120P		ITS 100 / CTS 100 (tillVVC)	
Utomhusgivare		OTS 100			

Utrustning inkluderad i Värme Primär (VP) krets
CIP ventil, Avtappningsventil, Avtappningsventil, CIP ventil

Utrustning inkluderad i Värme Sekundär 1 (VS1) krets
Säkerhetsventil, Avtappningsventil, CIP ventil

Utrustning inkluderad i Varmvatten (VV) krets
Säkerhetsventil, Avtappningsventil, CIP ventil, Backventil KV och VVC

Figure B.31: Heat exchanger and valve

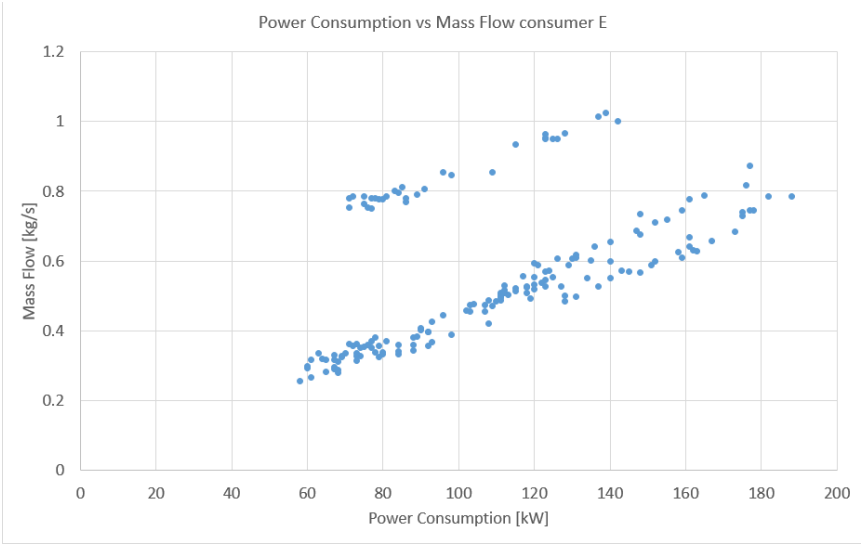

Figure B.32: Power consumption vs mass flow at consumer E

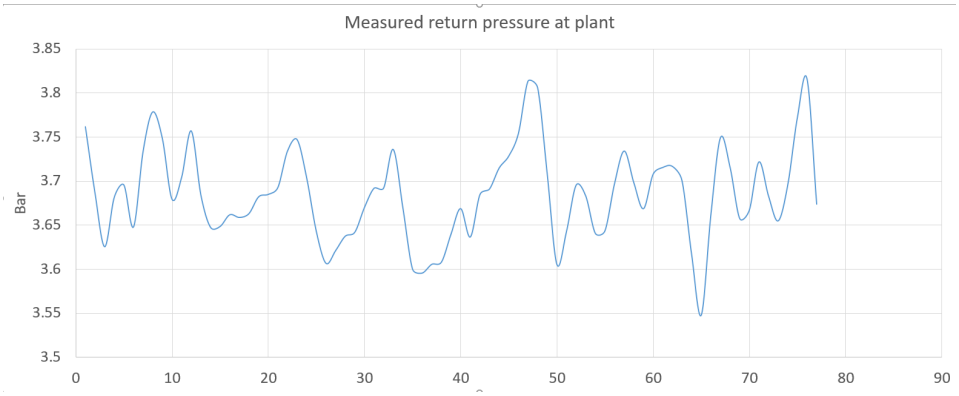

Figure B.33: Measured return pressure at plant during the first week of February 2019

Appendix C

Equations

$$
\begin{aligned}
q_a &= 0.0058 * Q_a + 0.1818 \\
q_b &= 0.0041 * Q_b + 0.0472 \\
q_c &= 0.0041 * Q_c - 0.0678 \\
q_d &= 0.0065 * Q_d + 0.1628 \\
q_e &= 0.0041 * Q_e + 0.0261 \\
q_f &= 0.0039 * Q_f + 0.0743 \\
q_g &= 0.0026 * Q_g + 0.0321 \\
q_h &= 0.004 * Q_h + 0.0247 \\
q_i &= 0.0055 * Q_i + 0.1952 \\
q_j &= 0.0037 * Q_j + 0.1053 \\
q_k &= 0.0062 * Q_k - 0.0341 \\
q_l &= 0.0057 * Q_l - 0.0554 \\
q_m &= 0.0034 * Q_m + 0.0803 \\
q_n &= 0.0039 * Q_n + 0.029 \\
q_o &= 0.0051 * Q_o + 0.2357 \\
q_p &= 0.0071 * Q_p - 0.4045
\end{aligned}
\tag{C.1}
$$

Bibliography

Bruyneel, Michaël (2019). *Sequential Convex Programming approach*. Last checked: 10.02.19. URL: https://www.researchgate.net/figure/Illustration-of-the-Sequential-Convex-Programming-approach_fig4_41714529.

Byun et al. (2019). *Study on the Development of an Optimal Heat Supply Control Algorithm for Group Energy Apartment Buildings According to the Variation of Outdoor Air Temperature*. Last checked: 11.02.19. URL: https://www.researchgate.net/figure/Schematic-diagram-of-district-heating-system_fig1_287301202.

CENSES, FME (2015). *CenSES Energy demand projections towards 2050*. Last checked: 01.02.19. URL: https://www.ntnu.no/documents/7414984/1265644753/Position-paper_Energy-Projections_utenbleed.pdf/b39bc144-cff6-46c3-82d9-37b1f8b2e04f.

Cengel, Yunus A. and Michael A.Boles (2011). *Thermodynamics An Engineering Approach*. Seventh. The McGraw-Hill.

Dyrset et al. (2017). *Training Event, Modelfit, CENIT and RealSim*. Cybernetica AS. 184 pp.

E24 (2019). *Norge har Europas laveste strømpriser*. Last checked: 01.02.19. URL: http://https://e24.no/energi/stroem/tross-dyreste-stroem-paa-aatte-aar-i-2018-norge-har-europas-laveste-stroempriser/24547531.

EngineeringToolbox (2019a). *Thermal conductivity of common materials*. Last checked: 11.11.18. URL: https://www.engineeringtoolbox.com/thermal-conductivity-d_429.html.

— (2019b). *Thermal conductivity of polyurethane insulation*. Last checked: 11.11.18. URL: https://www.engineeringtoolbox.com/polyurethane-insulation-k-values-d_1174.html.

Foss, Bjarne and Tor Aksel Heirung (2016). "Merging Optimization and Control". In:

Fox et al. (2016). *Fluid Mechanics*. Ninth. Wiley.

Giraud, Loïc et al. (2015). "Presentation, Validation and Application of the DistrictHeating Modelica Library". In: Grenoble, France.

Giraud, Loïc et al. (2017). “Optimal Control of District Heating Systems using Dynamic Simulation and Mixed Integer Linear Programming”. In: Grenoble, France.

Grundfos (2019). *TP 150-660 Pump*. Last checked: 25.03.19. URL: https://product-selection.grundfos.com/product-detail.product-detail.html?custid=GMA&productnumber=97927147&qcid=545665953.

Hamre, Andreas (2017). “Predictive Control of a District heating System”. Master Thesis. Norwegian University of Science and Technology.

Hermansson, Kristoffer and Christoffer Kos (2017). “Building and Simulating Dynamic Models of District Heating Networks with Modelica”. Master Thesis. Mälardalen University.

Hägg, Richard (2016). “Dynamic Simulation of District Heating Networks in Dymola”. Master Thesis. Lunds Universitet.

Kauko, Hanne et al. (2018). “Dynamic Modeling of local district heating grids with prosumers: A case study for Norway”. In: *Energy* 151, pp. 261–271.

Kiijärvi, Jukka (2019). *Darcy Friction Factor Formulae in Turbulent Pipe Flow*. Last checked: 11.11.18. URL: http://www.kolumbus.fi/jukka.kiijarvi/clunowa/fluid_mechanics/pdf_articles/darcy_friction_factor.pdf.

Larsen, Helge, Benny Bøhm, and Michael Wigbels (2004). “A comparison of aggregated models for simulation and operational optimisation of district heating networks”. In:

MET (2019). *Climate database*. Last checked: 01.05.19. URL: http://sharki.oslo.dnmi.no/portal/page?_pageid=73,39035,73_39049&_dad=portal&_schema=PORTAL.

Morvay, Zoran K. and Dusan D. (2008). *INDUSTRIAL INSULATION*. Last checked: 05.11.18. URL: https://www.wiley.com/legacy/wileychi/morvayindustrial/supp/toolbox10.pdf.

Møller, Sindre (2018). *Modeling and simulation of District Heating System*. Specialization Project.

NVE (2018). *Strømforbruk i Norge mot 2035*. Last checked: 01.02.19. URL: http://publikasjoner.nve.no/rapport/2018/rapport2018_43.pdf.

Nocedal, Jorge and Stephen Wright (2006). *Numerical Optimization*. Springer.

Patnia, Abhishek (2018). *Softmax*. Last checked: 25.02.19. URL: https://www.quora.com/Why-is-softmax-activate-function-called-softmax.

SNL (2019). *Fjernvarme*. Last checked: 10.02.19. URL: https://snl.no/fjernvarme.

Statkraft (2019a). *Fjernvarme*. Last checked: 09.03.19”. URL: https://www.statkraft.no/Energikilder/Fjernvarme/.

— (2019b). *Fjernvarme2*. Last checked: 09.03.19. URL: https://www.statkraftvarme.no/globalassets/old-contains-the-old-folder-structure/documents/faktaark_tcm84-14828.pdf.

— (2019c). *Legionella*. Last checked: 25.04.19. URL: https://www.statkraftvarme.no/om-fjernvarme/klima-og-miljo/legionella/.

Svenheim Rene, Anders (2016). “Model Predictive Control of District Heating Systems”. Master Thesis. Norwegian University of Science and Technology.

Thermopedia (2019). *Overall heat transfer coefficient*. Last checked: 17.11.18. URL: http://www.thermopedia.com/content/1007/.

Thomas, Philip (1999). *Simulation of Industrial Processes*. Butterworth Heinemann.

ToolBox, Engineering (2019). *Dynamic and Kinematic Viscosity*. Last checked: 29.10.18. URL: https://www.engineeringtoolbox.com/water-dynamic-kinematic-viscosity-d_596.html.

Utne, Åmund (2018). *Fjernvarme, Innføring i Teknologien*. Statkraft. 31 pp.

Wikipedia (2019). *Darcy–Weisbach equation*. Last checked: 04.11.18. URL: https://en.wikipedia.org/wiki/Darcy%E2%80%93Weisbach_equation.

Willersrud et al. (2013). "Short-term production optimization of offshore oil and gas production using nonlinear model predictive control". In: *Journal of Process Control* 23, pp. 215–223.

Yr.no (2019). *Temperatures*. Last checked: 11.04.19. URL: https://www.yr.no/sted/Norge/Tr%C3%B8ndelag/Stj%C3%B8rdal/Stj%C3%B8rdal/detaljert_statistikk.html.

ZHOU, Shou jun et al. (2014). "Dynamic modeling of thermal conditions for hot-water district-heating networks". In: *Hydrodynamics* 26, pp. 531–537.

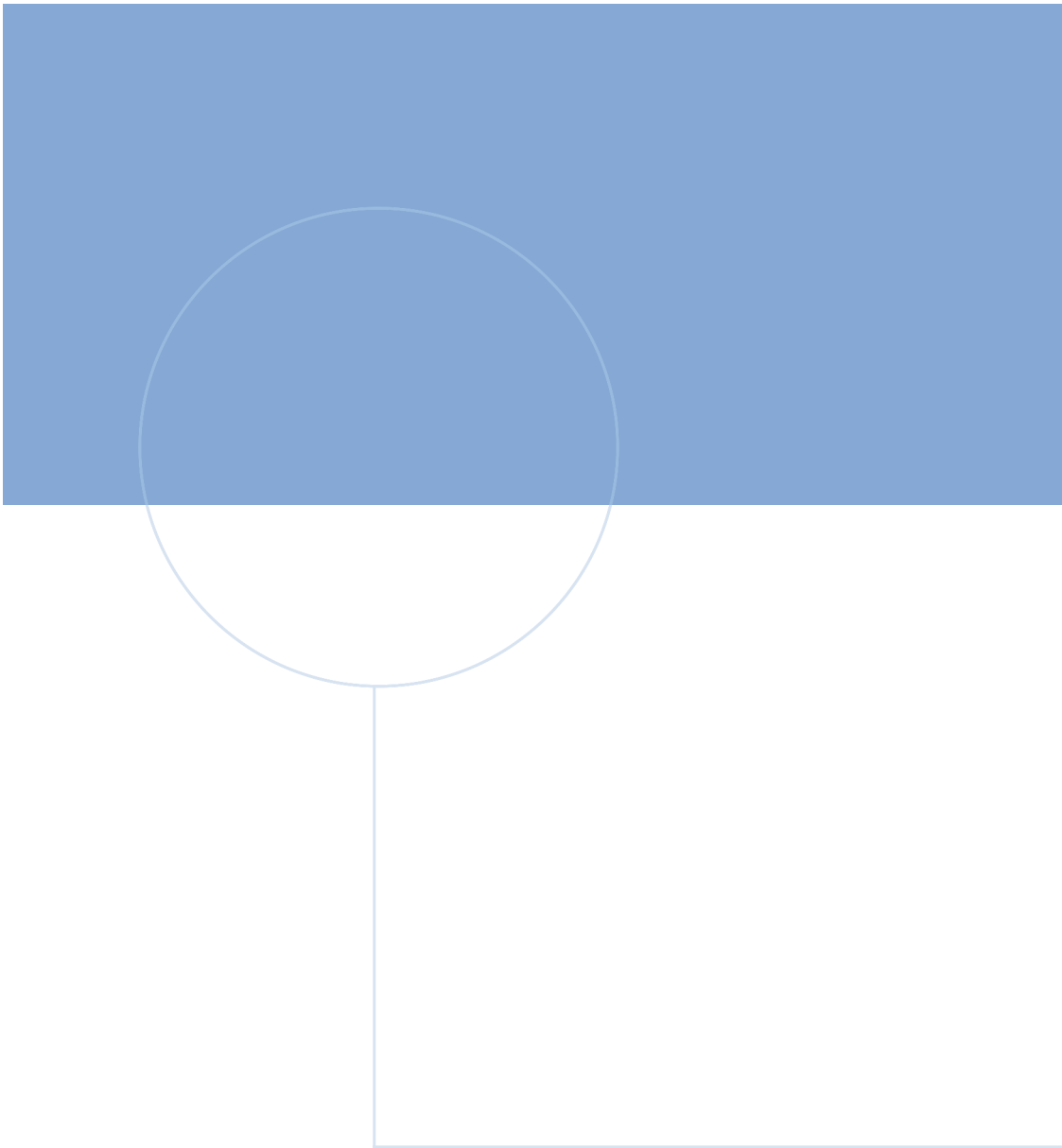

NTNU
Norwegian University of
Science and Technology